Charge transport and excited states in organic semiconductors

Song Jingyao

Department of Physics

Queen Mary, University of London

Supervisors – Dr. Theo Kreouzis

Dr. William Gillin

Dr. Natalie Stinglin-Stutzmann

July 2010

Submitted for the degree of Doctor of Philosophy

Declaration

I declare that all the work contained within this thesis is accomplished by myself during my study at Queen Mary, University of London.

Jingyao Song

Abstract

Organic semiconductors are of increasing technological interest in applications such as light emitting diodes, field effect transistors, and photovoltaic devices In order to reveal the basic principles behind these organic semiconductors, charge transport theory in these organic materials has been introduced and has been receiving increasing attention over the last few years. Although excitons are known to interact with free charges, the effect that excited states may have on the charge transport is not generally considered in the field of organic electronics. This occurs even though organic light emitting diodes (OLEDs) are known to contain large numbers of triplet states during operation. Indeed, it is quite possible that the mobility in working devices may well be a function of drive current, as the excited state population will change with operating conditions. This work is thus motivated by both technological and fundamental scientific interest.

In this thesis, the hole mobilities in both *poly-(3-hexylthiophene)* (P3TH) and *N,N'*-diphenyl-*N,N'*-bis(3-methylphenyl)-(1,1'-biphenyl)-4,4'-diamine (TPD) devices ($\mu_{Hole}^{P3HT} \approx 5.0\times10^{-5} cm^2/Vs$, $\mu_{Hole}^{TPD} \approx 5.0\times10^{-4} cm^2/Vs$) have been measured, and observed a remarkable mobility reduction (～15%) in ambipolar samples (in both P3HT and TPD) after applying a small DC offset bias. This correlated to the turn-on voltage in I-V characterization, and the luminescence in the ambipolar TPD sample. In the unipolar sample, however, there is no such behaviour. This strongly suggests that the reduction of the hole mobility is due to site blocking/interacting caused by the excited triplet states.

In further experiments in the presence of a magnetic field (500 mT), results an increase in the mobility (～5%) and steady state current density in ambipolar samples only, this is consistent with magnetically mediated inter-conversion of

(blocking/interacting) triplet states to the singlet states. The correlation between the magnetic mobility increase and the steady state current increase offers direct evidence for a microscopic mechanism behind organic magneto resistance (OMR).

Given the experimental evidence, we conclude that excitons (specifically triplet states play a critical role in charge transport in organic semiconductors.

Acknowledgment

Firstly, I would like to express my sincere thanks, appreciation and gratitude to all my supervisors: Dr. William Gillin, Dr. Theo Kreouzis and Dr. Natalie Stinglin-Stutzmann. I am thankful for their excellent guidance, valuable expertise and inexhaustible patience during all stages of my PhD study, which have enabled me to complete my research and write up this thesis. Also, without the financial support arranged by my supervisors, my studies at Queen Mary would have been impossible. I also want to thank my supervisors for giving me tons of support during my difficult job-hunting moments.

I would also like to thank all my colleagues in our group and office for their help with my experiments and studies. Especially, I would like to thank my ex-flat-mate and also my college Dr. Rui Zhang, for helping me arranges our accommodation. My thanks also go to Mr. Sijie Zhang and Dr. Emiliano Bilotti who, with incredible patience, helped me by correcting my writing mistakes. I want to thank Ken for explaining all the experimental equipment, and Geoff for repairing our machines, which were usually damaged by our careless operations.

I am deeply thankful to my parents, who enthusiastically supported all of my studies, and helped and guided me though difficult times. The rest of my family have also been incredibly supportive, particularly my grandparents.

Lastly, but most importantly, I thank my wife, Ling Liu, whose love and support has motivated me throughout, providing constant encouragement to me. I cannot express my appreciation through mere words: you make my life beautiful and worthwhile.

Contents

3. Experiment

4. P3HT Results

Figure list

Abbreviations list

Alq_3…… aluminium tris(8-hydroxyquinolinate)

BCP……..bathocuproine

CuPc…….....copper phthalocyanine

DI……..dark injection

FET……field effect transistor

MR……magnetoresistance

ITO……Indium tin oxide

OLD……...organic light emitting diode

OMR……organic magnetoresistance

OPV……organic photovoltaic

OTFT……organic thin film transistor

PLED……polymer light emitting diode

PTCBI……perylene tetracarboxylic derivative

P3HT…….....poly-(3-hexylthiophene)

TFT……...thin film transistor

ToF……time of flight

TPD……..*N,N'-diphenyl-N,N'-bis(3-methylphenyl)-(1,1'-biphenyl)-4,4'-diamine*

TPI……triplet-polaron interaction

Publications list

1. J. Y. Song, N. Stingelin, W. P. Gillin, and T. Kreouzis, *Reduced hole mobility due to the presence of excited states in poly-(3-hexylthiophene)*, APPLIED PHYSICS LETTERS **93**, 233306 (2008)
2. Sijie Zhang, Jingyao Song, T. Kreouzis and W.P. Gillin, *Measurement of the intersystem crossing rate in Aluminium tris(8- Hydroxyquinoline) and its modulation by an applied magnetic field*, Journal of Applied Physics. **106**, 043511 (2009)
3. J.Y.Song, A.J.Drew, N.Stingelin, W.P.Gillin and T.Kreouzis, *The effect of excited states and applied magnetic fields on the measured hole mobility in an organic semiconductor.* PHYSICS REVIEW B, **82**, 085205 (2010).
4. J.Y.Song, N.Stingelin, W.P.Gillin and T.Kreouzis, *blalanced ambipolar transport in N,N'-diphenyl-N,N'-bis(3-methylphenyl)-(1,1'-biphenyl)-4,4'-diamine (TPD)*. APPLIED PHYSICS LETTERS, submitted.
5. J.Y.Song, N.Stingelin, W.P.Gillin and T.Kreouzis, *Mobility research of intersystem crossing and organic magneto-resistance in N,N'-diphenyl-N,N'-bis(3-methylphenyl)-(1,1'-biphenyl)-4,4'-diamine (TPD).* PHYSICS REVIEW B, submitted.
6. Conference poster, Mobility due to the presence of excited states, SEMS poster presentation, Queen Mary university of London
7. Conference poster, Reduced hole mobility due to the presence of excited states in poly-(3-hexylthiophene), SID Organic Electronics
8. Invited conference talk, mobility change due to excited states, Mini-symposium on Organic Lasers and Hybrid Optical Structures.

Chapter one: Introduction

1.1. Brief history of organic devices

1.1.1. Organic light emitting diode

The beginning of organic LEDs can be traced back to the 1960s. Most early organic electroluminescent devices were based on anthracene crystal, where several hundred volts were required to obtain light emission. A significant step was made by Tang and Van Slyke in the 1980s[1, 2]. They produced a small molecule double-layer thin-film device based on aluminium tris(8-hydroxyquinolinate)(Alq_3), which is an electron transport material. The various layers were evaporated onto an indium tin oxide (ITO) electrode on top of a glass substrate. ITO works as a transparent anode, which is used to inject holes. On top of the ITO, there is a thin layer of N,N'-diphenyl-N,N'-bis(3-methylphenyl)-(1,1'-biphenyl)-4,4'-diamine (TPD), which is used to transport holes to the interface with Alq_3. Alq_3 is used to bring electrons to the interface with TPD, and excited states can be formed at this interface, from the recombination of these electron-hole pairs, light can be obtained from the device. A layer of Ag: Mg evaporated on top of Alq_3, is used to inject electrons, see figure (1.1.1)

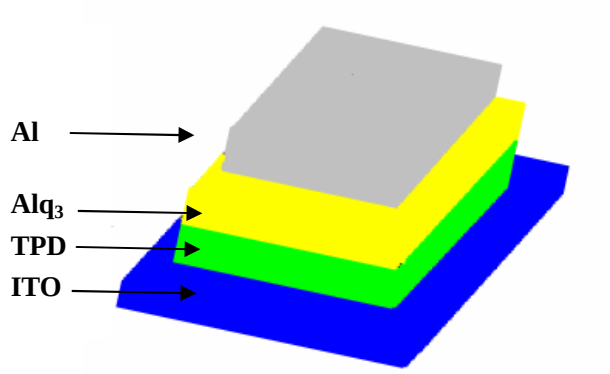

Figure 1.1.1 Structure of multilayer OLED

TPD is used for hole injection/transport, the anode is glass based ITO.

The unique feature of the device was that each layer was mainly used for unipolar charge injection and transport, for instance the work function of Al (Φ_{Al}) are relatively close to the LUMO of Alq_3 layer, and the work function of ITO (Φ_{ITO}) also matches with HOMO of TPD material. With small energy barriers at the electrodes interface, both electron and hole carriers injection/transport is highly optimised and the density is roughly balanced via similar mobility in the organic emitting diode, while the small energy barrier between TPD and Alq_3 layers could cause the charge carriers to accumulate at the interface. In figure 1.1.2 (b) electrons are accumulated at the LUMO level, this increases the possibility of recombination at the heterointerface. All of this could lead to an improvement of electroluminescence when compared with early anthracene devices.

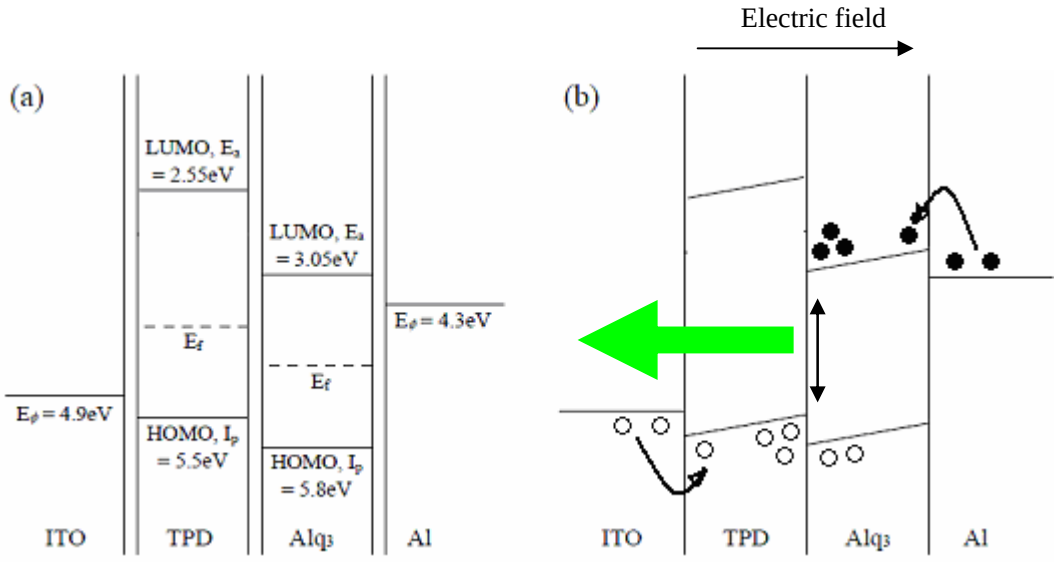

Figure 1.1.2 Schematic of energy levels

Schematic of the energy levels in Tang and Van Slyke's multilayer OLED: Eφ denotes the work function of the metals, and E_f is the Fermi energy, (b) shows charge injection, transport, recombination and light emission under applied potential. The multilayer device structure offers very low barriers for electrons and holes, while at same time it traps the charge carriers in an organic/organic interface to allow maximum recombination.

The first conjugated polymer-based device was discovered in 1989[3], by the group in the Cavendish laboratory. This device has a single layer structure, and uses poly (1, 4-phenylene) as both electron and hole transporting material, which is sandwiched between two electrodes, typically ITO and Al. Since then there has been extensive research on PLEDs[4].

Modern OLEDs are believed to have lots of advantages compared with traditional inorganic semiconductors, such as low cost, easy processing, and the possibility of large area fabrication. However they still currently present some problems, one of the disadvantages of organic materials in general is their sensitivity to an ambient environment, such as oxygen and moisture. For long-term usage of those materials, careful encapsulation can be used to avoid this problem.

1.1.2. Organic thin film transistor

The field-effect transistor (FET) was first proposed by J.E. Lilienfeld[5], who received a patent for his idea in 1930, and now thin film transistors (TFT) are widely used in computers, displays, and other electronic devices.

An organic thin film transistor (OTFT) is a three terminal device that consists of a gate, an insulator dielectric substrate, a semiconductor layer, and a source and drain (see figure 1.1.3). It can be used for amplification, switching, voltage stabilisation, signal modulation, and many other functions.

When the OTFT turns on, the gate voltage (Vg) (negative or positive) forces the holes (or electrons) to accumulate in a thin layer on the organic semiconductor at the interface with the insulator. The voltage between source and drain can make the holes (or electrons) drift across the interface, also the voltage potential between the source and gate can lead to a charge injection from the source electrode into the semiconductor.

When the OTFT turns off, the gate voltage Vg drives the holes (or electrons) away from the interface, so, even if a voltage is applied between source and drain, the current cannot flow though the channel, as there is a lack of charge accumulation.

With increases in the gate voltage, more and more mobile charges accumulate at the interface, which enhances the current flow between source and drain, and eventually reaches the saturation value.

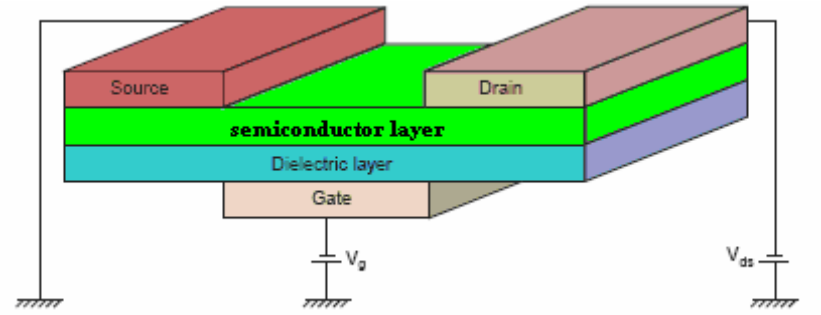

Figure 1.1.3 The structure of organic thin film transistor

This is a top contact bottom gate transistor, where source and drain are deposited on top of the semiconductor layer, and the gate contact is located at the bottom of the dielectric layer.

The typical characteristic is presented in figure 1.1.4. The voltage between the source and drain is constant, and the gate voltage is varies from 20 V to -60 V. When the gate voltage is above 0 V, the device is switched off and the leakage current is about 2×10^{-10} A. since there is no significant current flow through the device, the mobility of this device is too low to be detected. When the gate voltage is below 0 V, the device switched on, and the current gradually increase to 2×10^{-5} with the mobility between 0.5 to 1 cm^2/Vs. The saturated current divided by the off current is called on/off ratio which is around 10^5 in this figure.

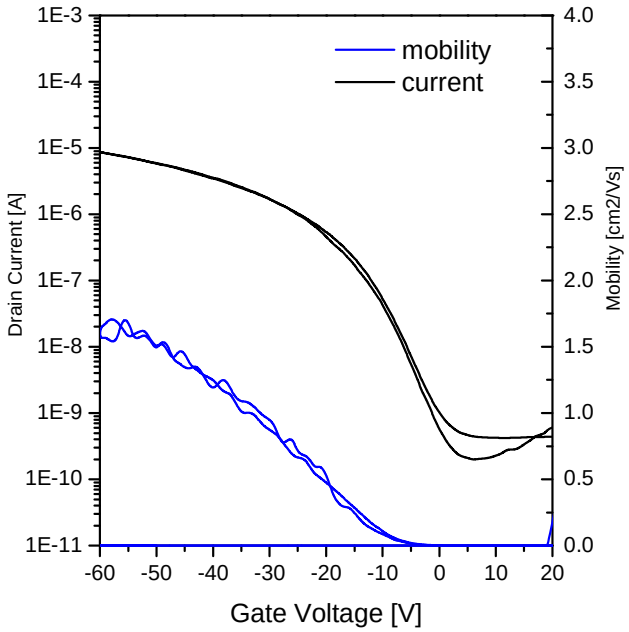

Figure 1.1.4 Characteristic of OTFT, the gate voltage was scanned from 20 V to -60 V, and then back again.

In 1986, the first organic thin film transistor (OTFT) was reported[6]. OTFT use organic semiconductors instead of the traditional semiconductor (silicon or gallium) layer. Compared to traditional materials, polymers have low melting points, hence they are easy to process, can be cheap, and suitable for large area application (such as big LCD displays). OTFT can also be flexible, so the OTFT board can be bent to fit a required shape, for application such as e-paper, LCD and so on.

The first OTFT was made using Polythiophene, but the properties of this OTFT were quite poor, for instance, the hole mobility was only $10^{-5}cm^{2/}Vs$, and the on/off ratio was only around 10^{3}[6] (the output current divided by the transfer current characteristic). Over the last 20 years or so, there has been significant progress in the OTFT field[7]. Not only have the electronic properties of OTFTs been greatly improved, but new fabrication techniques have also been found.

1.1.3. Photo-diode device

The room temperature charge carrier mobility in organic semiconductors is at least two orders of magnitude lower than in silicon based semiconductors. This does not mean that organic based photo-detectors cannot compete with traditional silicon based photo-detectors. For instance, organic semiconductors have very high optical absorption, which allows the organic photo-detector to be extremely thin, and still capture most of the incident photons.

The first organic photo-detector was invented by Peumans and his co-workers[8]. It is a multilayer structure device, and the energy level is shown in figure 1.1.5: copper phthalocyanine (CuPc) is chosen as a hole transporting layer, perylene tetracarboxylic derivative (PTCBI) is chosen as an electron transporting layer, and bathocuproine (BCP) is exploited to block the excited state diffusion, hence preventing the excited states dissociating at the Ag electrode surface. The whole system is under a reverse bias. The principle of this device is exactly opposed to the OLED system that was discovered by Tang and his co-workers. Firstly, the incident photons are absorbed by the device, which causes the formation of excited states at the CuPc and PTCBI interface. Due to the reverse bias, the excited states dissociate to free holes and electrons. Holes are carried via the HOMO level of CuPc hopping toward the ITO electrode, and electrons are carried by the LUMO level of PTCBI hopping toward the Ag electrode under the electric field. This allows a photo current through the detector. By analysing the photo current density, we can define the intensity of the incident light, thereby achieving the photo-detecting purpose.

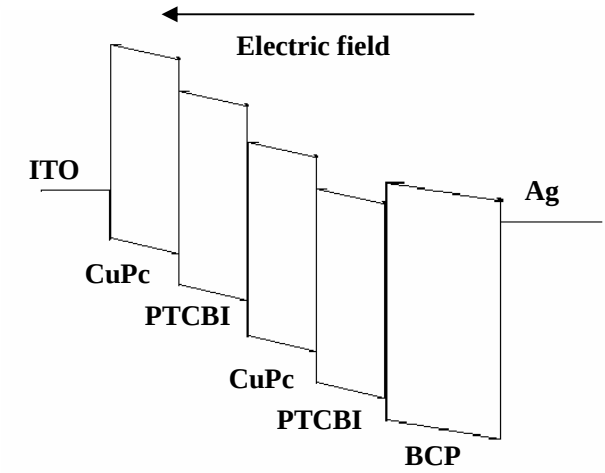

Figure 1.1.5 Energy level diagram of Peumans photo-detector device

The diagram presents the work function of both ITO and Ag, and also shows the HOMO and LUMO level of the organics. In order to achieve maximum photo current, the detector contains a multilayer structure of repeated CuPc and PTCBTI double layers.

1.2. Organic molecular structure and electronic properties

Organic semiconductors were initially employed in electroluminescence devices[9], but are increasingly applied to many other electronic devices, such as field effect transistors[10] and photovoltaic devices[11]. The application of organic materials depends on the unique semi-conducting behaviours of certain molecular structures. Two main semi-conducting organic materials will be fully described before further discussion, namely Poly-(3-hexylthiophene)[12] (also known as P3HT for short), and N,N'-diphenyl-N,N'-bis(3-methylphenyl)-4,4'-diamine (TPD). Both these materials are used throughout this work. Figure 1.2.1 (a), (b) shows the molecular structures of both P3HT and TPD[13].

The electronic states in these two organic materials play a crucial role in experimental semi-conducting devices. The benzene structure in these materials is an important example for explaining semi-conducting behaviour in organics, this is shown in figure 1.2.1 (c) (d). Each carbon has the charge occupancy $1s^2$, $2s^2$, $2p^2$, in order to form the bonds between the carbon atoms, sp2 hybridised bonds are formed. The 2s level mixes with two of the available 2p levels, which gives a configuration of $1s^2$, sp^2, sp^2, sp^2, p[14]. For a specific carbon atom, $1s^2$ is fully occupied, and three sp^2 hybridised bonds form three σ-bonds whose excitation energies are very high. The remaining p-orbitals, which are perpendicular to the molecule, form relatively weak π-bonds, and this π-π stack has a much lower energy. Because of the Pauli exclusion principle, the highest π (bonding) orbital that is occupied by electrons is called the highest occupied molecular orbital (HOMO), while the lowest π* (antibonding) orbital that is unoccupied by electrons is called the lowest unoccupied molecular orbital (LUMO) [15], HOMO and LUMO can, in some cases, be considered equivalent to the valence and conduction band for the hole and electron transport in an inorganic semiconductor. It is these orbitals that are responsible for the electronic properties of conjugated organics. The area of π-bond overlap and

charge delocalisation in a benzene ring[14] are shown in figure 1.2.1.(c) (d). The semi-conducting behaviour of organics depends on these small energy gaps between HOMO and LUMO[16], typically less then 3eV. Otherwise the charge injection will be prohibited by the large energy barrier at the interfaces between electrodes and semiconductor; therefore the organic will perform as an insulator.

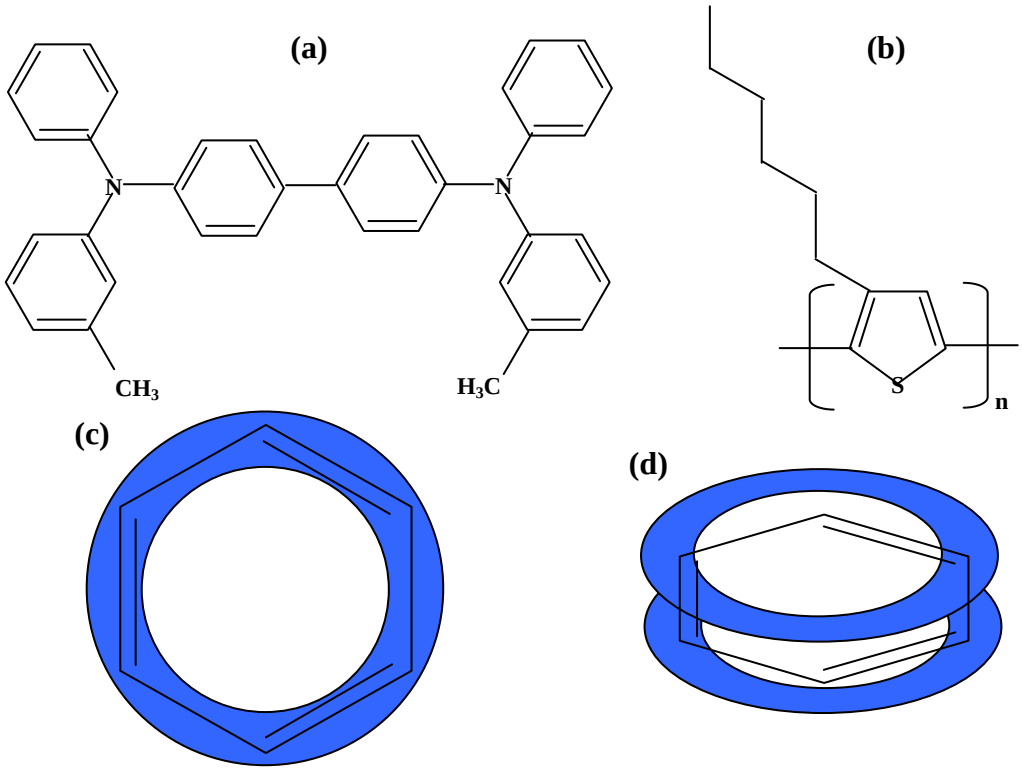

Figure 1.2.1 a) Molecular diagrams of TPD and b) P3HT and c) d) schematic of π-bonds orbitals in benzene

There are some similarities in charge transport between organic and inorganic semiconductors, though ordinarily charge transport in organic materials is different from that in inorganic crystalline semiconductors. This is mainly because, within the organics, the charge carrier is strongly localised to an individual site e.g. TPD molecule or P3HT polymer segment. The sites themselves are highly disordered. Doping them may radically change their charge transport characteristics, for example modifying the structure of the materials or serving as traps for carriers.

Figure 1.2.2, shows a typical model to explain charge hopping inside the organic diode structure, since the charge carriers are believed to be strongly localised (the localisation centres are called sites), and move by hopping across the material via these localised states under the electric bias. Depending on the relative energy distribution, a carrier can hop to the nearest neighbour, be trapped in lower energy sites or de-trap if the carriers have enough energy. In figure 1.2.2 (b), the HOMO and LUMO site energies are shifted under the electric field. If the electrodes are Ohmic contacts and charge injection is sufficient (quite a small energy barrier for charge injection), then the electrons are injected from the cathode, and hop via the LUMO sites from negative to positive (which can be understood as hopping from the high energy sites to the low energy sites). Conversely, the hole carriers can be injected from the anode and hop via the HOMO sites in the direction of the electric field. In figure 1.2.2 (c) (d), there is a large energy difference between the anode electrode (work function) and the HOMO level, and also a large barrier between cathode and the LUMO level, which makes the charge injection almost impossible under this reverse bias. Even though this model has been generally accepted and is broadly cited to explain many phenomena[17], it is still extremely challenging to develop a consistent theory for charge transport in organic devices.

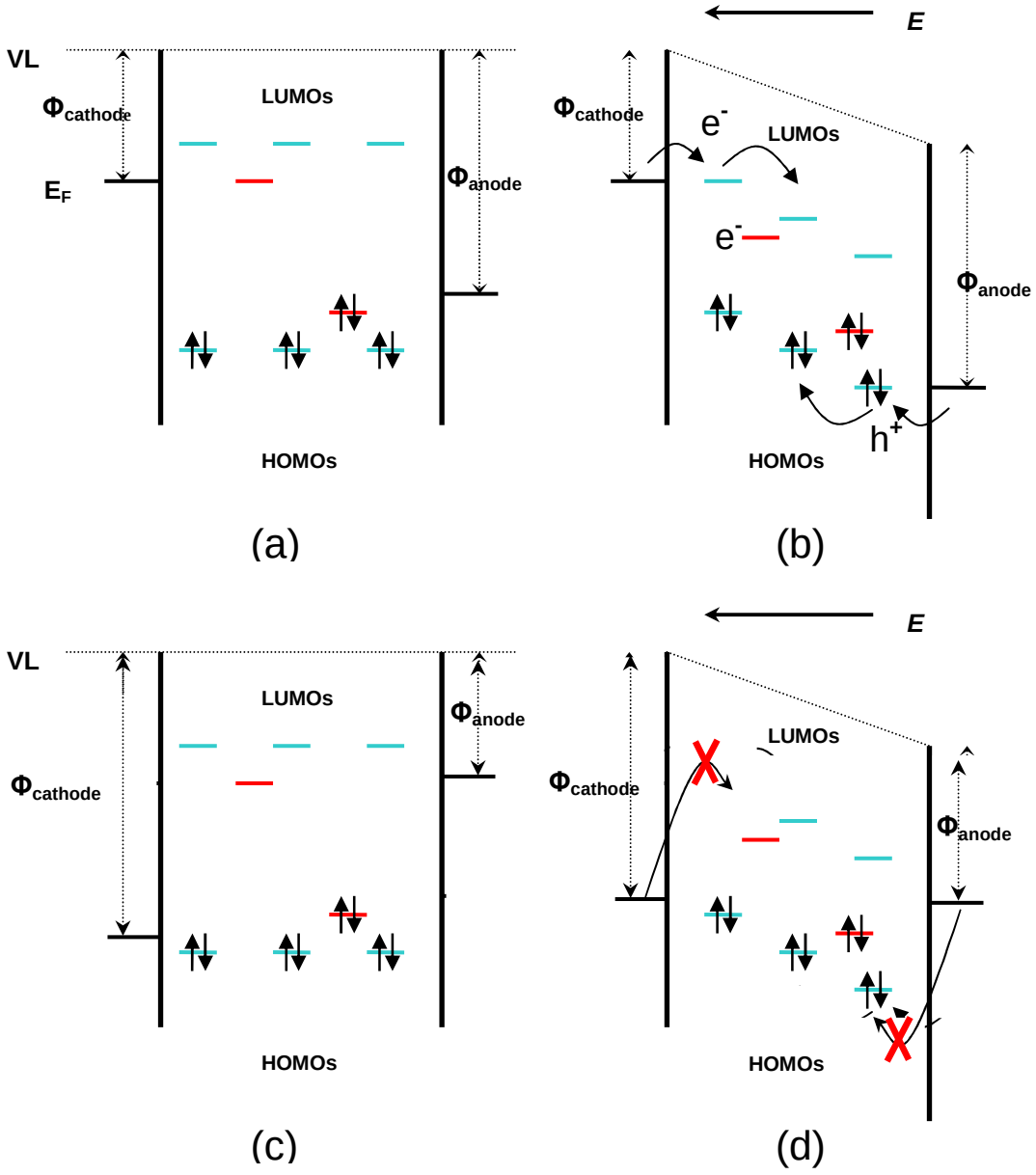

Figure 1.2.2 General case of hopping motion within a diode

The blue lines represent each molecule or "site" and the red lines represent the presence of a trap: (a) the hopping sites in organic materials with no applied bias applied, (b) with in forward bias applied[15]. (c) and (d) shows that the charge injection is prohibited under the reverse bias.

In order to define the charge transporting ability, a basic parameter is introduced, which is called free carrier mobility (see Equation 1.2.1). By definition, it is the drift velocity of free charge carriers normalised to the electric field.

$$v_d = \mu E \qquad \text{Equation 1.2.1}$$

where v_d, is drift velocity of the free charge carriers, μ means the carrier's mobility, and E is the electric field strength.

Since charge transport in amorphous organic materials occurs mainly by thermally activated hopping between localised states, the mobility usually increases strongly with electric field and charge concentration, and decreases with decreasing temperature. For instance, the relationship between charge mobility and electric field in highly field-dependent semiconductors is presented in equation 1.2.2, which is called Poole-Frenkel (PF) behaviour[18], and the Poole-Frenkel behavior can also be observed at a low electric field due to the trap filling mechanism in semi-conducting materials.

$$\mu = \mu_0 \exp(\beta\sqrt{E}) \qquad \text{Equation 1.2.2}$$

Where μ is the mobility of the sample, $\mu_0 = \mu\ (E=0,\ T)$ is the mobility under zero electric field, both $\mu_0 = \mu\ (E=0,\ T)$ and $\beta(T)$ are material-dependent parameters, which are also related to the temperature.

Due to the hopping conductivity mechanism and disordered nature of organic semiconductors, the mobility is not only field-dependent, but also strongly temperature-dependent. By using the Monte-Carlo simulations, Bässler and his co-workers[17] accomplished the temperature and electric field dependencies of the hopping mobility in the limit of high electric fields, which can be given by equation 1.2.3

$$\mu(\hat{\sigma},\sum,E)= \mu_0 \exp(-\frac{3}{2}\hat{\sigma}) \begin{cases} C\exp(\hat{\sigma}^2-\sum^2)E^{1/2}, & \sum \geqslant 1.5 \\ & \text{Equation 1.2.3} \\ C\exp(\hat{\sigma}^2-2.25^2)E^{1/2}, & \sum < 1.5 \end{cases}$$

Where μ_0 is a temperature dependent parameter, $\hat{\sigma}$ is disordered parameter, $\sum$ is the degree of positional disorder, E is electric field.

Dunlap and co-workers[19-21] studied the hopping mobility in random disorder systems and achieved an empirical equation (e.g. 1.2.4) for the mobility in amorphous semiconductor.

$$\mu = \mu_0 \exp\left\{-\left(\frac{3\sigma}{5k_BT}\right)^2 + C_0\left[\left(\frac{\sigma}{k_BT}\right)^{3/2} - \Gamma\right]\sqrt{\frac{eaE}{\sigma}}\right\} \qquad \text{Equation 1.2.4}$$

Where σ is a standard deviation of the energetic distribution of the density of states, T is the temperature and E is the electric field, while C_0=0.78 is empirical/fitting parameter, α is the minimal charge-dipole separation. Experience with the Gaussian Disordered Model (GDM) suggests that Γ characterises geometrical disorder and thus should depend upon transport site concentration.

The current density and voltage behaviour of organic semiconductors normally follow Mott-Gurney's law[22], which has been illustrated in figure 1.2.3.

In reality, there is a background concentration of charges n_0 (intrinsic charge concentration) in the semiconductor (due to thermal excitation or due to impurities/defects). As a result, when the injected carrier density n_i is much lower than n_0 at very low voltages, Ohm's law will be obeyed (in equation 1.2.5).

$$J = en_0\mu\frac{V}{d} \qquad \text{Equation 1.2.5}$$

Where e is the electronic charge, V is the voltage drop across the sample, and d is the

sample thickness (e = 1.6·10-19 C), where J is current density.

When the injected carrier density almost reaches the intrinsic charge density n_0 at the transition voltage V_{tr}, the I-V dependence will change as well: the injected charge carrier concentration becomes dominant, since the materials may contain low lying energy sites, and the charges will be captured by these empty traps. This can immobilise most of the injected carriers, leading to a greatly reduced current at lower injection levels. Since there is a finite number of shallow traps in the material, as the voltage finally reaches some critical voltage V_{TFL} all traps will be filled and the value of the current will increase to the space charge limited (SCL) trap-free value. This maximum current (SCL) is limited by the maximum amount of charge that can be injected into an semiconductor, due to Coulombic repulsion from charges already injected in the sample.

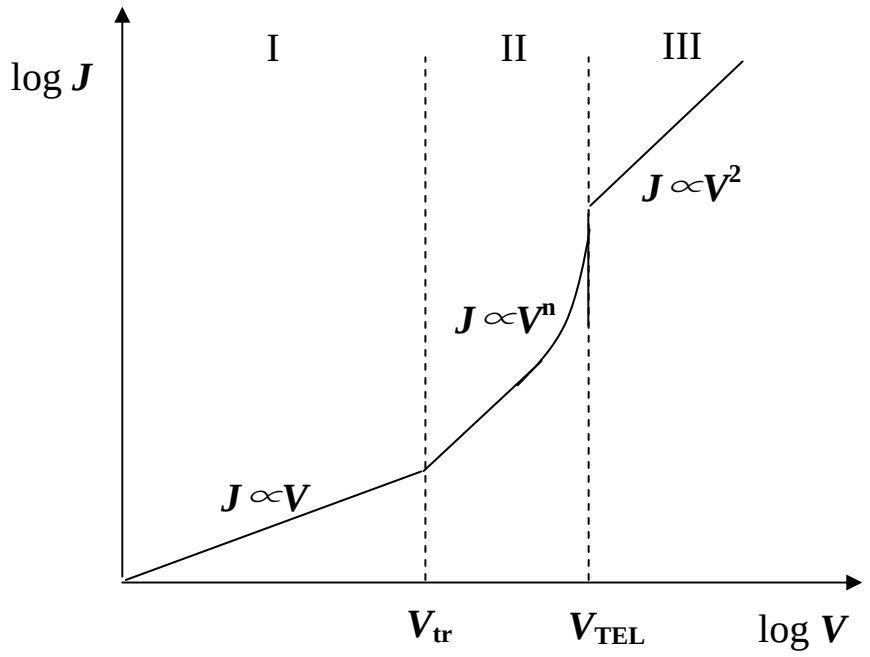

Figure 1.2.3 Schematic graph showing J vs V for an semiconductor with energy traps

(I) – ohmic region, (II) – trap-limited Space Charge Limited Current (SCLC), (III) – trap-free SCLC

1.3. Excited states in organic devices

1.3.1. Categories of excited states

Light emission from organic devices requires the formation of excited states. These are called excitons. Generally speaking, the exciton is an electron and hole pair. They attractively interact with each other via coulomb attraction. There are two different ways to classify the exciton.

An exciton can be categorised as Frenkel exciton if the electron-hole pair is located on the same molecular unit, or a Wannier-Mott exciton if the pair spans over a few adjacent molecular units, also known as transfer exciton[23]. Unlike inorganic semiconductors, the excitons in organic materials are mostly Frenkel excitons, which means that the exciton is localised on a single polymer unit or a small molecule.

The exciton can be classified by the different spin orientations of the electron-hole pair. The first group is called singlet states (indicated by figure 1.3.1 (b)[14]), whereby the electron and hole are orientated with spin anti-parallel and opposite (spin momentum m_s=0), and the total angular momentum equals to zero (S_{total}=0, with combination $\frac{1}{\sqrt{2}}(\downarrow\uparrow - \uparrow\downarrow)$). The second group is call triplet states (shown in figure 1.3.1 (c)), and contains three possible spin orientations. First, both electron and hole are spin up (with spin momentum m_s=1 and total angular momentum S_{total}=1). Secondly, both the electron and hole are spin down (m_s=-1, S_{total}=1). Thirdly, both of them are spin opposite but with a non-zero resultant spin component (m_s=0, S_{total}=1, with combination $\frac{1}{\sqrt{2}}(\uparrow\downarrow + \downarrow\uparrow)$)[24]

One can represent the different excitons by considering the precessing of the individual electron spins as in figure 1.3.1 (b) (c)

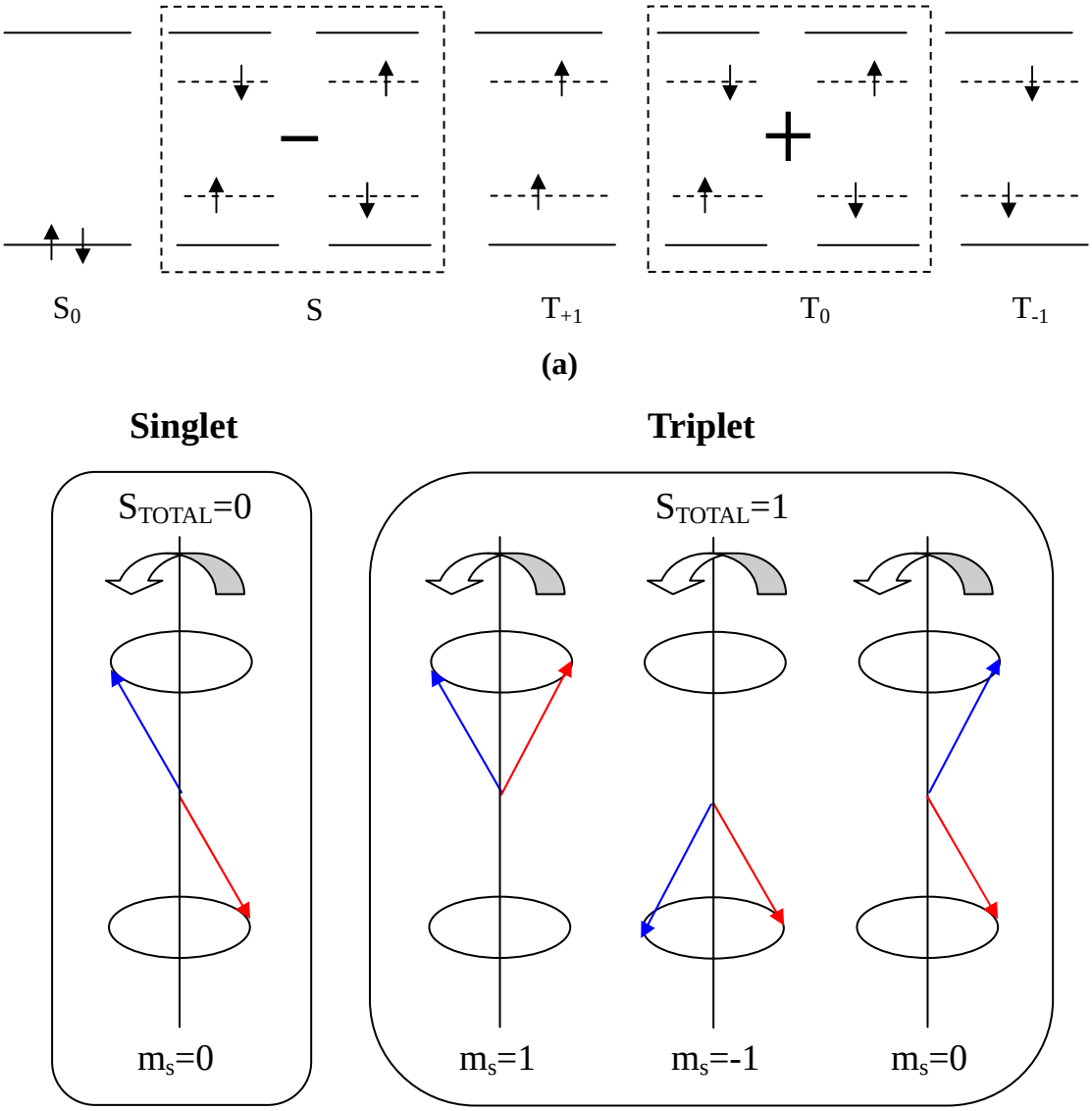

Figure 1.3.1 Exciton spin arrangements

Figure 1.3.1(a) represents the ground states, singlet and triplet, (b) and (c) indicate the spin momentum and angular momentum of singlet and triplet states.

Last but not least, because of the spin-allowed radiative decay, the singlet states have a much shorter lifetime, compared to the decay of triplet states, which is generally forbidden by the conservation of spin symmetry. Ordinarily, it is at least a factor of

one thousand shorter than triplets, for example the radiative recombination time for singlets in Alq_3 is of the order of 10- 20 ns whilst that for triplets is of the order of 25 μs^{-1} ms[25].

1.3.2. Generation of excited states

Excitons can be generated in two different ways: photo excitation (or photoluminescence) and electrical excitation (or electroluminescence). Both ways can achieve light emission in an OLED device.

Photo excitation is usually achieved using a laser. Light is incident on the diode and is absorbed by molecules in the organic semiconductor, the energy of the incident light lifts an electron into a higher energy state, leaving a hole behind it (see figure 1.3.2). However this excited state is very unstable, and it can easily lose energy. Both electron and hole recombine, emitting a photon. This is called photoluminescence. The exciton can also dissociate to a free electron and hole at the hetero-interface or at defects.

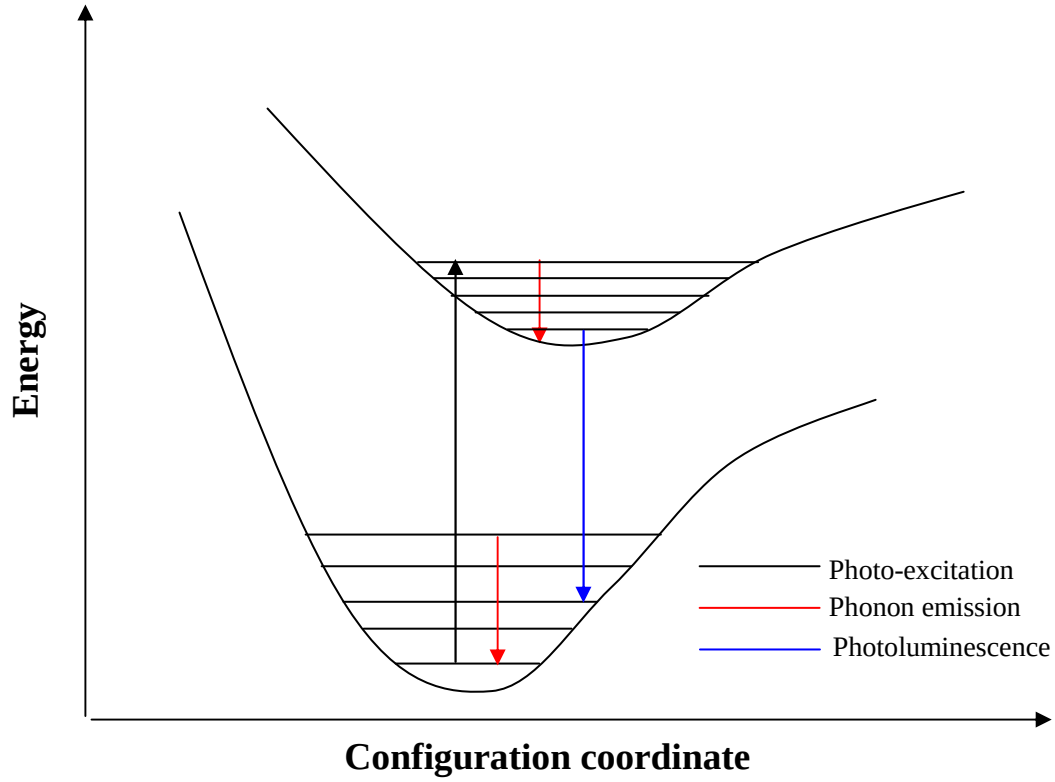

Figure 1.3.2 Schematic of photoluminescence process[14]

This figure represents (1) the photo-excitation from a ground state molecule to an excited state, (2+4) Phonon emission between vibrational levels, (3) Photoluminescence. The change in molecular potentials caused by the photo-excitation is indicated by the change in shape of the excited state potential and the shift along the configuration coordinate.

Electrical excitation can be observed by applying a voltage to an OLED device. Holes are injected from the anode into the HOMO level of the hole transport layer and meet with the electrons that have been injected from the cathode into the LUMO of the electron transport/emission layer. Once both types of charge are present in the emission layer[14] (or interface), excitons are generated by those electron hole pairs with required spin orientation. In this case, both singlets and triplets are formed. With singlet recombination, luminescence can be observed in the system, so it is called electroluminescence.

According to figure 1.3.1, given the random spin of electron and hole, the triplet/singlet generation ratio is 3:1. The spins of injected charge carriers from anode and cathode are random, without any external influences exciton formation is solely governed by spin statistics, so the electrical excitation causes 25% of excitons to form singlets, and 75% of excitons to form triplets.

1.4. Magnetic field effect on excited states

A small magnetic field can affect the spin-dynamics of electron-hole pairs, which lead to an inter-conversion between singlet and triplet. Since triplet excitons possess a magnetic moment, it is perhaps not surprising that they can be influenced by a magnetic field[26].

Organic magneto-resistance (OMR) was first observed in organic light emitting diode (OLED) structure by Kalinowski et al. in 2003[27]. They found that in an Alq_3 based OLED, both the light output and the current through the device were modulated by the presence of an applied magnetic field. The effect of the applied field on the light output was attributed to the hyperfine scale mixing of the singlet and triplet states [28, 29] resulting in an increased singlet concentration and hence greater efficiency, as well as a reduction in the triplet concentration. The effect of the field on the current through the device was attributed to this increase in singlet exciton concentration affecting the dissociation current in the device and reducing the role of free carrier trapping at triplet states[30].

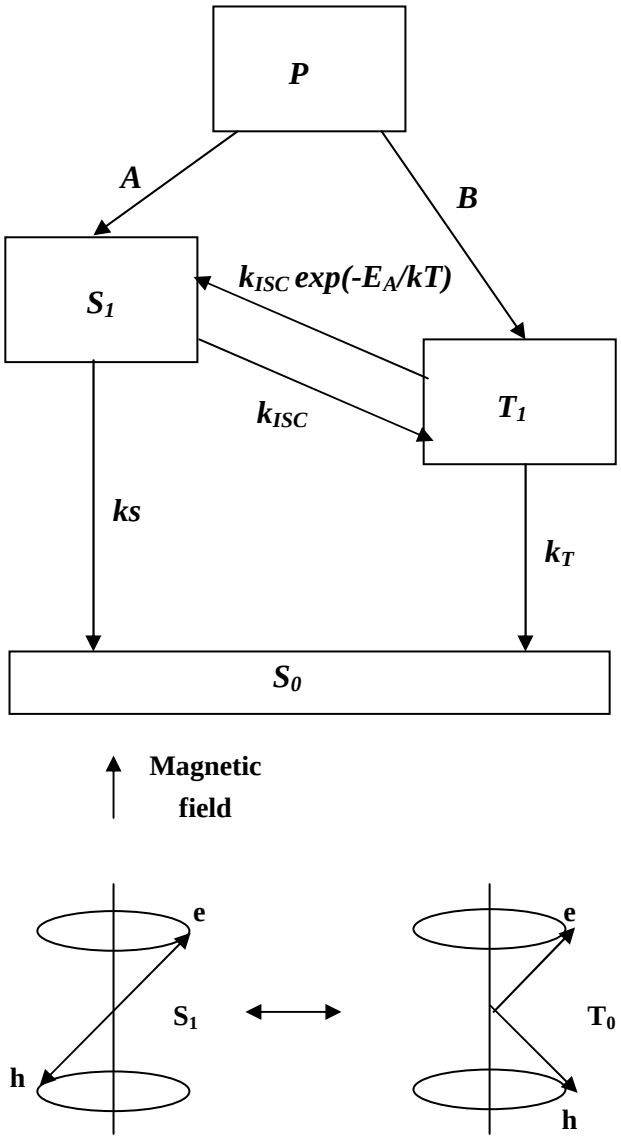

Figure 1.4.1 Relationship between different exited states

(a) A schematic diagram of the excitation and recombination pathways in an organic molecule. The excitation pump *P* produces no triplets under illumination (i.e., *B*=0), but in electrical pumping produces *A*=0.25 and *B*=0.75. (b) A vector diagram illustrating the increased singlet *m*=0 triplet intersystem crossing due to a magnetic field[31].

In figure 1.4.1 (a), we show a simple schematic diagram of the processes controlling the population of singlets and triplets within an organic molecule. There is an

excitation pump that can generate singlets or triplets, a recombination of either of these states, and an inter-system crossing between the two states. Also figure 1.4.1 (b) is a simple vector diagram showing how the presence of a magnetic field can act to alter the intersystem crossing between the two states. The effect of this magnetic field induced mixing would be able to increase in k_{ISC} (inter-system crossing rate) and would depend on the relative concentration of singlets and triplets as well as the temperature of the system. If the temperature was sufficiently high to overcome the potential barrier and if there were an excess of triplets in the system, increasing k_{ISC} would lead to a reduction in the triplet concentration. However, if there were an excess of singlets, then increasing k_{ISC} would lead to an increase in the triplet concentration[31].

For photo excitation most of the excited states are singlets therefore, due to the application of a magnetic field, the inter-system crossing rate k_{ISC} would increase, with the excess of singlet states caused by light absorption, increasing k_{ISC} could lead to an increase in the triplet concentration.

However, theoretically for electrical excitation, the triplets to singlets ratio is 3:1 if there is no external influence, so with this excess of triplet states in the system, increasing k_{ISC} would lead to a reduction in the triplet concentration.

Chapter two: Theory

2. Theory

2.1. Site blocking

Several microscopic mechanisms for the interaction between transiting holes and excited states may be considered (primarily long lived triplet states, for short lived singlets this effect is ignored). If the transiting hole has the same spin state as the hole on the triplet, the exciton acts as a blocked site for the transiting hole and will reduce the mobility. We note that the electron in the exciton cannot easily bind with the transiting hole (releasing its own hole for transport), as the triplet binding energy prevents this. It is possible that this interaction could occur but there would be some energetic barrier to overcome and hence, at the very least, there would be some degree of site blocking or transport delay. If the transiting hole has a different spin state to that on the exciton, then there are two possibilities. The triplet can be quenched (leaving a ground state) by the free carrier or can interact with it, but leaving a hole and triplet, resulting in an effective scattering interaction. These two processes are summarised in Equation 2.1.1[32].

$$T_1 + D_{\pm 1/2} \underset{k_{-1}}{\overset{k_1}{\Leftrightarrow}} (T_1 ... D_{\pm 1/2}) \overset{k_2}{\rightarrow} D_{\pm 1/2} + S_0^* \qquad \text{Equation 2.1.1}$$

Where T_1 means triplets state, $D_{\pm 1/2}$ represents the free charge carriers, and S_0^* is the ground singlets, and k_1 and k_{-1} denote the rate constants of formation and backscattering from a pair state ($T_1 \ldots D_{\pm 1/2}$), k_2 is the rate constant for triplet quenching.

Both of these processes will take some time and reduce the hole mobility. The net effect is that, on average, half of the triplet exciton sites are disallowed as transport sites, as far as the transiting holes are concerned, and the others would still cause interactions with the hole, which would be expected to reduce the mobility. All of these processes have been presented in Figure 2.1.1.

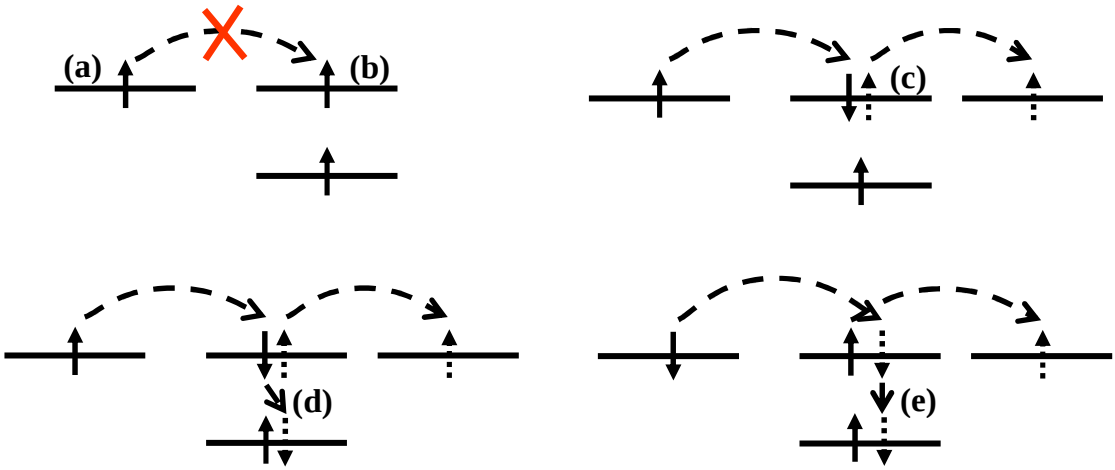

`

Figure 2.1.1 Schematic of possible reactions between exciton & charge carriers Fig (a) shows the free carrier, fig (b) represents the triplet state, fig (c) indicates the pair state ($T_1 \ldots D_{\pm 1/2}$). Fig (d) and fig (e) show the process of quenching, dashed line presents the hopping path of free charge carriers.

2.2. Magneto-resistance

A change in current due to a magnetic field through an organic device is known as organic-magneto-resistance (OMR).

There are two contrasting approaches to explaining OMR. One group of theories focuses on the role of excited states such as excitons, and several models have been established from this aspect, which will be introduced in the following paragraph (Frankevich model, Kalinowski model, and our QM model). Another approach is though the bipolaron model, which is thoroughly different from the excitation model

and will be introduced in section 2.3.

Frankevich[33] observed magnetic field effects in PPV derivatives in 1992. His research showed a sharp rise in a photo current of 3% under the magnetic field about 4 mT. When the magnetic field was greater than 4 mT the change in photocurrent was saturated.

The Frankevich explanation for this phenomenon is presented in figure 2.2.1. In this graph, $^{1}M_0$ is the ground state, and the excited states $^{1}M_1$ and $^{3}M_3$ are equivalent to singlet and triplet states. Above the excited states there are short range charge pair states $^{1}(P^{+}.P^{-})$ and $^{3}(P^{+}.P^{-})$, while on top of these there are long range charge pair states $^{1}(P^{+}\ldots P^{-})$ and $^{3}(P^{+}\ldots P^{-})$. Above all there are well-separated charge pairs P^{+}, P^{-}, which are respectively dissociated polarons. Each of these states has an equivalent behaviour to singlet and triplet states. Frankevich assumed the mixing between singlet states and triplet states can only occur in the long-range pairs. By applying an external field, the long range pairs are converted to singlet and triplet states with zero T_0 spin momentum, which reduced the population in T_{-1} and T_{+1}. This may help the long-range pair states' dissociation, hence increasing the photocurrent.

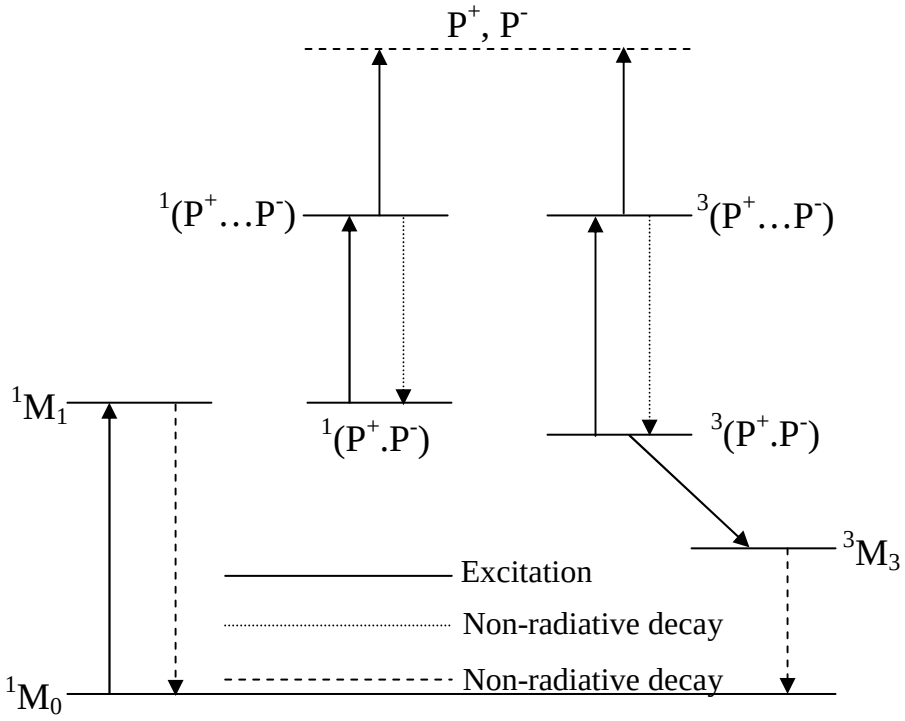

Figure 2.2.1 Frankevich model

Kalinowski et al.[34] found a sharp increase of photocurrent in the Alq_3 device under the magnetic field up to 65 mT and followed by a plateau or decrease for high field, and through this work they established a model which is shown in figure 2.2.2. The excited Alq_3 molecules can either radiatively decay or non-radiatively decay, with the decay rate k_r and k_{nr} respectively, and can also form a pair state 1(e…h), which is equivalent to the singlet characteristic. These pair states can revert to excited Alq_3 states (with rate k_{-1}) or possibly just dissociate to free electrons and holes (with rate k_1). Another possible pathway for this pair state is to transfer to a triplet-like pair state (with rate k_{tr}), which can also dissociate to free electrons and holes (with the rate k_3). Kalinowski assumed that the singlet pairs are more likely to dissociate to free charge carriers, so applying a magnetic field could increase the singlet population and lead to an increase in dissociated photo current.

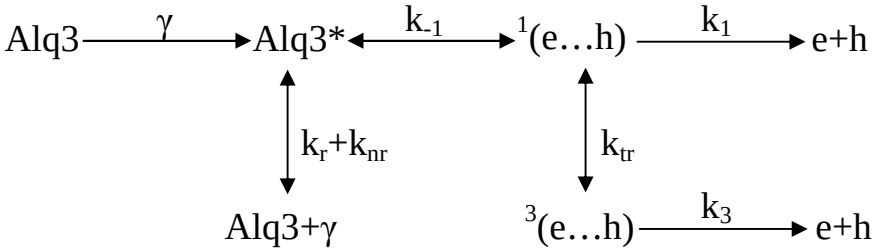

Figure 2.2.2 Kalinowski model

Although excitons are known to interact with free charges, the effect that excited states may have on the charge transport is not generally considered in these two models (even though these light emitting devices are known to contain large number of excited states). Neither of these approaches would predict a change in mobility with magnetic field. But, according to the site blocking theory in section 2.1, it is quite possible that the mobility in working devices may well be a function of drive current and magnetic field, as the excited state population will change with operating conditions.

Therefore, I believe that the inter-system crossing model provides a more detailed explanation, as shown in section 1.4, figure 1.4.1. A magnetic field can change the population ratio between triplet states and singlet states and thus enhance the working current and photo-luminescence in an organic diode. The mobility of charge carriers in an organic semi-conducting device could be correlated to the triplet concentration, as shown in section 2.1, since a magnetic field can affect the triplet concentration, it could also affect the mobility of carriers in these devices.

For example, electric-excitation mainly generates triplet states (triplet to singlet ratio 3:1, under no external influence), therefore with excess triplets inside the system, applying a magnetic field could increase the intersystem-cross rate $k_{ISC,}$ and lead to a decrease of triplet states. With fewer triplet states blocking/interacting with the free charge carriers (see section 2.1), the carrier mobility of this device should increase,

then enhance the current density of this device, as well as the luminescence intensity. This phenomenon might be a valid approach to explaining magneto-resistance in organic semiconductor systems. This thesis is motivated by this approach.

2.3. Bipolaron theory for MR

Another explanation of OMR is the bipolaron theory, which was established by groups at the University of Iowa and Eindhoven [35, 36]. If two electrons have different spin states, a bipolaron intermediate state can be formed (see figure 2.3.1 (a)). If they have the same spin, a bipolaron state cannot be formed. These bipolarons can be considered as electron trapping sites.

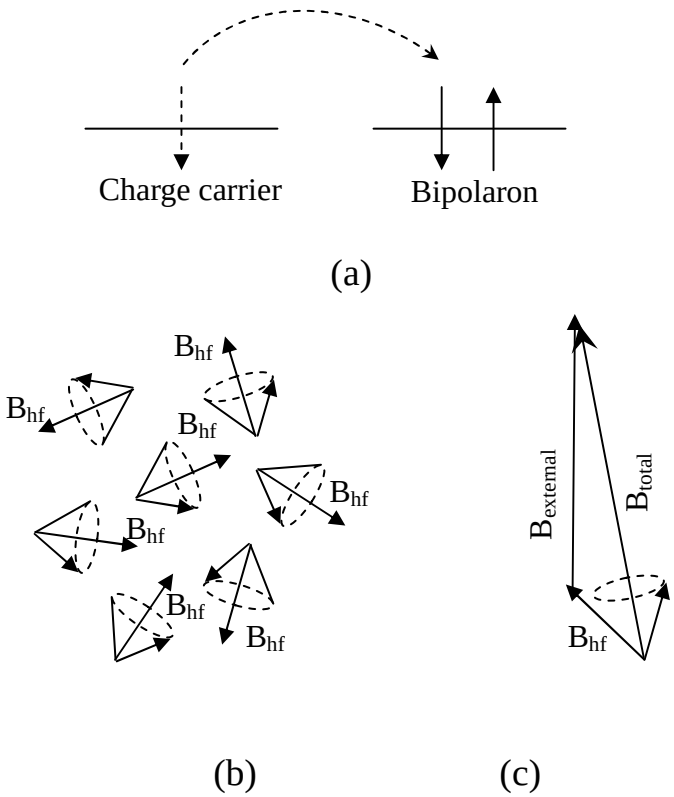

Figure 2.3.1 Schematic of bipolaron, hyperfine precession and total magnetic field precession of injected charge carriers, (a) bipolaron formation, (b) hyperfine precession, and (c) injected charge precess under total magnetic field

In the bipolaron model, it is suggested that conduction in disordered organic materials takes place by hopping of charge carriers between localized sites having a density of states (DOS) that is often assumed to be Gaussian, with a width δ~0.1–0.2 eV. Because of strong electron-phonon coupling, charges form polarons and the energy penalty U for having a doubly occupied site, i.e., a bipolaron, is modest. Experimental indications are that $U \sim \delta$. Because of strong on-site exchange effects, they assume that bipolarons occur only as spin singlets. Two polarons having the same spin component along a common quantization axis have zero singlet probability and cannot form a bipolaron. This ‘‘spin blocking’’ is the basic notion of their mechanism[35].

The hydrogen atoms generate a very small hyperfine field inside the organic semiconductors, and this is totally random due to spin statistics. Injected charge carriers will precess under this small hyperfine field (see figure 2.3.1 (b)), as charges hop across the bulk of the material, the spin state of these injected charges would flip with the random hyperfine field. Hence the spin of injected charges can flip to any possible direction due to the random hyperfine field, which could maximise the possibility of bipolaron formation. When an external magnetic field (much greater than the hyperfine field) is applied it dominates the total magnetic field in the organic material, therefore all the injected charges should precess with the overall magnetic field (see figure 2.3.1 (c)), causing a fixed possibility of bipolaron formation.

With less bipolaron formation under the external field compared to null magnetic field (random hyperfine precession), the device current, as well as the luminescence, should increase. This is the basic idea of bipolaron theory.

Chapter three: Experiment

3. Experiment

3.1. Materials

The materials used in our experiments are mainly P3HT and TPD. P3HT is provided by Merck Chemicals (molecular weight 44000 and 96% regioregularity) and used straight away. TPD is purchased from Sigma Aldrich with the purity > 99.9%, and then further purified via evaporation and deposition method to ensure the good performance. ITO is purchased from Sigma Aldrich as well, with the thickness of 125 nm and resistance about 50 Ω/sq. Gold is also purchased from Sigma Aldrich with the purity of 99.99%.

3.2. Sample

3.2.1. Unipolar and ambipolar P3HT devices

The typical device structure used in this chapter is presented in figure 3.2.1. It is a thin layer of P3HT film（≈1.5 μm), which is drop-cast from a chloroform-based solution on top of the etched ITO coated glass substrate (20 ×20 mm^2) with four gold contacts as bottom electrodes. On top of the thin organic film there is a strip of gold top contact for the unipolar device and aluminum electrode for the ambipolar device. All contacts are made through thermal evaporation. The overlap area of cathode electrode and anode electrode is the device region with a working area of

around 3mm^2.

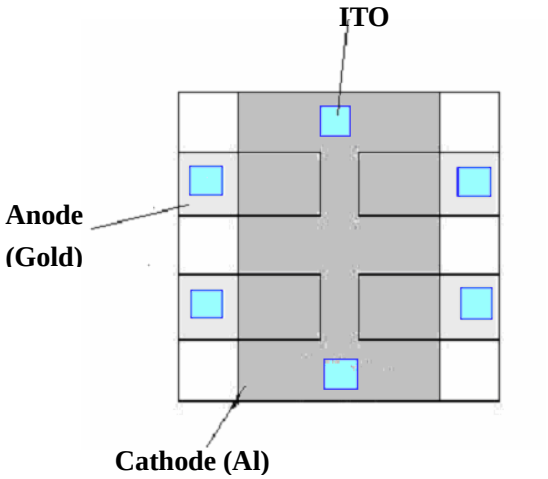

Figure 3.2.1 Geometrical configuration of the sample device, which is viewed from above

At the very bottom there are 6 ITO squares, which are etched from standard ITO substrates. Afterwards four gold electrodes are thermally evaporated on top of the etched substrates, and then a thin layer of P3HT film is drop cast from the chloroform solution. Finally, for the unipolar device a strip of gold is evaporated on top of the P3HT film, and for the ambipolar device, the top contacts are made by aluminum via thermal evaporation.

As gold is a very soft material, to prevent it being scratched by the contacting pin in the sample holder and hence lose contact, some small ITO squares are etched from the glass based ITO substrate, so even if the contacting pins penetrate the soft gold electrodes, the ITO squares can still provide a good electrical contact.

3.2.2. Unipolar and ambipolar TPD devices

The device structure (fig 3.1.2) is similar to the P3HT sample, which was introduced in section 3.1.1. A thin layer of TPD（≈610 nm) was thermally evaporated and deposited on top of the etched ITO substrate (20×20 mm^2), then a strip of aluminum was deposited on top of the organic semiconductor for the ambipolar, but for the

unipolar device, ITO and gold were designed to work as anode and cathode, as both of them had the TPD material sandwiched in between. The structure of this sample was shown in figure 3.2.2. Obviously a new mask was required to etch the ITO substrates to this new pattern with four bottom anode electrodes, and the shape was presented in figure 3.2.2. The overlap area of cathode and anode was the device region with the working area of around $3mm^2$.

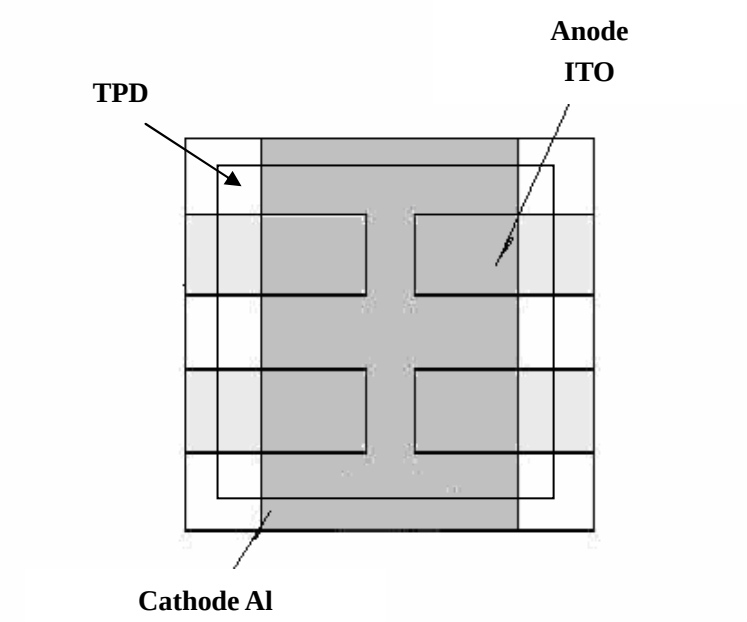

Figure 3.2.2 Schematic of the TPD device, top view

On the bottom of the substrate there are four strips of etched ITO contacts that work as cathode electrodes, and then a thin layer (normally around 616 nm) of TPD is thermally evaporated on top, finally, a thin layer of anode material (Al around 1000 Å in these experiments) is deposited above the TPD semi-conducting layer.

3.3. Sample preparation

3.3.1. Cleaning, etching and plasma-treatment

It must be emphasised that the sample preparation step is a key issue in this

experiment, and as such is explained by the following paragraph.

1. Cleaning ITO substrates

- Thoroughly clean the ITO substrates with detergent (put the wash powder on top of the glass, rinse it with water and hand cleaning).
- Ultrasonic bath in a water solution of detergent for 15 min
- Change the detergent water, ultrasonic bath in distilled water for 15 min and repeat this process once more.
- Ultrasonic bath in acetone for 10 min and repeat this process one more time.
- Ultrasonic bath in chloroform for five minutes, and repeat this process once more, then dry the sample via nitrogen gun.

2. Etching ITO substrates

- Spin-casting photoresist (S1818G2) on top of ITO substrates (spin speed 2000 rpm for 20 s, followed by 40000 rpm for 1 min).
- Thermally cure the sample in an oven at 100°C for 15 min.
- Wait for five minutes, let the sample cool down, and then cover it with the mask, exposing it to UV light (350 nm) for 1 min.
- Wash the uncovered photoresist by $Na(OH)_2$ (25%) with distilled water (75%) solution for two minutes, and then rinse it in the distilled water.
- Soak the substrates in HCl (48% volume percentage), distilled water (50% volume percentage) and H_2NO_3 (2% volume percentage) solution at 48-50℃ for 1.5 min, then rapidly transfer to distilled water to wash away the acids.
- Quick ultrasonic clean of the substrates in acetone and chloroform twice, the sample must be dried between each ultrasonic treatment.

Then a plasma treatment is used to modify the substrates surface condition using a Diner Electronic femto Plasma system. The purpose of this modification is to remove any remaining organic residuals from the patterned ITO and also increase the work

function of the ITO electrodes[37]. During the treatment, this system is evacuated by a rotary pump using pressure around ~0.3 mbar, and then oxygen gas is introduced into the chamber via a needle valve. In order to make sure that there is enough oxygen in the chamber, the gas flow rate was set to keep the chamber pressure around ~1.5 mbar for at least five minutes. Eventually, the pressure is adjusted to 0.2 ~0.3 mbar by the oxygen needle valve, and the generator power is set to 30 W for five minutes.

3.3.2. Deposition

For P3HT device, the electrodes are thermally evaporated and deposited, and the organic layer is processed using drop-casting.

1. Deposition of bottom contact

- Ultrasonic bath separately in acetone and chloroform solution twice, and dry the sample via nitrogen gun.
- Move the sample to evaporation chamber (home built) pump the pressure to 1.5×10^{-5} mbar, choose the right mask and power, thermally evaporate (Au or Al) under 1 Å/s for the first 10 nm, and 2Å/s till the thickness reaches 50 nm.
- Wait for the sample to cool down before moving it out of the chamber.

2. Drop-casting

- Carefully weigh 7 mg of P3HT, dissolve it into 1 ml chloroform solvent.
- Gently heat the solution up to 35℃ if it has not dissolved properly.
- Drop four drops (each drop approx. 0.15 ml) of P3HT-chloroform solution on top of the substrate. Cover it with a funnel to slow down the chloroform evaporation and prevent the air-flow. This will ensure a good quality organic film, with a very smooth surface.

For the TPD device, the whole sublimation process is completed under thermal

evaporation and deposition using a Kurt J. Lesker spectros evaporation system.

Once the cleanly preparations are complete, the substrate was sent into the evaporation system for TPD layer fabrication. This transfer time must be kept to a minimum in order to prevent the oxygen trapping on top of the substrates. Since TPD is a small molecule organic semiconductor, thermal evaporation-deposition is chosen to build this device rather than the lesser quality drop-casting method, which gives a rough film. A Kurt J. Lesker SPECTROS evaporation system is deployed for TPD growth, and the schematic of this system is presented in figure 3.3.1. It consists of two vacuum chambers, one acting as a load lock, used for loading the substrates to the ultra high vacuum evaporation chamber, while the other contains the equipment for both organic and metallic evaporation. The substrate sample holder is loaded onto a transfer arm in the load lock, which can be evacuated using scroll and turbo-molecular pumps to produce a pressure around 10^{-7} mbar. The main chamber is evacuated using a scroll and helium cryo-pump to a pressure around 10^{-8} mbar, this may increase to ~10^{-7} mbar during evaporation. Inside the main chamber are six boron-nitride crucibles for organic sublimation and two sources for metal deposition, in this case only one of the organic crucibles has been used for TPD sublimation, one titanium-diboride crucible is designed for aluminium deposition, and another molybdenum crucible is used for gold deposition.

Above the crucibles is a cassette where the substrate holder can be supported. The cassette can be moved in height and contains the masks needed for the organic and metallic layer growth. During evaporation the cassette is rotated in order to improve the uniformity of the layers. This arrangement of crucibles and masks allows for all layers to be grown without breaking vacuum. Both metallic and organic crucibles are resistively heated. Deposition is controlled through a calibrated quartz crystal monitor. Once the TPD layer is finished, the mask can be changed to continue cathode deposition. Once the cathode layer (Au or Al) has been deposited above the

TPD molecular layer, the whole evaporation process is complete.

When the device is complete, it can be returned to the load lock for access. The required preparation method for materials will depend on the device structure. The most common device structure consists of 610 nm of TPD sublimed onto the ITO substrate, which is purchased from Aldrich. After a change of masks, the aluminum or gold cathode is ready to be evaporated, and in this experiment it is grown to approximately 1000 Å. The overlap area of ITO and cathode layers defines the shape of our device.

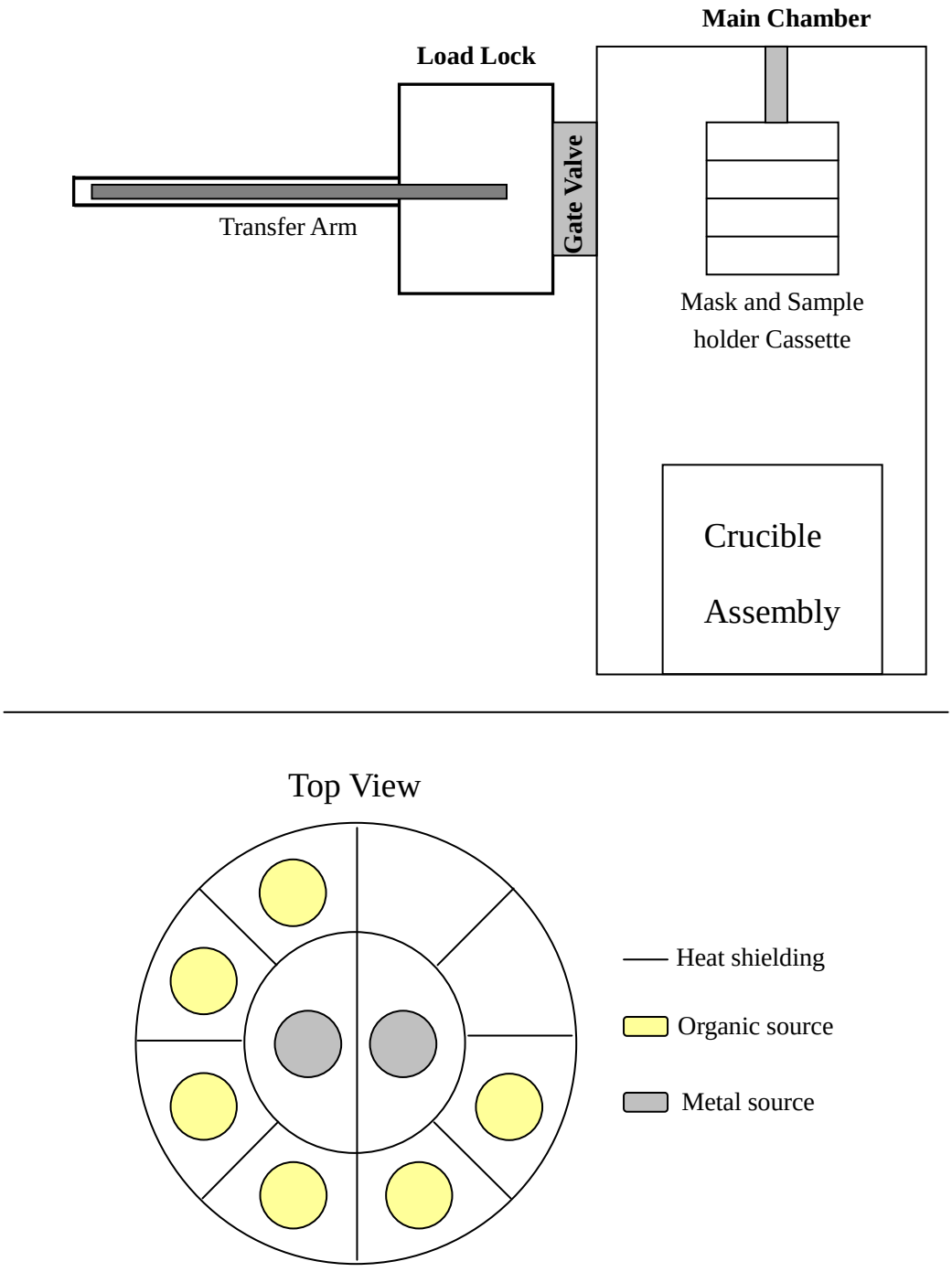

Figure 3.3.1 Kurt J. Lesker SPECTROS evaporation system[14]

The top pane shows a schematic of the whole system. The bottom pane shows a schematic of the crucible assembly.

All sample preparation steps are processed inside a clean room with a particle density

of less then 10000 p/m^3. Organic solvents are purchased from Sigma-Aldrich, and the P3HT is provided by Merck-chemical.

Once the device has been fabricated, it is immediately transferred to a sample holder and evacuated. This can prevent any unnecessary oxidization and contaminations.

All devices are placed in an electrical sample holder for testing, as shown in figure 3.3.2. The sample holder is built in a manner that allows electrical access from one side via a LEMO connector which is a 6 pin adapter[14]. Four of these pins, which correspond to the bottom anode electrodes, are connected to four BNC connectors, and marked separately, so which electrode has been used can be easily recognized during measurement. Two other pins, which are related to the top cathode electrodes, are connected together and lead to just one BNC connector. This kind of design makes the electrical circuit connection more convenient. The other side of the holder gives optical access for luminescent measurements, or for use as a laser incidence window. The sample holder can be evacuated though the vacuum port by using a Leybold PT50 pumping station giving pressure of ~10^{-5}mbar. As P3HT is not very stable in atmosphere due to the oxidization and degradation, all the experiments are kept in a high vacuum environment.

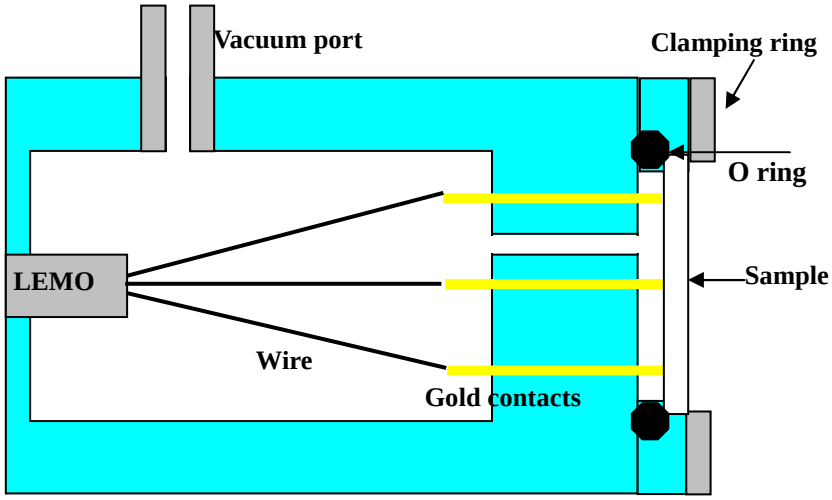

Figure 3.3.2 Schematic of the sample holder used for all electrical and luminosity measurements[14]

There is a vacuum port channel for evacuating the holder and the sample, which is located on top of this sample holder. This diagram also represents the electrical connections, including the spring-loaded gold contacts, which are used to maintain a gentle but constant contact with the electrodes of the sample. The glass substrate seals against an O ring. The clamping ring ensures that the sample is held securely and that a good vacuum seal is achieved.

3.4. IV characterisation

A Keithley 236 source-measure unit was used to take IV measurements, by providing a series of constant voltages while recording the current density through the device. From the source-measure unit, a triax cable leads to an adapter to connect to the LEMO connector on the sample holder. The adapter from the triax lead to the LEMO connector is kept as short as possible in order to minimise noise[14]. This setup allows for measurements of current from 10^{-12} to 10^{-1} Amps. Luminosity was measured using a Newport 1830C optical power meter. For measuring luminosity there is a silicon photo-diode (818-SL) and matching integrating sphere (819M). This setup comes pre-calibrated and allows for absolute measurements of luminosity at a certain wavelength. As the luminescent spectra of OLEDs are broad, the power meter is not capable of giving absolute power measurements for these devices under all luminescence wavelengths. In order to get a useful measurement, the power meter is set to the peak wavelength of the emission spectrum of the sample. As this work is mainly focused on a certain device, the problems regarding power measurements are negligible since the devices are not being compared to other devices with different emission spectra.

3.5. Dark injection (DI)

3.5.1. Standard DI

The dark injection transient current technique (DI) [38, 39] is often used to measure the mobility of the device. This method is based on applying a voltage pulse to the sample in a dark environment and recording the current flow through the device. This is displayed as a voltage across a load resistor on an oscilloscope. Mobility can be calculated from this transient time by measuring how long it takes these charge carriers to drift across the sample.

Figure 3.4.1 is the schematic of the dark injection experiment set up. The pulse generator output applied to the injective electrode, and the shape of the voltage step, is shown in fig 3.4.1 (b). As charge carriers are injected into the unipolar device, the current density increases. When the front edge of charge carriers almost reaches the counter-electrode, there is a reduction in charge injection, causing a reduction of the dark current. The dark current eventually reaches the steady state dark current I_{SCL}. As a result of this, a current density peak appears on the oscilloscope, as shown in figure 3.4.1 (c). This can be explained by the voltage drop between the frontier charge carriers and counter electrode. As the front edge keeps drifting toward the counter electrode, the gap between the frontier charges and counter electrode decreases, leading the driving electric field ($E=V/d$) to increase at the beginning of the injection. But the maximum amount of charge that can be injected into the organic semiconductor is limited by the coulombic repulsion from the charges already injected into the sample[15]. This eventually forces the dark injection current down, hence the dark current increases at the beginning then drops down until it finally reaches the steady state I_{SCL}. The time at which the turning point of the dark-current occurs, is called the dark injection transient time (or t_{DI} for short), and this relates to the time it takes for the frontier charge carriers to hop across the device. t_{DI} is a vital element for the mobility calculation.

The curve in figure 3.4.1 (c) is considered as an ideal model, which means that during the charge drift there is no presence of traps or diffusion, and an ideal Ohmic contact[40] is used. This contact can sustain the space-charge-limit current through the sample, and act like an infinite reservoir of charges. In this experiment, gold contacts are attached to the organic as electrodes, since the work function of gold is quite close to the HOMO level of P3HT, implying that only an extremely small energy barrier exists for hole injection, thereby it can be considered as an Ohmic contact.

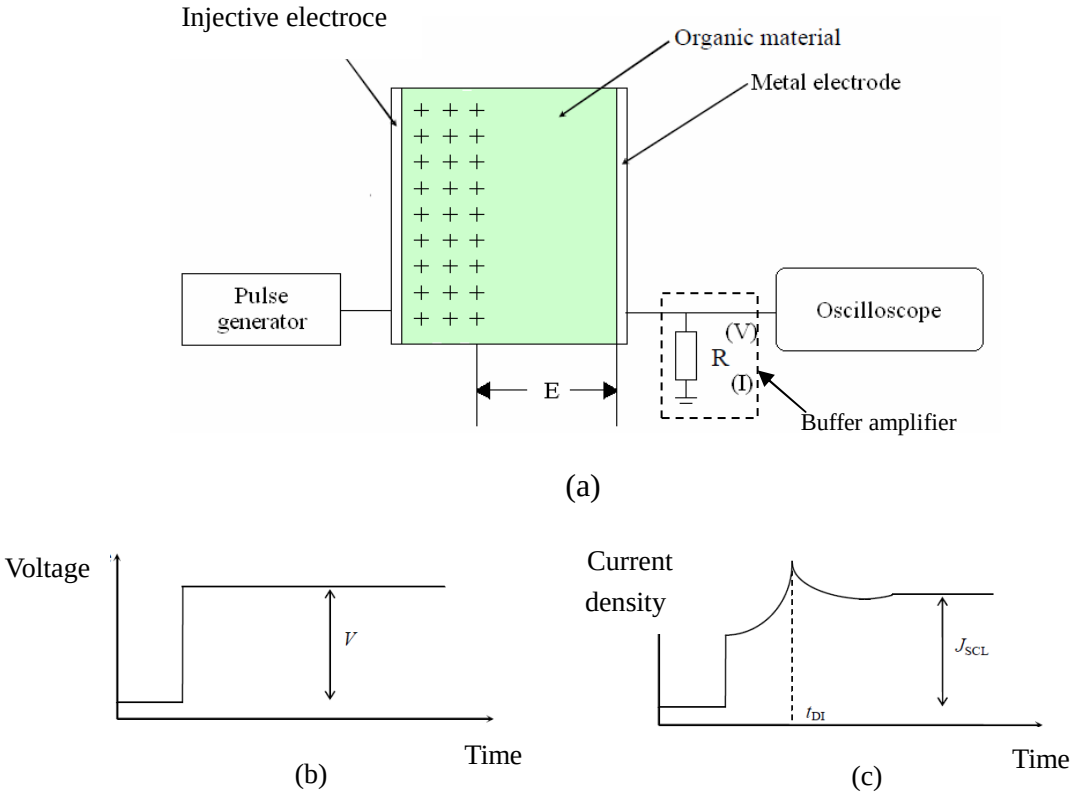

Figure 3.4.1 The schematic of the dark injection measurement

(a) The Dark-injection experiment set-up, where the oscilloscope is used to measure the voltage across the resistance R of the buffer amplifier, then the current flowing through the device can be given by V/R. (b) The applied step voltage as function of time, (c) the current density J flowing through the device as a function of time.

A buffer amplifier is used to protect the oscilloscope, in case the sample short-circuits results in a large current passing through the sample and damaging the costly oscilloscope. It also allows the load resistor, which determines the RC time constant, to be varied.

According to equation 3.4.1, in order to calculate the mobility of the charge carriers, the transit time (t_{trans}) – which is the time taken for free charge carriers to drift across the device under a space-charge-free environment – must be found. It means that all the charge carriers are driven only by the uniform electric field and not disturbed by each other's own electric field (or coulombic force).

$$\mu = \frac{d^2}{Vt_{trans}} = v_d/E \qquad \text{Equation 3.4.1}$$

μ is the charge carrier mobility, d is the distance between two electrodes, V is the voltage drop across the electrodes, and t_{trans} is the transit time.

The space-charge-free transit time t_{trans} can be obtained from the dark injection transit time (t_{DI}). The relationship between t_{DI} and t_{trans} is presented in equation 3.4.2. To meet the requirement of this equation we assume that it is a trap-free device.

$$t_{DI} = 2(1\text{-}e^{-1/2})\cdot t_{trans} \approx 0.786\cdot t_{trans} \qquad \text{Equation 3.4.2}$$

Thereby: $\mu = 0.786\, d^2/Vt_{DI}$

Where t_{DI} indicates the dark injection transit time, and the numerical factor 0.786 relates the DI time to the transit time[40].

As shown in equation 3.4.2, during dark injection measurement the carriers actually arrive at the counter-electrode much faster than in the space-charge-free case. This is because the voltage across the sample is mainly dropped across the time-dependent gap *d(t)* between the leading edge and the opposite electrode (see figure 3.4.1 (a)). So, the electric field which drives the front carriers edge toward the counter electrode

($E=V/d(t)$) is increasing and is higher than the value of the electric field in the space-charge-free environment (V/d). This results in a faster transit time across the device for the frontier carriers. The overshoot of the current density above the SCL value J_{SCL} can be easily understood in terms of the amount of injected charge before the time t_{DI}. Due to a higher average electric field at $t < t_{DI}$, the amount of injected charge is some 10% higher than that in the steady-state SCL situation, which results in a higher current density $J(t_{DI}) \gg 1.2 \times J_{SCL}$[40]. Finally, at times $t > t_{DI}$ the current density eventually relaxes towards the steady-state value J_{SCL} as in figure 3.4.1 (c)[15].

In a real dark injection system, the DI peak (shown in figure 3.4.2) is different from the ideal curve. This is due to diffusive broadening, the field-dependence of the carrier mobility, trap filling, and the presence of RC displacement current decay at short times. Charge trapping especially can have a very pronounced effect on the shape of the SCL transient, and strong trapping may even cause the DI transit peak to disappear.

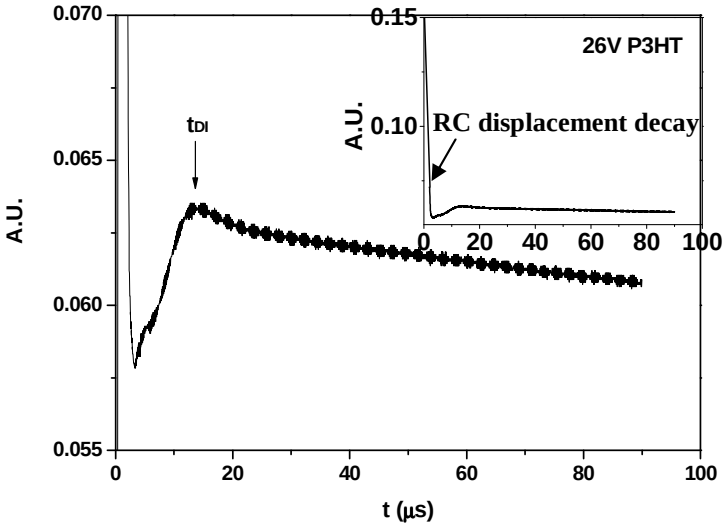

Figure 3.4.2 Typical DI space charge limited hole current transient curve

This measurement is under 26 volts for the P3HT device (both cathode and anode electrodes are gold and the thickness of P3HT between two electrodes is roughly equal to 1.5 μm).

Besides the broadening of the dark injection transit peak, the RC displacement decay is also observed at short times in a real DI curve (see figure 3.4.2). Depending on the decay time, this might shadow the DI peak, and the decay time of RC displacement is proportional to the RC, which is shown in equation 3.4.3.

$$\tau = C \sum R \qquad \text{Equation 3.4.3}$$

where τ is the RC displacement time constant, and R is the total resistance of the measuring circuit (including the cable resistance, the electrode resistance, the sample resistance and the load resistance of the amplifier, $R=R_{cable}+R_{electrode}+R_{sample}+R_{load}$), while C is the capacitance of the device (typically several nF in our samples).

During the dark injection experiment, we have to reduce the duration of RC displacement current as much as possible. Fast charge carriers (under a high electric field for example), can result in a DI transit peak moving towards the RC displacement peak. So, if the RC peak is too broad, the DI transit time (t_{DI}) might hide and disappear inside the RC displacement peak. According to equation 3.4.3, we can either reduce the capacitance of the sample to reduce the RC decay time, and this can be achieved by decreasing the electrode area or increasing the sample thickness (according to equation 3.4.4), or we can reduce the resistance in the whole experimental circuit, this is normally accomplished by decreasing the load resistance of the buffer amplifier. It looks like that a decrease in the device area or increase in the device thickness will cause the sample resistance to increase thereby compensating for any decrease in sample capacitance. However, R is not only determined by the device resistance, but by the resistance of the entire circuit (equation 3.4.3.). Therefore, a change in the area can have a beneficial effect on the RC decay time. Carrying out the experiment at a lower electric field is an alternative solution, which means t_{DI} is relatively larger than it is in high electric field, so the DI transit peak might move out of the RC displacement shadow. The drawback of this

method is that it sacrifices the high field data points, because of the limited measuring window. This may not always be a valid option, especially in a thick device. In order to reach the required electric field, an extremely large voltage becomes compulsory.

Since our sample consists of two parallel metal electrodes and a semiconducting layer in between, it can be considered as a parallel plate capacitor, and the capacitance is given by equation 3.4.4

$$C = \varepsilon_0 \varepsilon_r \frac{S}{d} \qquad \text{Equation 3.4.4}$$

C is capacitance, ε_0 is Permittivity of vacuum ε_r dielectric constant, S is the electrode overlap area and d is the distance between both electrodes.

Generally speaking, the dark injection transit current method is a mature technique to calculate mobility in amorphous organic materials and it has been intensively used in mobility measurements[41, 42].

In this experiment, a Berkley nucleonics (model 6040) pulse generator supplied the voltage step needed to carry out the DI experiment, which was connected directly to the substrate electrode. The DI current transient was observed as a voltage drop across a load resistor (typically 479Ω) connected to the input of a buffer amplifier whose output was digitised using a Tektronix TDS2002 oscilloscope. In this experiment, signal averaging over several pulses was carried out to reduce white noise at a frequency of 5 Hz.

3.5.2. DI with photo-excitation

For traditional dark injection measurements, only holes or electrons are supposedly injected into the unipolar device. Since exciton formation requires both holes and electrons, this indicates that excitons do not exist inside the unipolar device during

DI operation. In order to investigate the effects of excited states, excitons must be generated inside the unipolar device, and perhaps the only option is via photo-excitation. A laser has been deployed to pump the molecules to excited states.

To understand the light absorption behaviour of P3HT, UV visible absorption spectra are used, shown in figure 3.4.3. Clearly the absorption peak is around 550 nm. So a green laser (LCS-DTL-316) was chosen for this purpose with an output wavelength of 532 nm, which is quite close to the absorption peak of P3HT, to achieve maximum excition density inside the device.

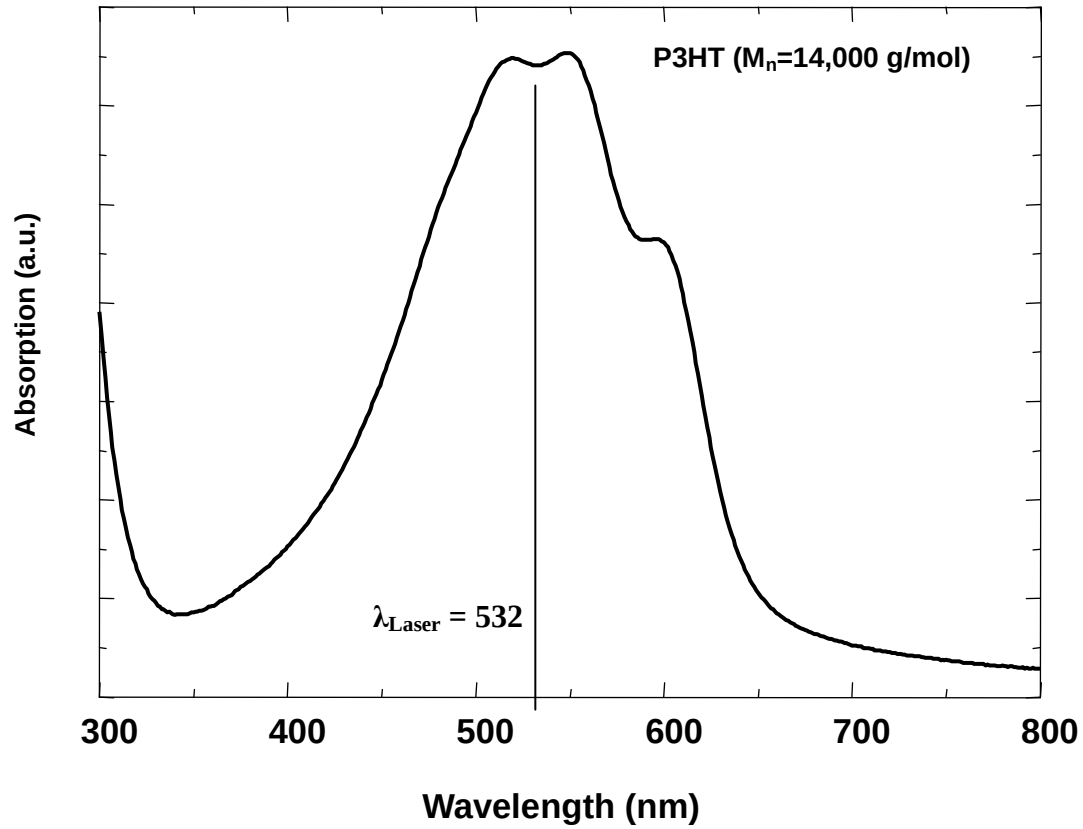

Figure 3.4.3 Absorption spectrum diagram of P3HT

The absorption peak of P3HT is roughly around 550 nm, it is very close to the laser (LCS-DTL-316) wavelength that is used in this experiment for exciting the molecule from ground states, data was obtained via UV-Visible spectrum (Hitachi U-3000 spectrophotometer) on a P3HT coated quartz.

The experimental set up is shown in figure 3.4.4. The idea of this experiment is to investigate the role of excitons on charge carrier transport. During the operation excitions are generated by an adjustable laser source, gradually increasing the optical intensity of the laser, and more ground states were pumped to excited states. Due to the photo-excitation mechanism, most of these excited states are singlets (as discussed in chapter 1.2.3). As part of these singlets transfer to triplet states by inter-system crossing, however, we assume that the triplets population could also increase with the laser intensity, the assumption being that more and more free charge carriers would be caught by those triplet states, hence delaying the charge carriers drifting across the device.

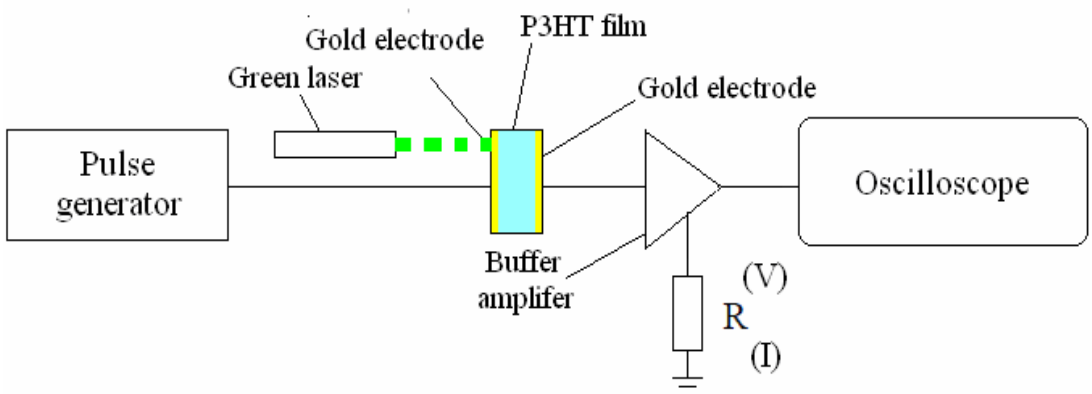

Figure 3.4.4 Schematic of the dark injection measurement with laser to generate enough excitons inside the sample

The pulse generator provides a voltage step to the sample, and the oscilloscope is used to record the current density drops on the load resistance R (in this experiment it is 479Ω). An adjustable green laser is used to generate excitons inside the sample, and the laser is illuminating the whole device.

3.5.3. DI with electric excitation

Normally, the dark injection technique is applied to unipolar devices, which means the work function of the cathode and anode contacts are both close to HOMO level, or LUMO level, so technically, only holes or electrons can be injected into the semiconductor. As the excitons require both hole and electron, unipolar devices are not viable, therefore ambipolar devices are built to achieve electric excitation. Both holes and electrons are injected using an anode with a work function close to the HOMO level for hole injection, and a cathode for electron injection which has a smaller work function close to the LUMO level. Although the device has been changed to ambipolar, there is not much difference in the hole mobility due to contact change. So the dark injection results for this ambipolar device are still valid in this specific case.

For this method, excited states are generated inside the system by a small DC offset bias, therefore an adjustable DC Voltage source is needed, also a summing amplifier is deployed to add the DC offset voltage to the pulse signal. This adjustable DC voltage source and summing amplifier are hand built. Figure 3.4.5 shows the structure of the DC offset source, whereby a variable resistor is used to distribute the voltage, and a multimeter is connected parallel to the DC output to monitor the offset value. Moreover the output for this voltage source is designed to be negative ($-V_{DC\ offset}$), as the positive pole of the batteries is grounded. The reason for this kind of arrangement is to match with the summing amplifier, which is actually a differential amplifier.

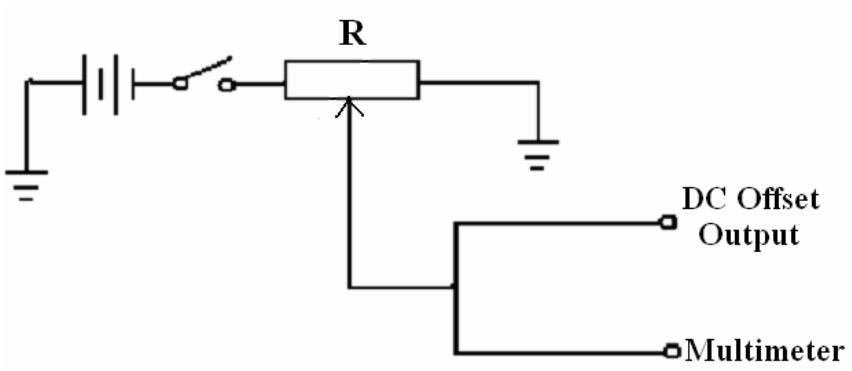

Figure 3.4.5 Schematic of the variable DC offset source

The battery is 18 volts, which is more than enough for the measurements, the variable resistance can be changed from 0~1kΩ, and the multimeter model is Wavetek Meterman 27XT. The DC offset output is adjustable and depends on the distribution of the variable resistance *R*.

The structure of the summing amplifier is presented in figure 3.4.6. It is built using four identical resistances, each one of them is 100 kΩ, with an ER27AB-LM6171-BIN operational amplifier. The output voltage is $V_{out} = V_{In+} - V_{In-}$. As the DC offset voltage output is a negative value ($-V_{DC\ offset}$), the real output of this amplifier is $V_{out}=V_{pulse}-(-V_{DC\ offset})$, so $V_{out}=V_{pulse}+V_{DC\ offset}$, which achieves the original purpose, adding the DC offset voltage to the pulse signal (from the pulse generator).

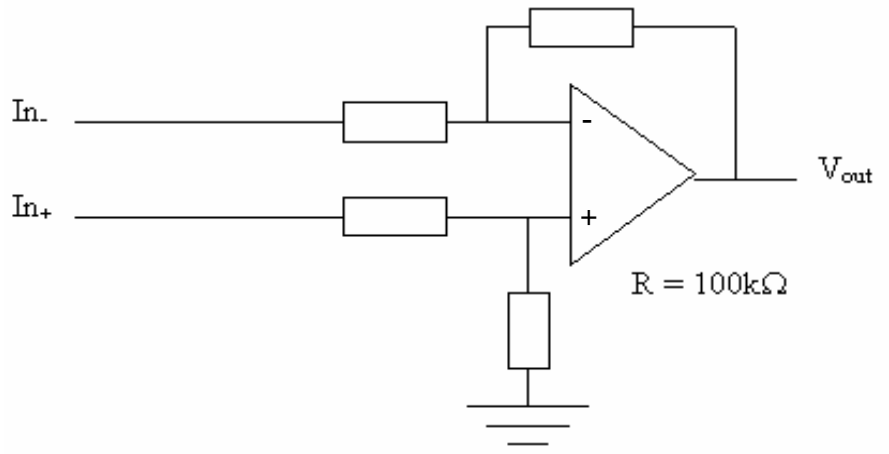

Figure 3.4.6 Schematic of the summing amplifier

The experimental arrangement is presented in figure 3.4.7. A Berkley nucleonics pulse generator supplying the voltage step was connected directly to the substrate electrode (in the case of no offset) or fed into one of the inputs of a summing amplifier, with the other input connected to a DC supply (in the case of measurements with offset voltage), and the summing amplifier output is then connected to the substrate electrodes. Before carrying out the DI measurements, the summing amplifier output was monitored using a Tektronix TDS2002 oscilloscope and the size of the offset and absolute value of the voltage step (V_0) was recorded and, where necessary, adjusted.

An ambipolar device is deployed to achieve exciton generation (more specifically, mainly triplet generation), and the mechanism of this experiment is pre-generating excited states into the system by the DC offset voltage before the dark injection measurement, and keeping the voltage step (V_0) at the same absolute value (see figure 3.4.7). When the DC offset voltage is less than the turn-on voltage of the sample, only hole carriers can be pre-injected into the system. As exciton formation is prohibited, the mobility of the device should be more all less the same as that with a zero offset voltage. If we gently increase the DC offset voltage above turn-on voltage, both holes and electrons can be pre-injected into the device via the Au anode and Al cathode, leading to exciton formation inside the device (mostly triplet states 3:1).

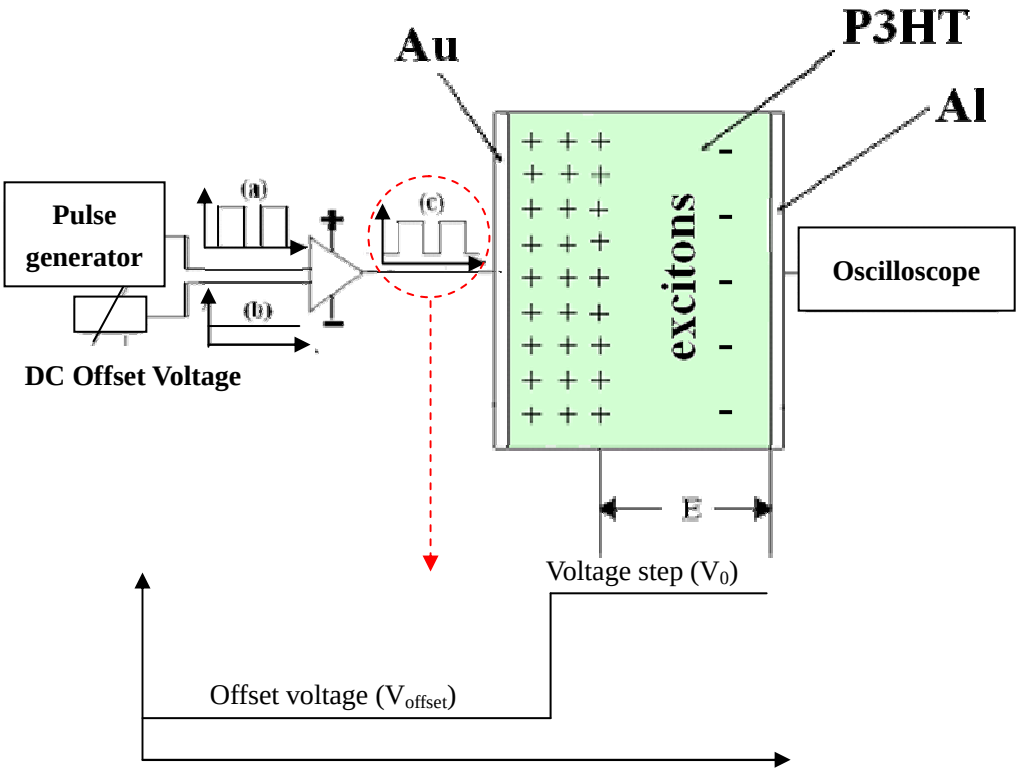

Figure 3.4.7 Experimental setup for the ambipolar device

The variable DC voltage source can provide a DC offset bias for the system, and the summing amplifier is used to add this DC offset to the pulse generator. Therefore figure (a) represents the shape of the step voltage from pulse generator, figure (b) shows the shape of the offset voltage from the variable DC voltage source, and figure (c) is the shape of the voltage pulse after the combination via the summing amplifier.

In order to test whether a mobility change is due to the effect of excited states (mainly triplets) and not some mechanism related to the current density in the device, a unipolar device (Au-P3HT-Au) was used to make a comparison. There are several reasons for introducing the unipolar device. Firstly, the different electrodes may affect the sample mobility, e.g. the impurities of the electrodes may cause different potential drops at the interface and lead to different electric fields across the

semiconductor, therefore the unipolar device can be used to test this possibility in this experiment. Secondly, as only holes can be injected into a unipolar device, triplet formation is prohibited even under a large offset voltage. Thirdly, the DI measurement might be disturbed by the DC offset voltage, as the dark injection is highly dependent on the electric field inside the sample, the pre-applied DC offset voltage could affect the internal electric field distribution. So, by comparing the mobility data of the unipolar device with a variety of DC offset voltages (including zero offset voltage) we can test whether the DC offset bias disturbs the measurement or not. If the mobility of this unipolar device were the same under different DC offset values (including zero offset voltage), this would mean that the pre-applied DC offset voltage does not influence the internal electric field, so the DI technique is still capable of this measurement.

Lastly, and most importantly, if the experimental results agree with these assumptions, the mobility change for the ambipolar device could only be caused by the excited states, as the only difference between unipolar and ambipolar devices is the existence of excited states, while all other possibilities have been ruled out according to previous discussions.

3.6. Time of flight (electron and hole mobility)

Another classic method to investigate charge transport is the time of flight (ToF) technique, which is capable of both electron and hole mobility measurements. It was introduced into the field of organic crystals by Kepler[43] and Leblanc[44] in 1959-1960. In this method, a thin sheet of excited states (electron-hole pairs) is generated next to the semi transparent contact by absorption of a short duration strong optical laser pulse. If it is an asymmetric device, a reverse bias is applied to the device, by using a small work function electrode as anode and a large work function electrode as cathode. As a result, an electric field is applied to the sample without introducing

any charge injection, this design is very efficient for charge extraction. If the laser is incident on the anode, then, under the influence of the applied electric field, electrons combine at the anode and a sheet of remaining hole charge carriers will move across the device under the electric field, eventually reaching the counter electrode. The hole mobility can be detected in this way. On the other hand, if the laser is shone on the cathode, the hole combines with this electrode and leaves the electrons to move under the applied field and drift to the anode electrode, hence the electron mobility can be obtained. This process is represented in figure 3.5.1 (a). A sheet of charge carriers is drifting across the sample under the electric field. In an ideal case there will be a constant photo generated current passing through the device which suddenly falls to zero as the sheet of charge carriers reaches the counter-electrode[15], (represented by the solid line in the *J-t* dependence in Figure. 3.5.1 (b)).

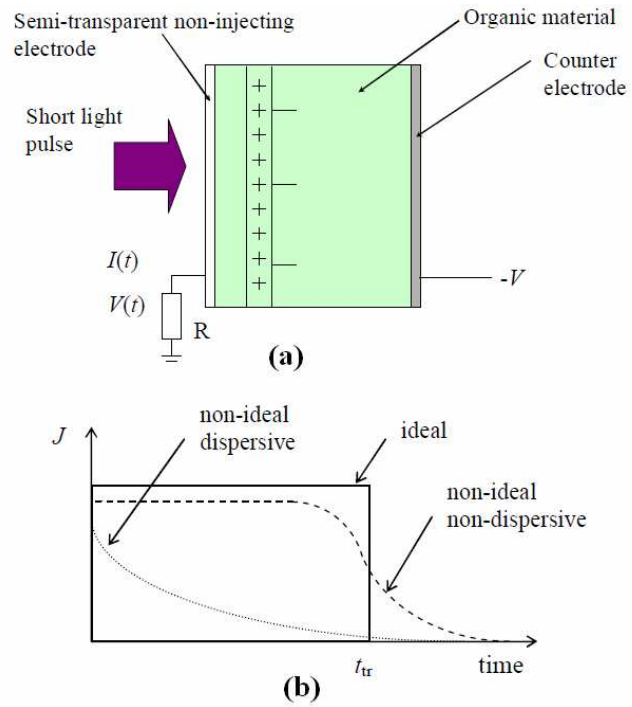

Figure 3.5.1 Schematic diagram of time of flight[15]

Diagram (a) experiment set up, and graph (b) time of flight transient results on oscilloscope.

In a real situation, however, ToF transients would not be this ideal shape. Realistically, there will be a finite absorption depth of the incident light, resulting in a finite thickness of a sheet of free charges carriers. Moreover, there will be a diffusive broadening of the distribution of drifting charge carriers and mobility variations. As a result of these effects, assuming that most of the carriers have a constant average drift velocity (so called non-dispersive transport), the observed ToF signals would have a shape similar to the dashed line which is shown in Figure. 3.5.1 (b). It is still possible to determine the average transit time and, normally, the transit time in this case has been generally accepted as the moment when half of the charge carriers have reached the counter electrode ($t_{trans}=t_{1/2}$, and the broad distribution $W=(t_0-t_{1/2})/t_{1/2,}$ see figure 3.5.2 (a)). However, in many cases the situation is quite different as the charge carriers in a photo-generated sheet move with a very broad distribution of drift velocities, resulting in an almost featureless photocurrent transient, such as the dotted line in Figure 3.5.1 (b). This type of transient is called dispersive and is observed in many amorphous organic materials. In order to analyse such transients they are usually plotted in *log I – log t* representations where a knee, corresponding to a characteristic transit time, can often be seen (see figure 3.5.2 (b) and (c)). By knowing the transit time t_{trans} of charges across the device, we can find out the charge mobility μ from equation 3.4.1, in section 3.4.1.

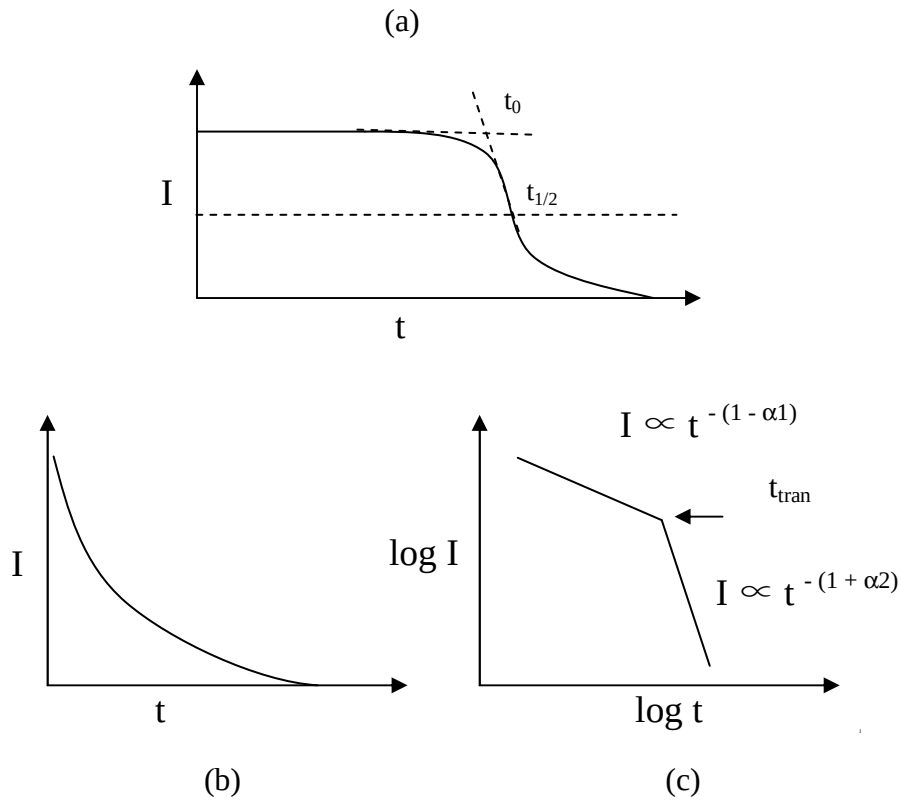

Figure 3.5.2 The ToF transit time calculation

Where t_0 is the fastest transit time and $t_{1/2}$ is the average transit time. Figure 3.5.2 (a) non-dispersive behaviour with linear plot, and the transit time is half of the fastest arrival, (b) dispersive behaviour with linear plot where there is no obvious feature, (c) dispersive behaviour with double-log plot, where there is a clearly seen correspondence to the transit time.

The electrical contacts in the time of flight experiment are different from dark injection, as generally they are blocking contacts. This kind of contact usually has a large energy barrier for charge injection, making it almost impossible, hence the charge carriers are solely created by the light absorption. Ideally, it can be considered as a space-charge-free environment, because a very low population of charge carriers is generated inside the system via photo-excitation, hence the electric field perturbation caused by these charge carriers is not that significant, so the charge

carriers can be considered to be driven only by the uniform electric field.

The absorption depth of the optical excitation must be significantly smaller than the thickness of the organic semi-conducting film. Otherwise, as the light penetrates the sample, charge carriers are not only generated next to the semi-transparent electrode but also created inside the bulk of the device, so the charge carrier travelled distance is not the sample thickness any more. In addition, the spatial distribution of charge carriers inside the sample may cause the time of flight signal to broaden and become dispersive. In order to keep the result convincing, the minimum thickness of a ToF sample must be far more than the penetration depth parameter δ, which is the inverse of extinction coefficient α at the laser wavelength for a given material. The required minimum distance between both electrodes can be obtained using equation 3.5.1, and equation 3.5.2.

$$\delta = \frac{1}{\alpha(\lambda)} \qquad \text{Equation 3.5.1}$$

$$\delta \leq \frac{d}{10} \qquad \text{Equation 3.5.2}$$

d is the thickness of the device, δ is the penetration depth, and α is the extinction coefficient.

The extinction coefficient is a crucial element for searching the minimum thickness of a ToF device, hence UV-visible absorption spectroscopy is used to investigate this parameter. Usually this technique is used to measure the optical density (OD_a) for absorption of the sample. The OD is defined in equation 3.5.3.

$$OD_\lambda = log(I_0/I) \qquad \text{Equation 3.5.3}$$

Where OD_λ is the optical density of light at a certain wavelength, λ, I_0 is the intensity of the incident light, and I is the intensity of the transmitted light through a sample of thickness x.

Since transmission at a given wavelength is related to both incident light and transmitted light intensity, as the extinction coefficient α (see the equation 3.5.4), equations 3.5.3 and 3.5.4 can be brought together to allow direct measurement of the excitation coefficient, and calculate the penetration depth using equation 3.5.5.

$$I/I_0 = e^{-\alpha(\lambda)x} \qquad \text{Equation 3.5.4}$$

α is the extinction coefficient of a certain light with the wavelength λ, and x is the thickness of the device

$$\alpha(\lambda) = \ln(I_0 / I) \times (1/x) = \frac{\log(I_0 / I)}{x \times \log e} = 2.3 \times \log(I_0 / I) \times (1/x) = 2.3 \times OD_\lambda / x$$

Equation 3.5.5

The relationship between extinction coefficient and optical density under the maximum absorption wavelength, λ.

Last but not least, the optical pulse duration must be short compared to the transit time for charge carriers across the sample, if the optical pulse step lasts too long, it will generate fresh charges carriers while drift is occurring and distort the time ToF signal, so that the transit time of charge carriers cannot be properly detected. Low-intensity optical pulses are used so that the photo-generated charge carrier density does not significantly disturb the uniform electric field (see equation 3.5.6) in the structure to keep the photocurrent in the space-charge-free condition.

This condition is:

$$q_{photogenerated} = \int_0^\infty Idt << CV \qquad \text{Equation 3.5.6}$$

where q is photogenerated charges, I is instant current, t is time, C is sample capacitance and V is voltage.

The absorption depth of the optical excitation must be much smaller than the

thickness of the organic semi-conducting film, as discussed earlier in this section. Therefore, before a time-of-flight experiment, the minimum thickness of the sample must be calculated out via equation 3.5.1 to equation 3.5.5. Otherwise, with a random sample thickness, the obtained mobility value is not convincing. In order to achieve this purpose, a UV visible absorption spectrum is used to obtain all necessary parameters. The spectrum of a quartz-based TPD device with a thickness of 2000 Å is shown in figure 3.5.3, with a maximum absorption at approximately 350 nm.

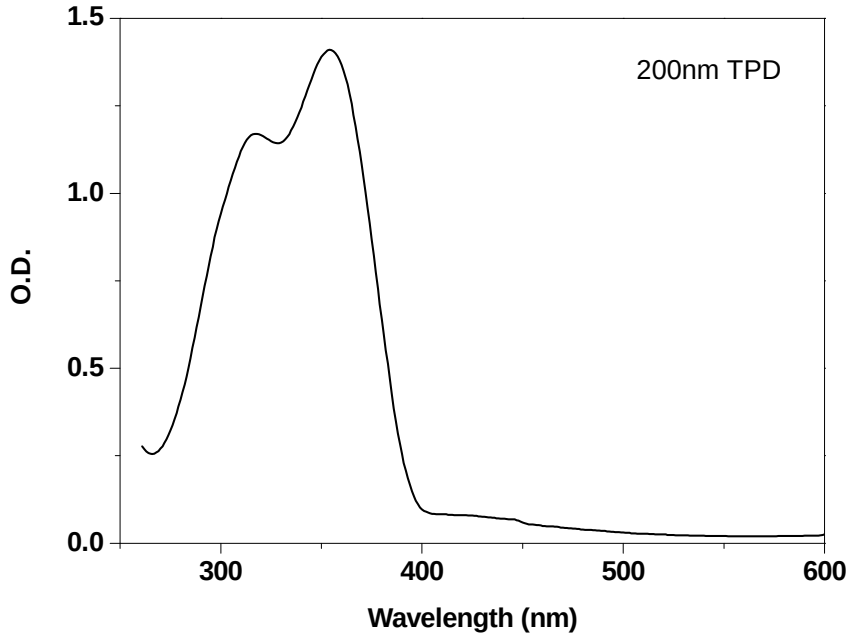

Figure 3.5.3 Absorption spectrum of TPD

The sample is thermally deposited (via Kurt J. Lesker spectros evaporation system) on top of a quartz substrate with the thickness 2000 Å, and the measurement is taken by using UV-visible spectrum (Hitachi U-3000 spectrophotometer).

The minimum sample thickness is calculated as follows:

$d \geqslant 10\delta$

As $\delta = 1/\alpha$ (according to equation 3.5.1),

So $d \geqslant 10/\alpha(\lambda)$

According to equation 3.5.5 $\alpha(\lambda) = 2.3 \times OD_\lambda / x$

So $d \geq \frac{10}{2.3 \times OD_\lambda / x}$

As OD_λ=1.41, x=2000 Å, λ=355 nm (this is the wavelength of our laser output)

Therefore $d \geqslant$ 616 nm

d means the minimum sample thickness which is 616 nm after the final calculation, OD_λ is about 1.41 and sample thickness x is 2000 Å.

Therefore, the chosen sample thickness is around 610 nm.

As the experiments must take place under reverse bias, the ITO electrode is chosen as the cathode, and aluminum is used as the anode, because the work function of ITO (4.9 eV) is quite far from LUMO level (2.55 eV) of TPD and the work function of aluminum (4.3 eV) is quite far away from HOMO level (5.5 eV). As a result, the applied voltage can only provide an electric field to the sample without introducing any extra charge carriers into the system, because of the large energy barrier.

A laser pulse (made by Big Sky Laser Quantel, which output Nd:YAG doubled 532 nm and tripled 355 nm) is used to generate a thin layer of excitons into the system, a pulse generator (mode: TTi TG1010A Programmable 10 MHz DDS Function Generator) is set at 3 Hz to apply the reverse electric bias for the ToF measurement, and an oscilloscope (mode: Agilent infiniium) is deployed to record the ToF result.

A voltage pulse is triggered 700 μs before the laser pulse to provide the electric field for the ToF measurement, and the voltage step lasts approximately 30 ms, which is long enough for the charge carriers to drift across the sample. Figure 3.5.4 presents the ToF curve on the oscilloscope, the voltage step started at -7×10^{-4} (given by the first RC displacement peak), which means it starts 700 μs before the laser pulse is triggered (indicated by the second displacement peak), and the beginning of the laser pulse is defined as time zero on the oscilloscope.

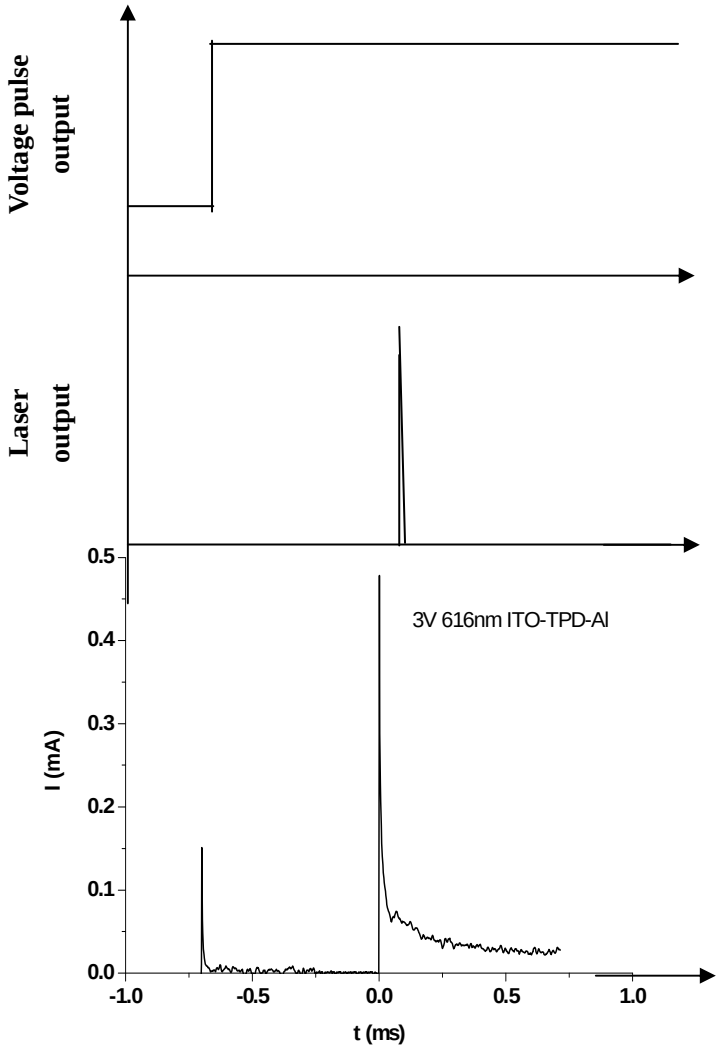

Figure 3.5.4 Current versus time plot of ToF measurement

This is the hole mobility measurement curve for TPD with a thickness of 610 nm, under 3 volts reverse bias.

The device is set under a reverse bias, and placed in the sample holder in a high vacuum environment with pressure set to $\sim 5\times 10^{-5}$ mbar. The hole mobility in a sample is obtained by having the laser incident on the aluminium anode, and the electron mobility is measured by shining the laser on the ITO cathode.

3.7. DI in thin TPD devices

Since TPD films are thin, even a small voltage pulse can sustain the dark injection measurement. It is not necessary to use a high voltage generator, instead, a more accurate and delicate pulse generator (model: TTi TG1010A Programmable 10MHZ DDS Funcion Generator) is used to give a voltage pulse and a DC offset voltage at the same time. The summing amplifier is no longer necessary. As a small voltage pulse cannot damage the oscilloscope, the buffer amplifier is also removed. A more sensitive oscilloscope (model: Agilent infiniium) is used for data collection. Any light output from the device is observed using a Thorn EMI 9202V S-20 Photomultiplier and SignalRecovery 7265 lock-in amplifier. The schematic is simplified in figure 3.6.1.

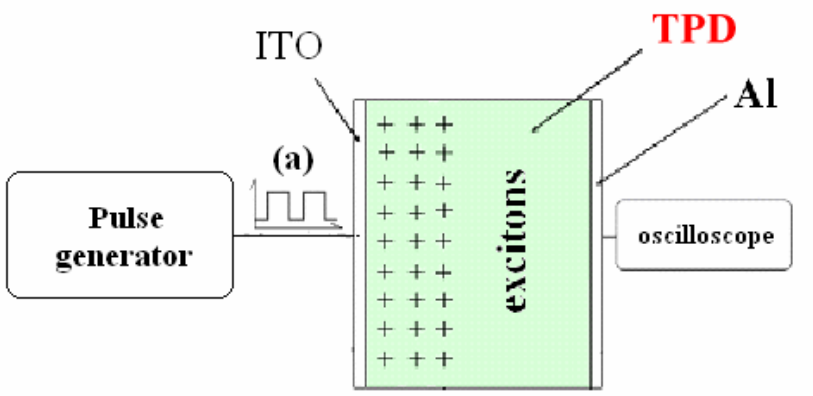

Figure 3.6.1 Schematic of the electric measurement circuit for a TPD device

The pulse generator is set with the frequency of 3 Hz, and the input resistance of the oscilloscope set to 50 Ω, figure (a) represents the shape of the voltage pulse given by the pulse generator, which contains both the step pulse and the DC offset voltage.

The experimental method is an exact repetition of that in section 3.4.1, except the pulse generator is more sophisticated, as it can provide both voltage pulse and offset at the same time. Also the oscilloscope is more sensitive, and the resolution is 16 bits

instead of 8 bits.

3.8. ToF with forward bias

This experiment is different from the traditional time-of-flight measurement, as we know that ToF experiments are normally taken under space-charge-free condition, with two blocking electrodes providing the electric field without injecting any free charge carriers into the system. However in this specific case, we need to generate excited states inside our sample to observe the effects of excitons. Therefore blocking electrodes are not suitable, instead Ohmic contacts are used to inject both electrons and holes into the device. As the work function of ITO (4.9 eV) is quite close to the HOMO level of TPD (5.5 eV), it is chosen as the anode electrode for both unipolar and ambipolar devices, while aluminium is chosen as a cathode electrode for ambipolar devices even though it is not very efficient for electron injection. On the other hand, gold is used as a cathode for unipolar devices, as it is expected to be considerably worse than aluminium at electron injection.

The sample structure is typical of dark injection devices (introduced in chapter five). The ambipolar devices are still fabricated by ITO anode, aluminium cathode with TPD semiconductor sandwiched in-between while unipolar devices were composed using ITO-TPD-Au structure, hence all preparations are exactly as same as in chapter five.

The experiment set up is represented in figure 3.7.1. During this experiment, a laser pulse (made by Big Sky Laser Quantel) is used to generate a thin layer of free charge carriers behind the transparent ITO electrode, a pulse generator (model TTi TG1010A Programmable 10MHZ DDS Function Generator) is set at 3 Hz and not only provides the electric bias for the ToF measurement, but also generates triplet states inside the sample, while an Agilent infiniium oscilloscope is deployed to record the ToF results.

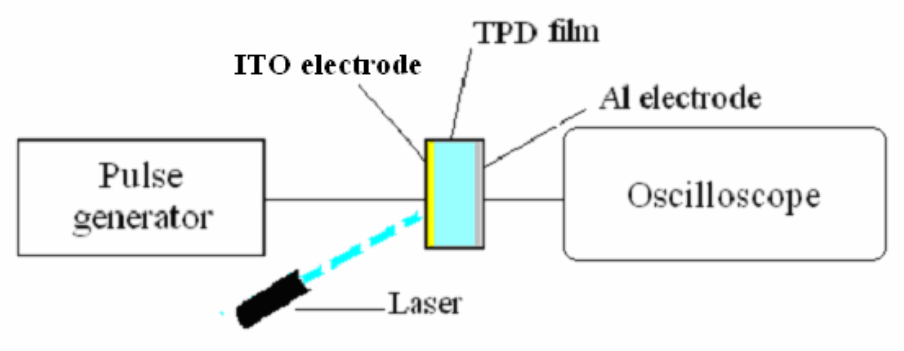

Figure 3.7.1 Schematic of time-of-flight measurement

The laser is incident to the anode electrode, therefore a thin layer of electron-hole pairs are generated beside the ITO electrode, under the electric bias provided by the pulse generator, electrons in this thin layer recombine with the anode contact immediately, leaving the holes to drift across the sample and finally reach the counter-electrode. Nevertheless, the pulse generator is not only used to provide electric field, it is also used for the injection of charge carriers.

The timing of this experiment is similar to the one in section 3.5. The principle of this experiment is to provide a voltage step to the sample device before the laser pulse is triggered, hence hole and electron pairs are pre-generated in the ambipolar sample via ITO and alumina ohmic contacts, which eventually leads to the formation of triplets, then triggers the laser pulse and observes the behaviour of time-of-flight results with the formation of excitions. As we gently raise the step voltage, the concentration of excited states would also increase, and as a result the observed hole mobility of the device would be affected by the presence of triplet states. In order to make a comparison, a unipolar device is also deployed. Theoretically, for unipolar devices only a hole can be injected into the sample from the anode electrode and extracted by cathode contact. Exited states could not, therefore, be generated inside the device, hence the mobility of the unipolar sample should not be affected by the step voltage.

3.9. MR measured by DI and ToF

At the first stage of this experiment the sample mobility is measured by DI, and excited states are pre-generated by a DC offset voltage. A magnetic field is provided by 10 Neodymium Disc Magnets, and the field intensity is measured by Hirst GM05 meter, given an average value of 0.52±0.005 T.

Another test is to use time of flight technique to compare the DI results in the presence of a magnetic field. The samples are measured under reverse bias, so the contacts do not provide charge injection. The magnetic field is provided by a U shape Neodymium Magnet with a field intensity of around 0.2 T.

The device is still made from TPD, with the structure identical to that used in section 3.1, so the preparation processes are also exactly the same as those introduced in chapter three. Ambipolar and unipolar devices are also used to make the comparison.

The dark injection experimental set up is exactly the same as for the dark injection experiment (see figure 3.6.1, in section 3.6).

In order to probe changes in charge transport due to magnetic fields, DI measurements on the diode structures are carried out by repeatedly placing and removing a small neodymium magnet (magnetic field typically 500 mT) directly above the sample. These are carried out on both Al and Au cathode samples, at different DC offset values.

According to chapter 1.4, if the device is excited by electric excitation then most excited states are triplets, therefore a large DC offset voltage (higher than turn-on voltage) could generate more triplet states inside the device than singlet states (and the ratio is 3:1, under no external influence). According to figure 1.4.1 in chapter 1.4, by applying a large magnetic field, the high concentration of triplet states can inter-convert to singlet states via intersystem crossing. Therefore we suggest that the reduction of the triplet population can lower the scattering/blocking effect on free charge carriers, and lead to an increase in carrier mobility. When we increase the

offset bias, more triplets are generated inside the device, and under the influence of a magnetic field more triplet states would transfer to singlet states via intersystem crossing. As a result, the mobility improvement, due to the effect of a magnetic field, would also increase.

The time of flight experimental set up is similar to that in chapter four. In order to investigate the effect of the magnetic field, the ToF measurements are carried out by repeatedly placing and removing a small U shape neodymium magnet directly above the sample. These are carried out on both hole and electron mobility measurements. The reason for choosing a U shape magnet is that the gap between two magnet poles can provide the magnetic field without blocking the laser beam, and the schematic of this arrangement is presented in figure 3.8.1. The magnetic field is measured by the Gauss meter behind the substrates (which is the non linear magnetic field intensity effect on the sample) and is about 0.2mT.

The experiments are carried out under reverse bias so both contacts behave as blocking electrodes, and no extra charge carriers can be injected into the device, hence electric-excitation is prohibited and photo-excitation mainly generates singlet states, which have an extremely short lifetime and cannot act as charge blocking sites, so applying the magnetic field should not affect the ToF mobility too much due to a lack of triplet excitons.

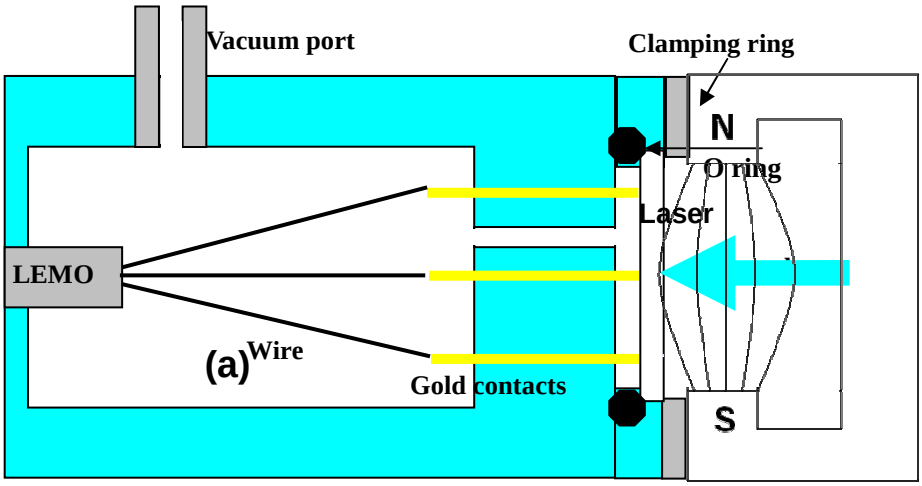

Figure 3.8.1 Schematic of ToF measurement with magnetic field

Figure 3.8.1 (a) shows the ToF measurement setup with magnetic field, and the side view of the U magnet.

Chapter four: P3HT Results

4. P3HT Results

4.1. DI in P3HT

The dark injection technique[38, 39] was chosen to measure the hole mobility in poly-(3-hexythiophene) devices, as it is much more suitable for both dispersive and non-dispersive materials when compared to the time-of-flight technique. As P3HT is a typical dispersive organic semiconductor, it is usually easier to measure using the dark injection technique.

The dark mobility in P3HT is measured using the dark injection technique, and is compared with the literature to confirm the validity of our experimental technique. If the samples are carefully prepared and all testing steps are followed, then our results must agree with other research.

Figure 4.1.1 presents the current versus time (1.05 μm thick P3HT) on the oscilloscope traces, and the arrows indicate the DI transit time. Obviously, the DI transit time scales correctly with the increasing drive voltage, for instance the transit time at 60 V is nearly half of that at 30 V, which obeys the mobility equation 3.4.1.

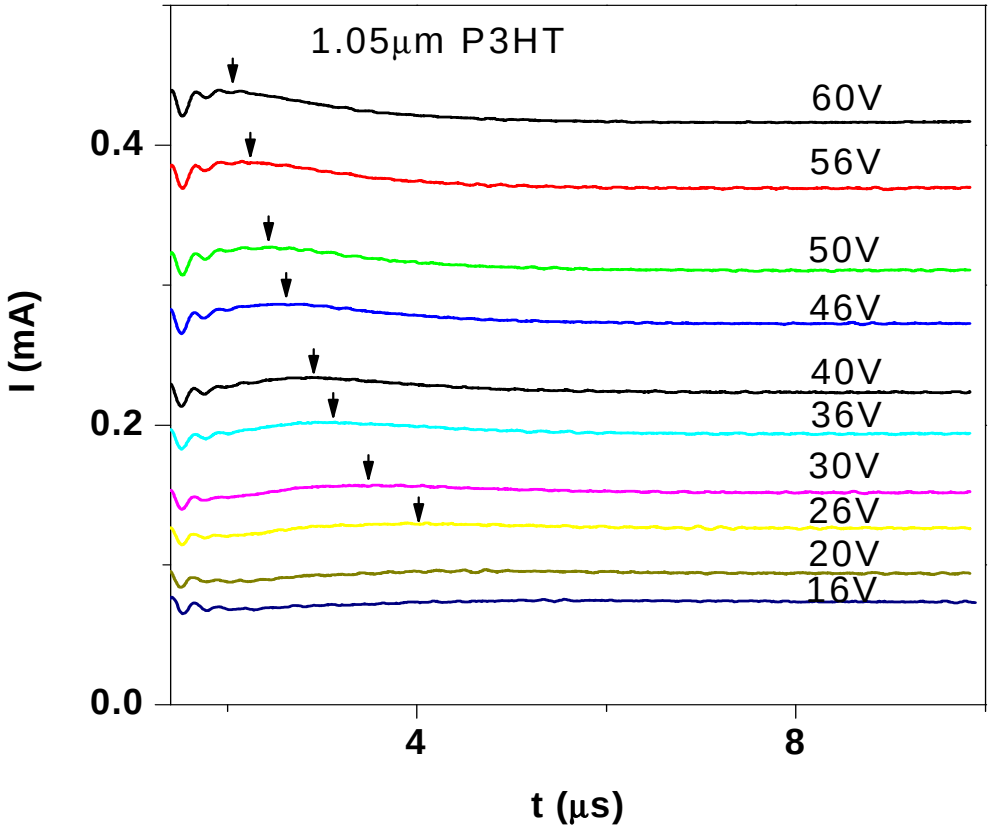

Figure 4.1.1 Current versus time of P3HT device

Clear dark injection transit peaks are indicated by the arrows for bias≥26 V.

Drift velocity can be obtained using the sample thickness divided by the space charge free transit time ($\sim 0.785 t_{DI}$). Figure 4.1.2 presents the drift velocity versus the electric field. According to equation 1.1.1 in chapter one, $\mu = v_d / E$, μ is mobility, v_d denotes charge carrier velocity and E represents the electric field. So the slope of this schematic is the mobility of the P3HT sample, which is around $6.33 \times 10^{-5} (cm^2/Vs)$, and it is comparable to those reported in the literature for P3HT[45, 46]. The linear fit of this data does not pass through the origin, which indicates a slight field dependence of the mobility or a systematic error in some measurements.

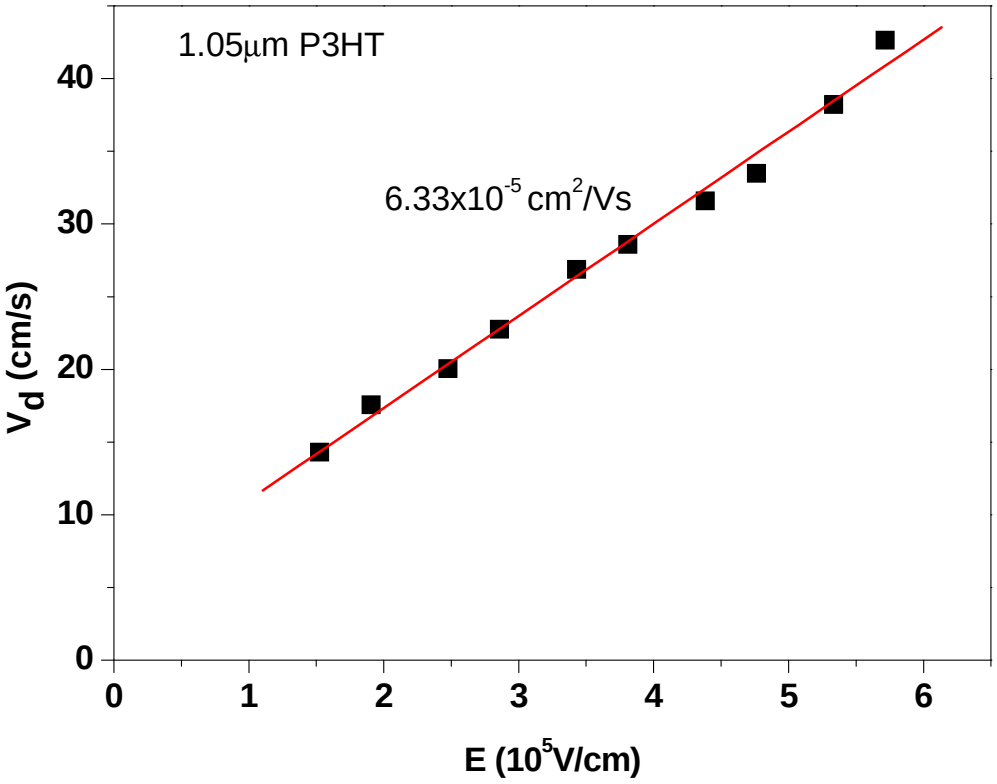

Figure 4.1.2 Drifting velocity versus electric field

The calculated hole mobilities, using the same data in figure 4.1.2, are also shown as a Poole–Frenkel plot in Fig. 4.1.3. In this figure all the mobilities are measured under a reasonable electric field (E>1000 V/cm). Less than this value, may experience trap filling, and the mobility could increase rapidly with electric field, leading to inconsistent results). The average mobility for drift velocity versus electric field (～6 ×$10^{-5}$$cm^2$/Vs) agrees with not very field dependent mobility in figure 4.1.3 (～8× $10^{-5}$$cm^2$/Vs). This information is also confirmed in our experimental techniques and data collections.

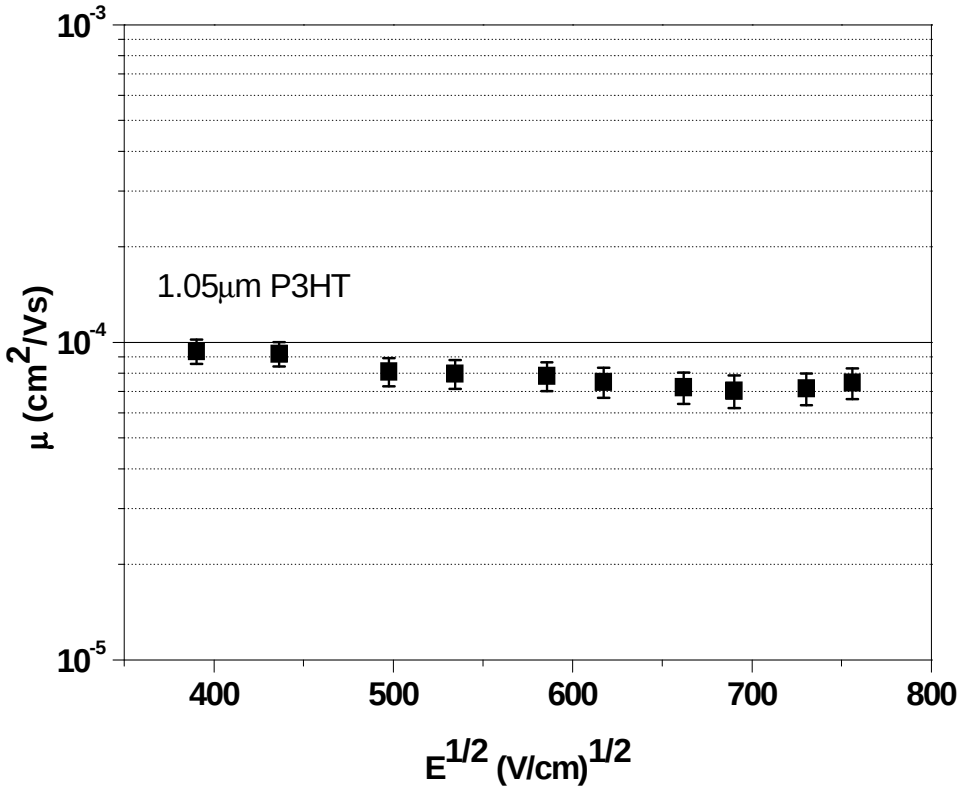

Figure 4.1.3 Poole–Frenkel plot of P3HT sample. The sample thickness is 1.05 μm.

4.2. DI with photo-excitation in P3HT

4.2.1. Results

This experiment involves two parts, first a comparison of the mobility in a dark environment and under a laser incidence. Theoretically, excited states do not exist inside the sample under a dark environment. In contrast, with 2 mW laser incidence excited states can be generated, which might cause mobility variations.

Figure 4.2.1 shows the DI curve for P3HT device (1.4 μm) in a dark environment, and the DI transit time scaling correctly with the voltage bias. Figure 4.2.2 presents the current versus time for the same device but with 2mW laser incidence. According to this figure, it is obvious that the DI technique is still capable of mobility

measurements, even though the device is not under the dark environment anymore. All the measurements are taken under the same electric field as that in figure 4.2.1, to provide a good comparison. The current density in this graph is slightly higher than in figure 4.2.1, which could be caused by the trap filling due to exciton dissociation. In these graphs (figure 4.2.1 and figure 4.2.2), there is a small bump in front of the DI peak, which might be due to the amplifier oscillation. As it does not move with the electric field, it cannot be the DI turning point.

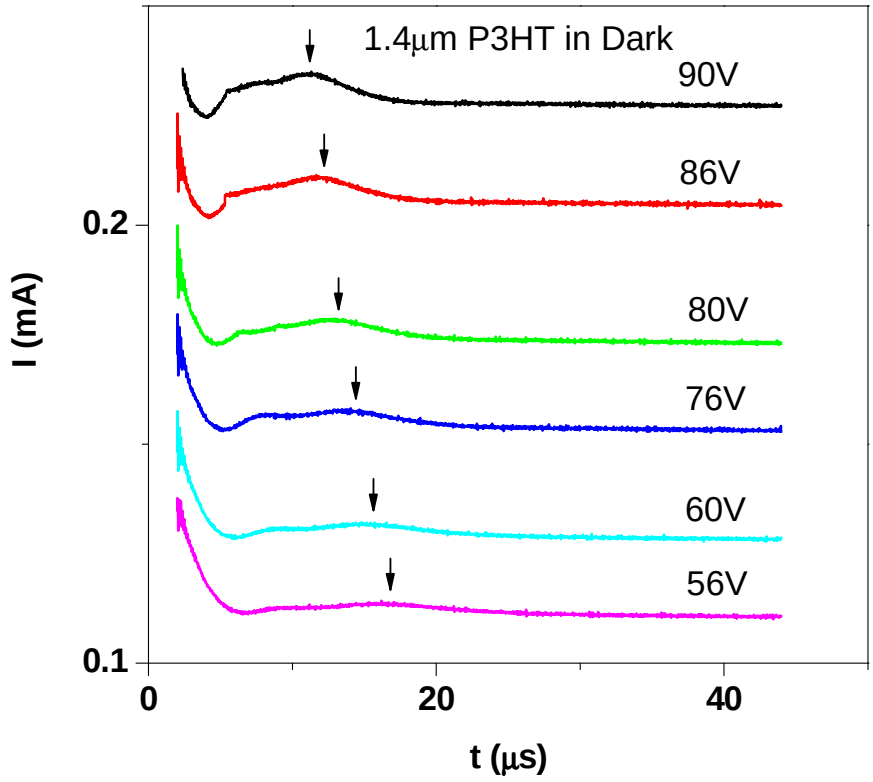

Figure 4.2.1 Current versus time of P3HT device in a dark environment

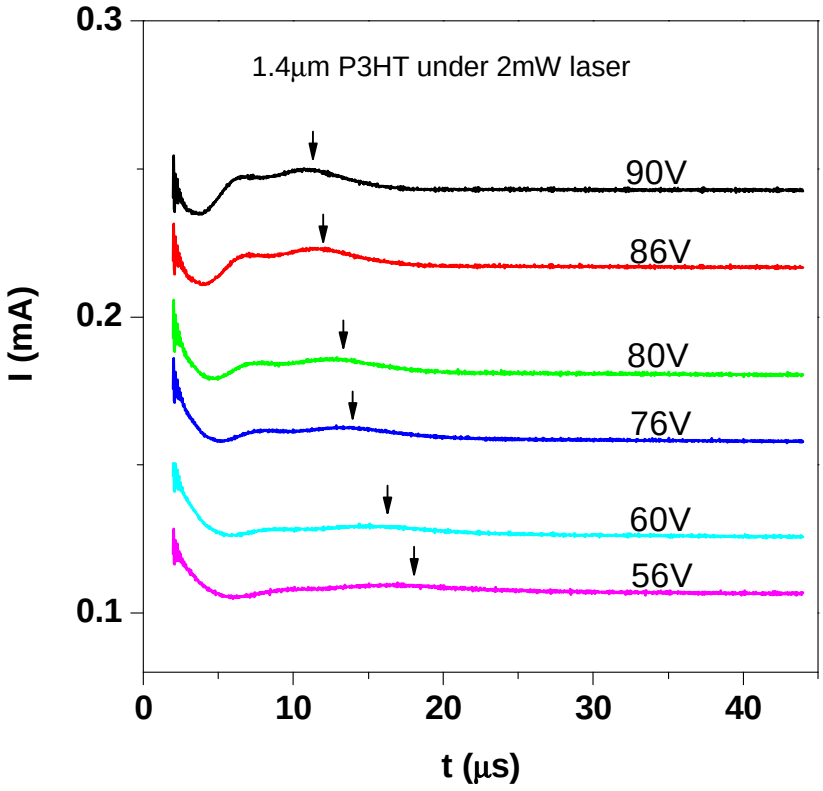

Figure 4.2.2 DI curve for P3HT device under 2mw laser incidence

At the second stage, we increased the laser intensity step by step, while recording the mobility of the sample at given voltage. The current trace on the oscilloscope is present in figure 4.2.3, the transit time decreases as the laser intensity increases, indicating that the mobility in the device increases as a function of laser intensity. In order to pick the transit time more accurately, the DI transit peak is fitted with a cubic polynomial curve. Thus the transit time can be calculated by the derivative of the fitted equation. Most importantly, in order to eliminate unnecessary artificial errors, all the transit times are chosen in this way throughout this thesis.

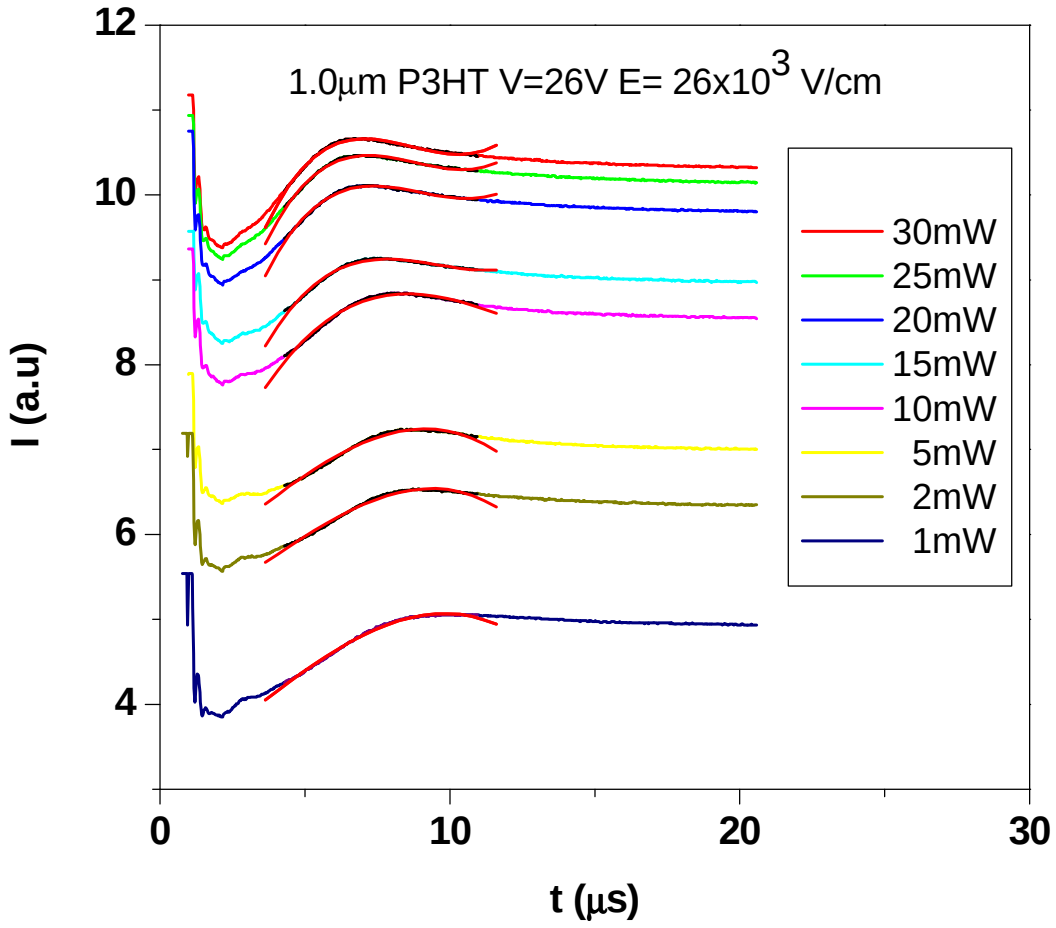

Figure 4.2.3 Current versus time under different laser intensity

4.2.2. Discussion

For the first part of the experiment, by calculating the mobility and drift velocity from figure 4.2.1 and figure 4.2.2, the drift velocity versus electric field is plotted in figure 4.2.4 for both measurement conditions. According to this, the mobility of the device in the dark has no significant difference from the mobility under 2 mW green laser incidence.

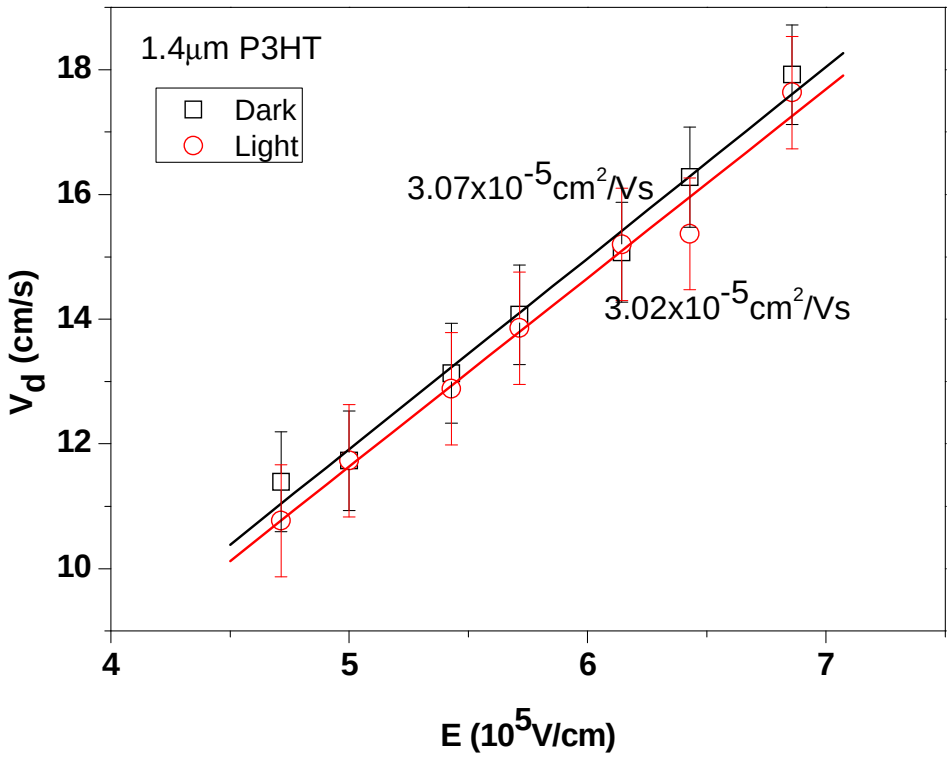

Figure 4.2.4 Carriers drift velocity versus electric field

For the sample in the dark environment, the mobility is around (3.07±0.42) × 10^{-5} cm^2/Vs, and for the sample under the 2mw laser incidence, the mobility is around (3.02±0.47) ×10^{-5} cm^2/Vs.

Figure 4.2.5 shows the Poole–Frenkel plot for data both under the dark environment and laser incidence. However, there is not much difference between both conditions. Therefore the result does not firmly back up our assumption.

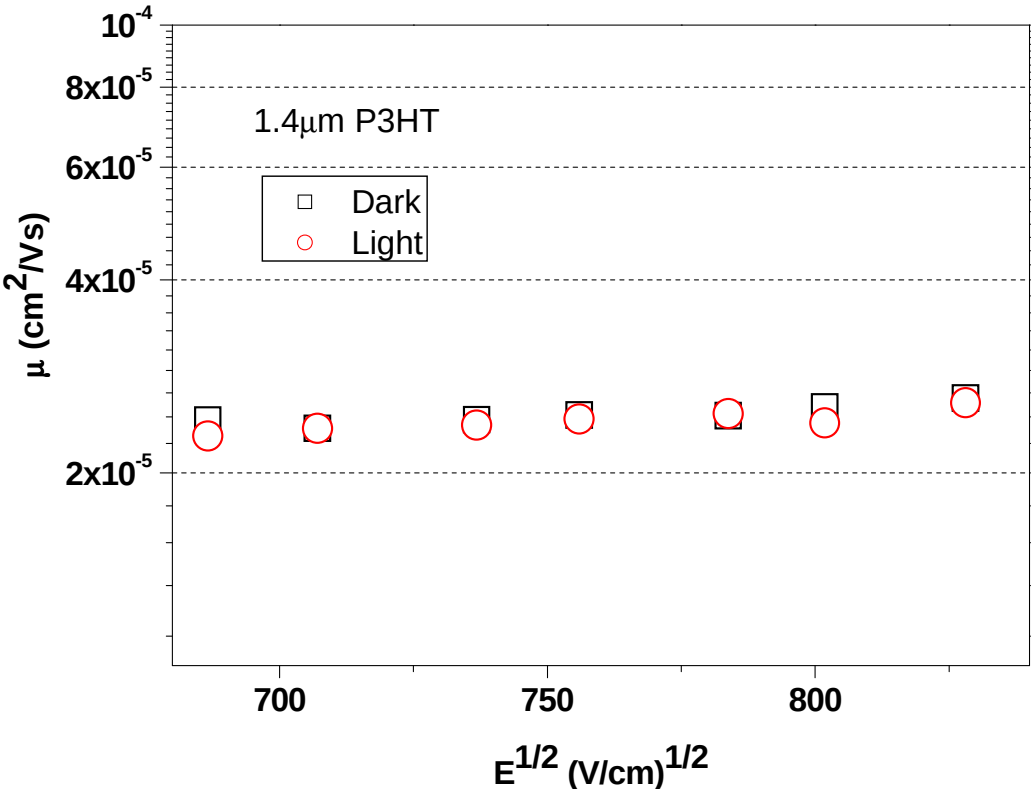

Figure 4.2.5 Poole–Frenkel plot of P3HT sample with the thickness of 1.4 μm The mobility is measured both under the dark environment and laser incidence.

Figure 4.2.6 represents the steady state current density both under dark environment and under 2 mW laser incidences. At lower electric field both current densities are quite similar and no significant differences can be observed. However, at higher electric field the current densities are slightly higher after laser incidences. This might be due to the de-trapping at high electric field. Since singlets can dissociate to free electron and hole pairs at the interface or at defects, or within the bulk material itself, there will be more charge carriers in the device under the laser incidences. With more charge carriers trapped at the lower energy site, it is more likely to de-trap under higher electric field. This can therefore lead to an increased current density at higher electric field under the laser incidences.

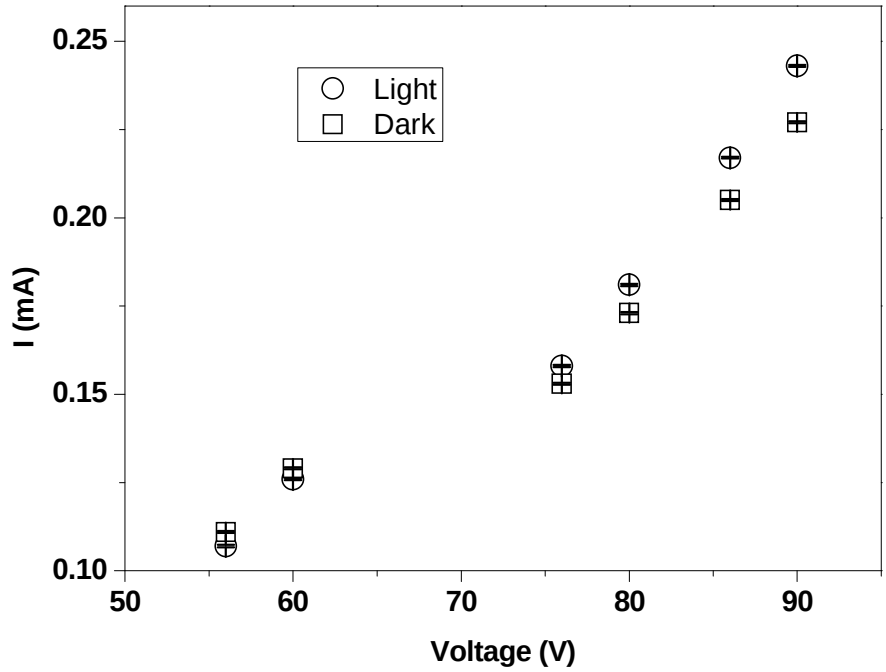

Figure 4.2.6 Steady state current density versus applied voltage

Currents are measured both under the dark environment and 2 mW laser incidence.

In the second stage of the experiment, we gradually increased the laser intensity. Theoretically, the mobility of the sample should decrease as the optical intensity increases, resulting in more and more triplet generation via inter-system crossing. But the reality is contrary, according to figure 4.2.7 the transit time decreases as the laser intensity increases, indicating that the mobility in the device increases as a function of laser intensity (see figure 4.2.7). This is exactly opposite to our original suggestion. So this phenomenon confirmed that the mobility change in this case is not due to the reaction between triplet states and free charge carriers, but to some other unknown mechanism that must take place inside the device.

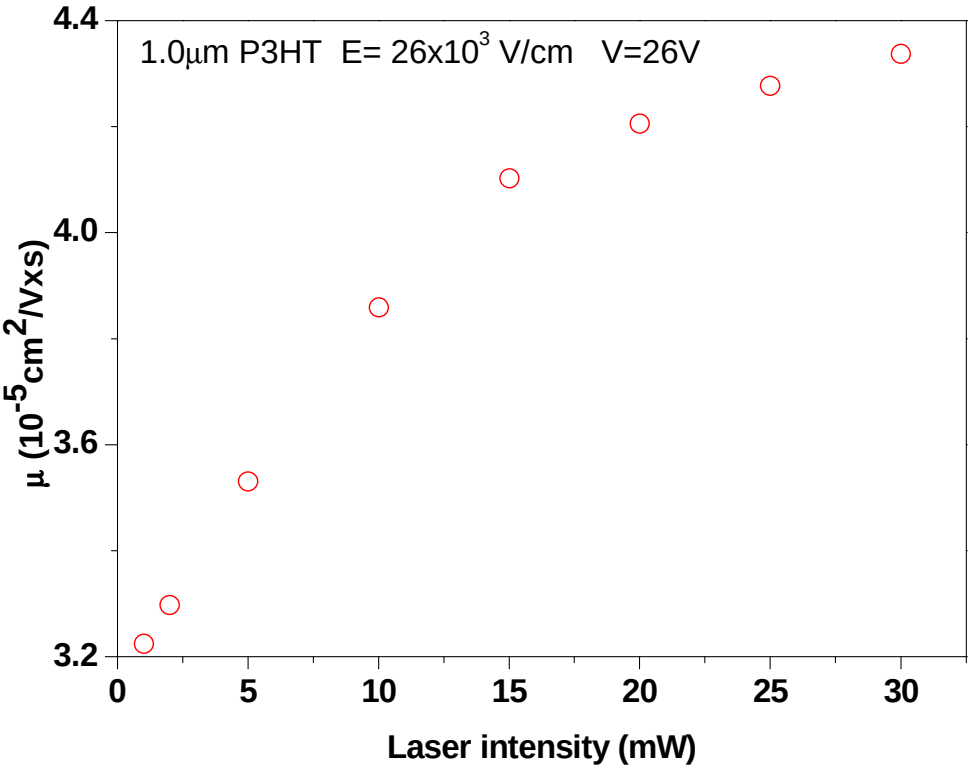

Figure 4.2.7 Mobility of the P3HT device as a function of incident light intensity The increase of incident laser intensity enhances the mobility of the device, this is not expected by our assumption, but might be due to the trap filling inside the P3HT unipolar device.

After careful consideration, we realised that some critical mechanism was missing at the very beginning of our assumption. Except for the small amount of triplet states caused by the intersystem crossing, most of the excited states photo-excited inside the system are singlets, so the effect of these vast singlet states cannot be ignored in this situation. Singlet states are widely reckoned to have a very short lifetime. According to what we have discussed before, it can dissociate to free electron and hole pairs at the interface or at defects, or within the bulk material itself, and this is the principle of how organic photovoltaic devices works. In the OPV system the organic molecule can be excited by light absorption. These light excited singlets can

dissociate to electron and hole carriers, Therefore generating current flow through the device.

In this experiment, as we gradually increase the intensity of the laser, the singlet population should increase as well. As a result of the huge population of singlet states generated, exciton dissociation is inevitable (just like the situation in photovoltaic devices), so these dissociated free charge carriers could fill up some lower energetic trapping sites and lead to a sample mobility increase.

In conclusion, this phenomenon can be explained that, with a very low intensity incident laser (2mW), the singlet concentration is too low to generate enough dissociated charge carriers. Hence the lower energy sites were not filled up by the free carriers, thus the mobility of the device hardly changed at beginning. As the laser intensity increases, the singlet population should increase very rapidly. With more singlets dissociated to free charge carriers, then the lower energy traps start filling up causing the sample mobility to increase as a function of laser intensity.

Even though we are able to provide a plausible explanation, it is built on too many assumptions, which makes the conclusions not convincing. Other experiments were set up to test the effect of excited states on charge transport. In these, a small DC offset voltage is used to achieve electrical excitation instead of photo-excitation, as discussed in chapter three.

4.3. DI with electric-excitation in P3HT

4.3.1. Results

According to figure 4.3.1 (a,c,d), hole DI transients show a clear space-charge cusp in the ambipolar device (Au-P3HT-Al) and the transit time scales correctly with the applied voltage pulse. This suggests that the electron injection and transport within these devices is not balanced with that of the holes, as observed in some cases for

P3HT[46]. Indeed, we prepared our devices in air, which is likely to result in strong electron trapping, limiting electron transport in a more pronounced fashion compared to the hole transport. Figure 4.3.1(b) shows that, if keeping the total voltage pulse step stable and increasing the DC offset voltage to 8 volts, the transit time is still clearly detectable but becomes longer.

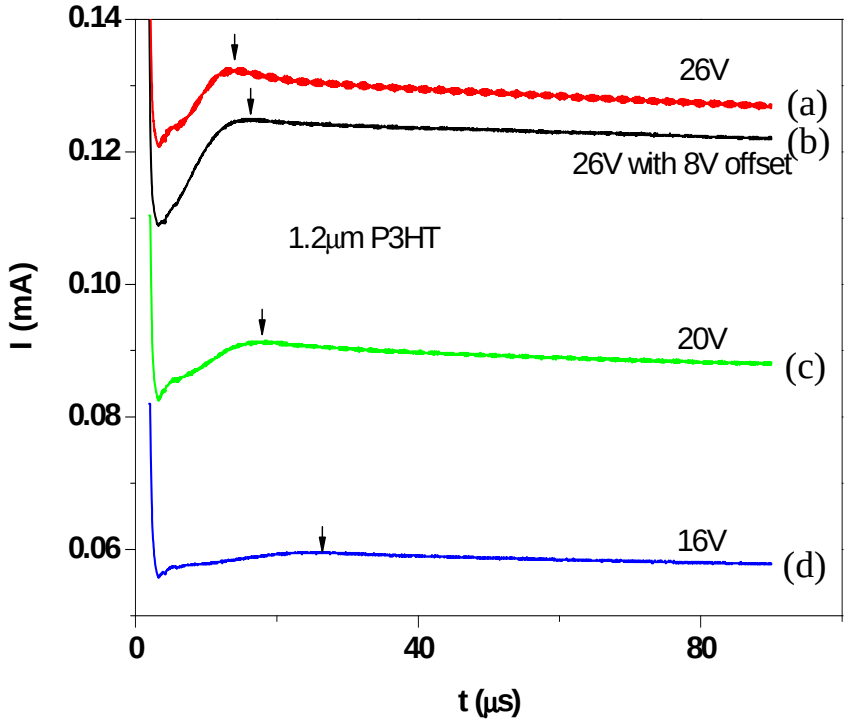

Figure 4.3.1 Oscilloscope trace of ambipolar P3HT sample: figure (a), (b) and (c) show the DI transients obtained under 26V, 20V and 16V bias without the offset. Fig (d) shows the DI transient under 26V with the offset. The mobilities are calculated using the equation 1.1.1

The calculated hole mobilities are shown as a Poole–Frenkel plot in figure 4.3.2, showing a slight electric field dependence both with and without offset (in this specific case, the offset voltage is 8V), and are comparable to those reported in the literature for P3HT[45, 46] and also our own data in chapter two. It is also confirmed by the velocity versus electric field plot (see fig 4.3.3), as both of them are not

passing through the original coordinate point. In these graphs it is clear that, under the same electric field, the mobility of the ambipolar device with 8V offset voltage is obviously less than the mobility with 0V offset.

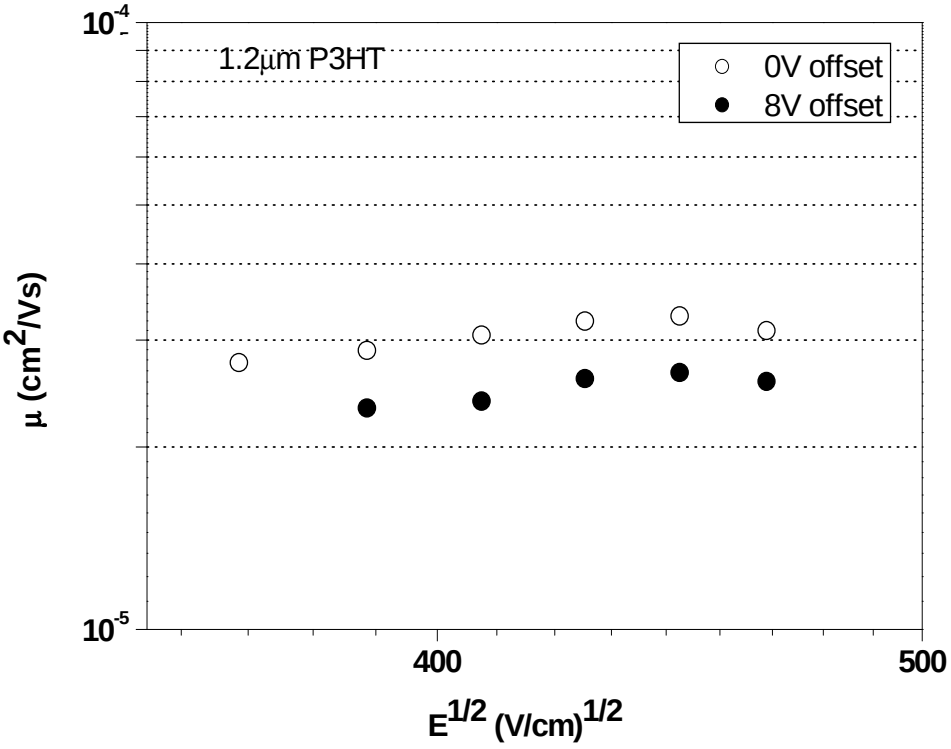

Figure 4.3.2 Mobility versus the electric field with and without offset voltage
The filled circles represent the mobility of the device with zero offset voltage, and the open circles represent the mobility with 8 volts offset voltage. The mobility of the device with 8 volts offset voltage is clearly less than the mobility of the device with no offset voltage.

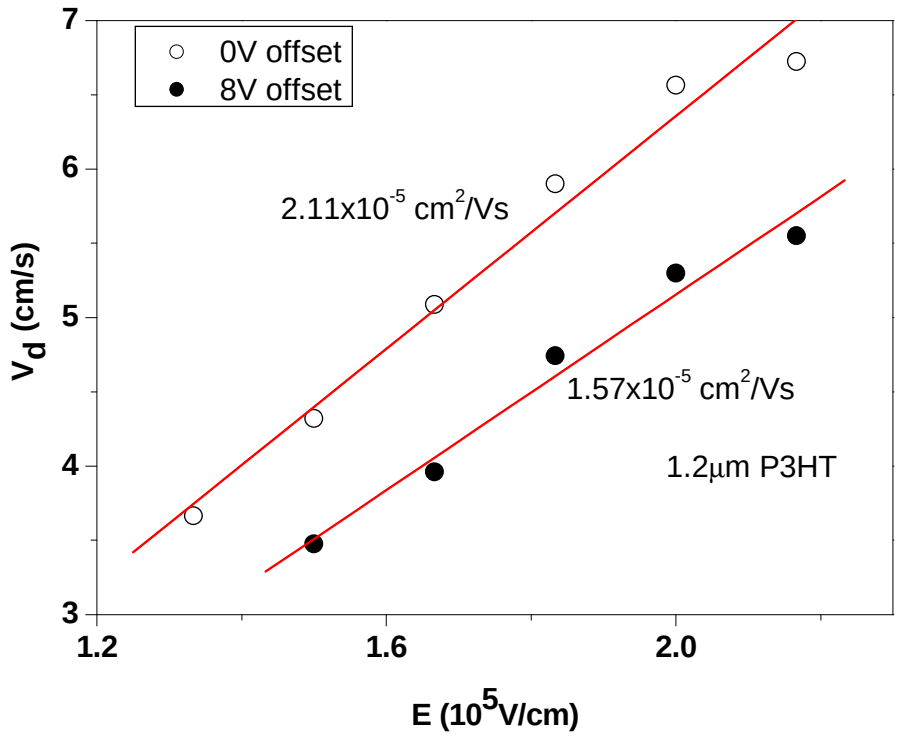

Figure 4.3.3 Velocity versus electric field

The average mobility under 0 V offset is 2.11×10^{-5} cm^2/Vs, and the average mobility under 8 V offset is 1.57×10^{-5} cm^2/Vs.

Figure 4.3.4 presents the raw DI transit curve for an ambipolar device. In order to keep the experiment under the same conditions all the measurements are taken under the voltage step V_0 of 26 V, therefore the internal electric field is always the same. As the offset voltage increases, the DI transit peak shifts to longer times, indicating that the increase of offset voltage can lead to a mobility decrease in the ambipolar P3HT device.

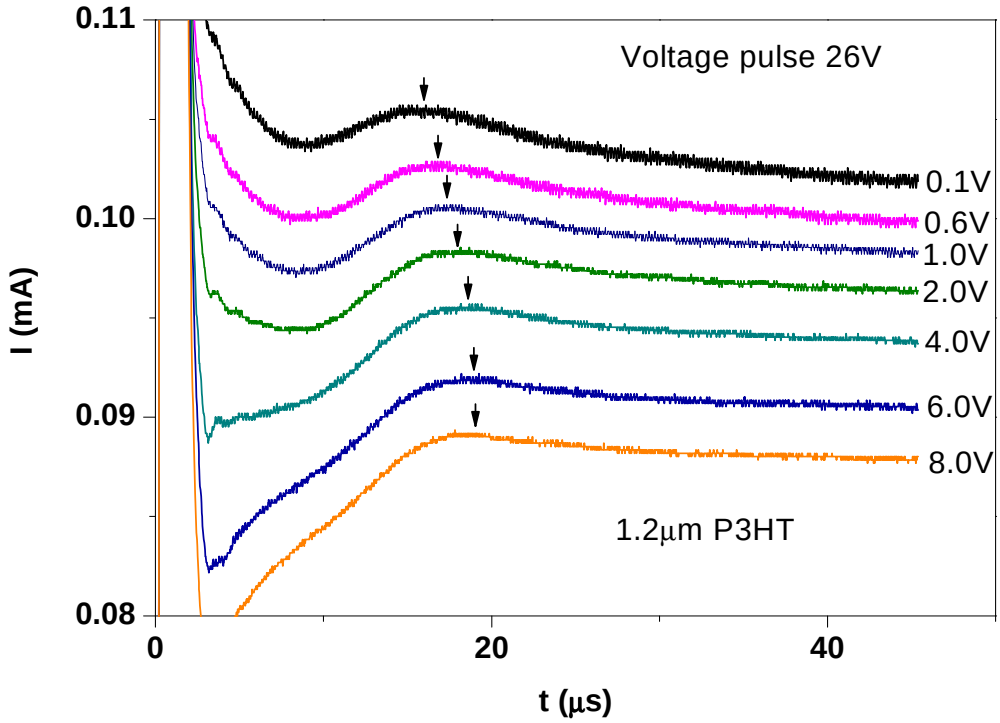

Figure 4.3.4 Current versus time for the ambipolar device under different offset voltage

The thickness of this ambipolar device is 1.2 μm. Although the offset voltage varies from 0.1 V to 8.0 V, the absolute voltage step applied on the device is kept at 26 volts throughout the whole experiment, which ensures that all data is collected under the same conditions.

Figure 4.3.5 shows the current versus time for the unipolar device, all the data is also collected at 26 V for comparison with figure 3.3.4. In this case the DI transit time is not affected by the offset voltage, indicating that the hole mobility is not related to the offset voltage in the unipolar system.

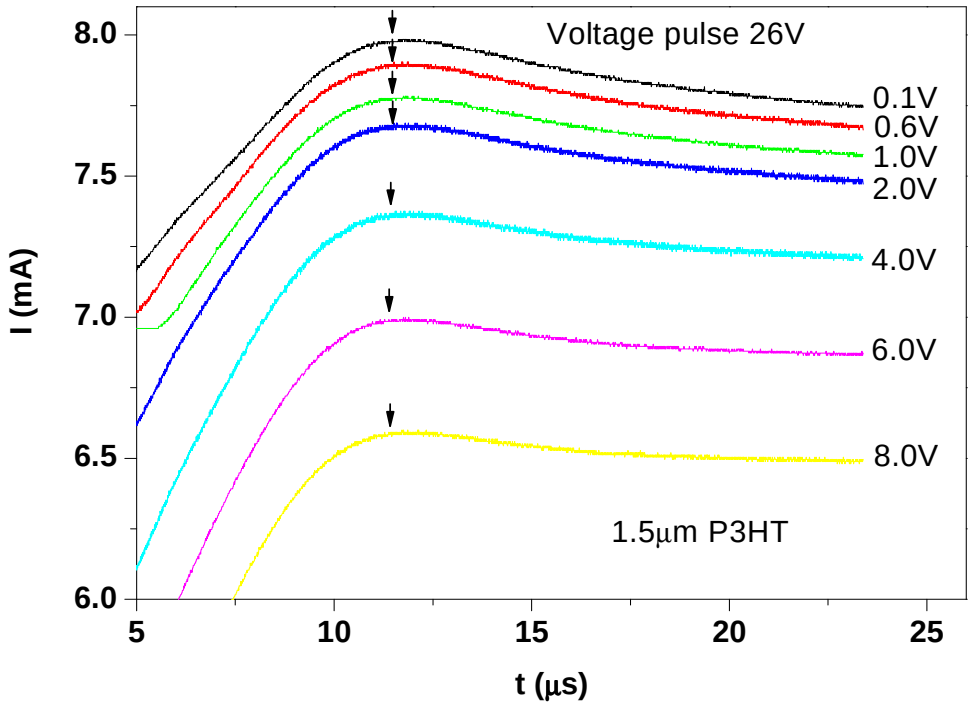

Figure 4.3.5 Current versus time for the unipolar device under different offset voltage

The thickness of this unipolar device is 1.5 μm. Although the offset voltage varies from 0.1 V to 8.0 V, the absolute voltage step applied on the device is kept at 26 V throughout the whole experiment for comparison with figure 3.3.4.

4.3.2. Discussion

After carefully fitting and analysing the *I-t* curves in figure 4.3.4 and figure 4.3.5, the hole mobility in both unipolar and ambipolar devices can be obtained. Figure 4.3.6 shows the mobility ratio, defined as the calculated mobility with nonzero offset, divided by the mobility at zero offset, i.e. μ(offset≠0)/μ(offset=0), versus the offset for three hole-only (Au–P3HT-Au) and three ambipolar (Au–P3HT-Al) devices. The hole-only devices show virtually no change in hole mobility irrespective of the offset, up to 8 V, strongly suggesting that at the experimental carrier concentrations, all hole traps are filled (if there were unfilled hole traps, then an increase in measured

mobility would result from the increased offset). For offset voltages below ~0.6 V, the data obtained for ambipolar structures is similar to those observed for hole-only devices in so far as the mobility is unaffected. This is because with the DC offset voltage less than the turn on voltage of ambipolar P3HT devices (see figure 4.3.7, the inflection point is ~0.8 V), only holes can be pre-injected into the system, thus exciton generation is prohibited. The hole mobility behaves as though it was in a unipolar device. When the offset voltage >~1 V, we observe a marked decrease in mobility as a function of offset voltage in the ambipolar architectures. This can be explained when the DC offset voltage is higher than the sample turn on voltage: both electrons and holes are pre-injected into the system and cause excited states formation, as a result of excited triplet sites interaction with free charge carriers, the hole mobility would be expected to drop. If the DC offset voltage keeps increasing, more triplet excitons are pre-generated inside the device, which can cause the hole mobility to decrease further.

We also note that the average zero offset P3HT hole mobilities for the two types of sample (unipolar and ambipolar) are in agreement, given sample to sample variation, being $\mu_{Au-Au}=(5.1\pm0.9)\times10^{-5}$ cm^2/Vs and $\mu_{Au-Al}=(4.8\pm1.8)\times10^{-5}$ cm^2/Vs. This shows that there is no difference in the samples due to the use of gold or aluminium as the top contact, such as from metal diffusion into the device.

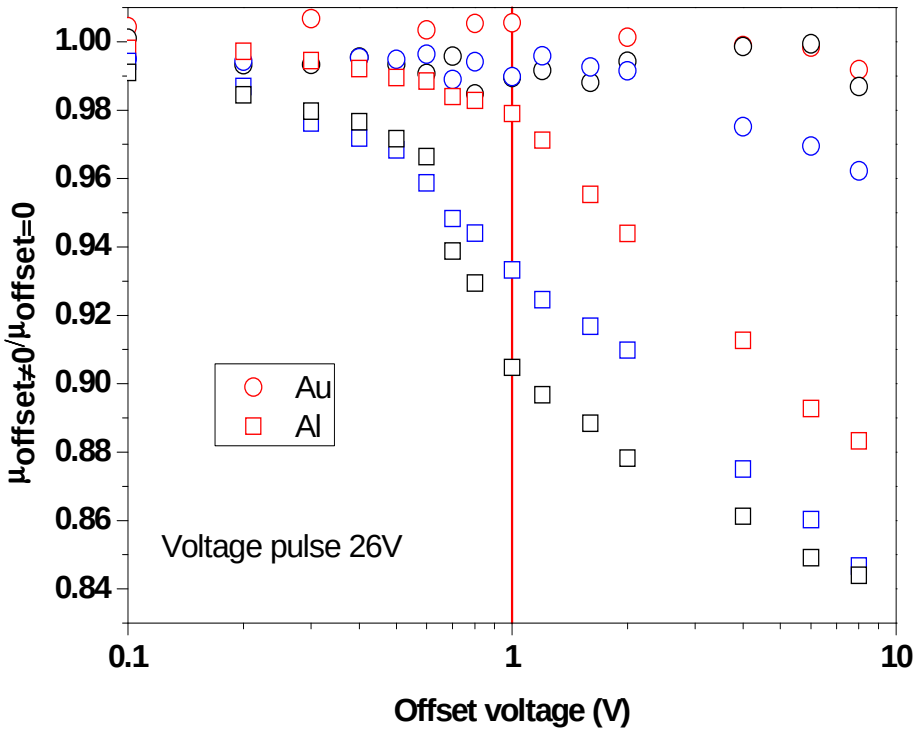

Figure 4.3.6 Mobility ratio versus the offset voltage in P3HT devices

With regards to the reproducibility, three unipolar (Au-P3HT-Au) and three ambipolar (Au-P3HT-Al) devices have been measured to confirm the reproducibility of this experiment.

The mobility reduction (in figure 4.3.6) could be argued that the reduction in mobility actually correlated with the injection of electrons and hence columbic trapping may be the cause rather than interactions with triplets. The role of trapped charge on current transport has been studied theoretically by Rackovsky *et al.*[47]. They demonstrated that trapped charge levels above ~10^{13} cm^{-3} would affect carrier mobility if the trapped charge was acting as shallow traps. In our system the electron concentration in the layers can be estimated to be at least 10^{6} times lower than the level needed to affect the dark injection pulse and any trapping of holes with free electrons would be likely to produce the excitons that we are considering

($J = en_0\mu\frac{V}{d}$, so $n_0 = \frac{I \times d}{e \times \mu \times s \times V}$, where e is electron charge, n_0 is the population of charge carriers, μ is the charge mobility, V is the voltage across the device and I is the current flow through the sample).

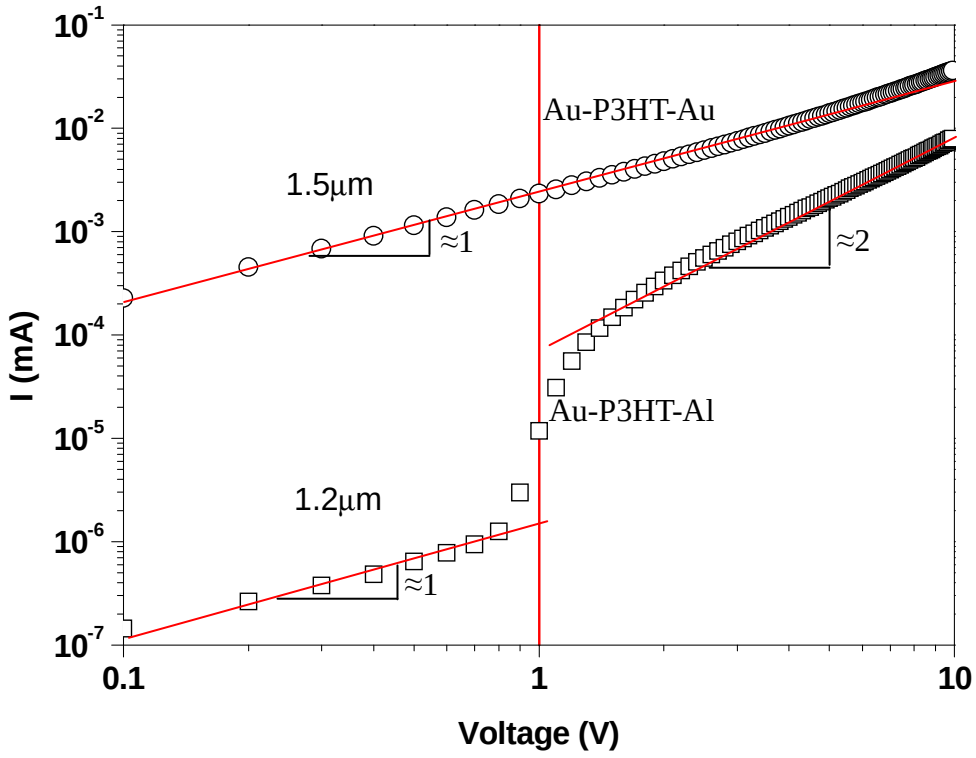

Figure 4.3.7 I-V characteristic for both ambipolar and unipolar devices
Clearly the turn on voltage for the Au-P3HT-Al ambipolar device is around 0.8V, but for the unipolar (Au-P3HT-Au) device the current density increases very smoothly with the applied voltage, therefore there is no inflection point on the curve.

Figure 4.3.7 shows the current-voltage characteristics (measured by a Keithley 236 source-measure unit) of the two types of device investigated here. We note that the hole-only characteristic displays no sharp transitions and tends towards Ohmic ($I \propto V$) regime. It also shows much higher current densities at low voltage compared to the

ambipolar device. The latter can be due to a combination of factors, such as interpenetration of the evaporated gold within the organic layer (effectively reducing the device thickness) and the efficient hole injection and extraction by gold. The ambipolar structures show typical diode device behaviour consisting of a hole-only current at low voltages, a sharp increase in current at ~0.8V (the turn-on, associated with the onset of electron injection), and a space-charge limited ($I \propto V^2$) regime developing at high voltages. Note that the onset of electron injection in figure 3.3.7 (~0.8 V) corresponds to the onset of mobility reduction (~0.6 to 1 V) seen in figure 3.3.6.

The IV characteristic in figure 4.3.7 followed Mott-Gurney law[22] perfectly. As the current density is high enough to fill up all charge trapping sites, the unipolar device is under a trap-free, high field limit condition, leading the current density proportional to the applied voltage, $J \propto V_{applied}$. So the slope of the IV curve in a double log plot is approximately 1.

However for the ambipolar device, when the voltage is much less than 1 V, the device follows Ohm's law. The current density is proportional to the applied voltage, $J \propto V_{applied}$, with the slope of this IV characteristic at about 1. When applied voltage is around 1 V, the injected charge carrier density is still too low to fill up those low energetic sites inside the organic, the charges will be captured by these empty traps, and thereby immobilise most of the injected carriers, leading to a greatly reduced current at lower injection levels, with $J \propto V_{applied}^{n}$. When applied voltage is higher than 2 volts, all traps will be filled and the current will reach the space charge limited trap-free condition. According to Mott-Gurney law, the current density should be proportional to the square of applied voltage $J \propto V_{applied}^{2}$, and indeed the slope of the IV characteristic curve is 1.98 (with R^2=0.999) above 2 V in the ambipolar device.

We attribute the reduction in hole mobility (figure 4.3.6) to interactions of the holes with excited states present in the P3HT. This is for the following reasons. If the

lengthening of the DI arrival time were solely due to the injection of electrons into P3HT and the corresponding electrostatic screening effect of these electrons, then the arrival time would not be affected by the offset.

Clearly, electrons will be readily trapped in our devices and, as a consequence, will directly interact (electrostatically) with injected holes. We observe an offset hole current, however, prior to the application of the DI step, therefore, it is reasonable to assume that all trapped electrons will have formed a bound electron-hole pair before the DI measurement is carried out. Given the long time (~200 ms) for which the offset is applied before the DI experiment is carried out, it might be argued that most bound pairs would be in the form of triplet excitons. Triplet excitons, however, are long lived, thus can be expected to diffuse throughout the bulk of the P3HT film prior to the DI pulse being applied[48].

Chapter five: TPD Results

5. TPD results

5.1. Time of Flight (electron and hole) in TPD

5.1.1. Results

Figures 5.1.1 (a), (b) and (c) show ToF hole photocurrent transients, and figures 5.1.1(d), (e) and (f) present the ToF electron photocurrent transients for an ITO-TPD-Al architecture, both of them measured from 3 volts to 8 volts reverse bias. The transit time t_{trans} can be obtained from the inflection point in the log-log plot of current versus time[49], which scales correctly with the applied bias, and it is clearly detectable for both hole and electron photocurrents. This suggests that even though TPD is used for hole transport purposes, surprisingly, it can transport both holes and electrons, both mobilities of this sample are calculated using equation 5.1.1.

$$\mu = \frac{d^2}{Vt} \qquad \text{Equation 5.1.1}$$

Where d is the sample thickness, V is pulse voltage amplitude, and t[50] is the transient time (t_{trans}).

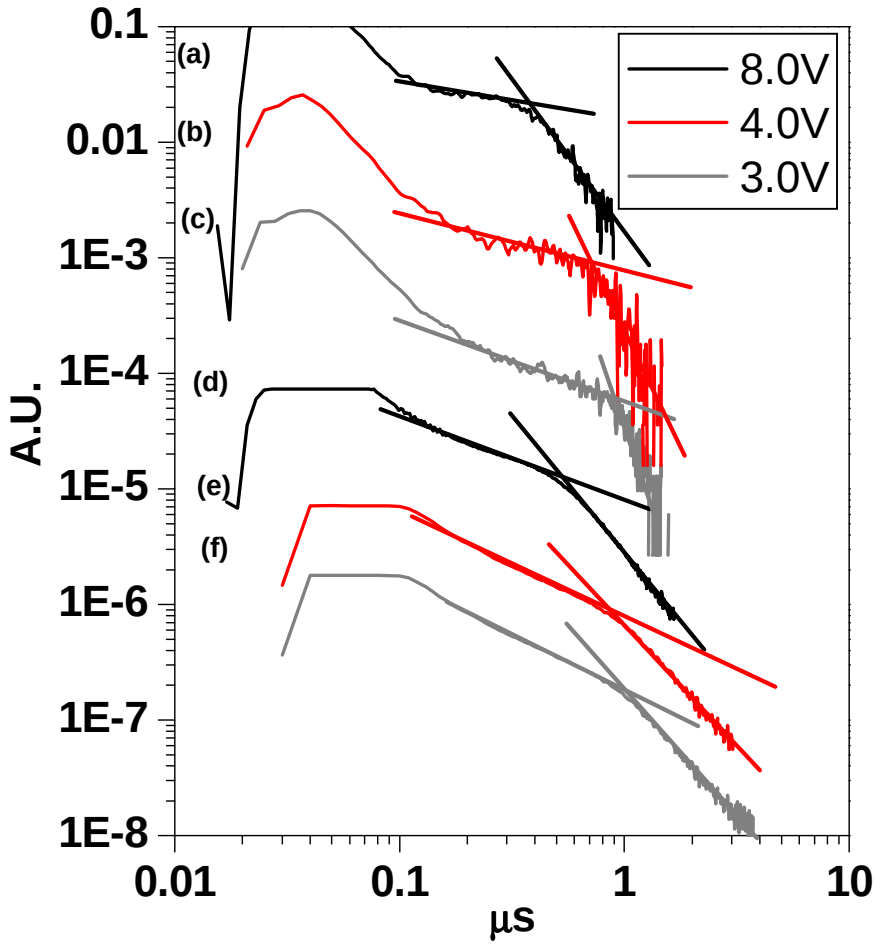

Figure 5.1.1 Typical time of flight currents obtained in a 600 nm thick TPD devices

Figures (a) (b) and (c) are hole photocurrents at 8 V, 4 V, 3 V reverse bias, and figures (d) (e) and (f) are electron photocurrents at 8 V, 4 V, 3 V reverse bias. The inflection time t is used for mobility calculation.

The photocurrent transients are dispersive in figure 5.1.1, possessing a decay with a characteristic ‘‘knee’’ on a double logarithmic plot. Dispersive transport is an indication of disorder, which may be due to trap states in the hole transporting TPD[17]. Note that, the photocurrent transients become less dispersive as the electric field increases, this can be attributed to fast carrier de-trapping under the influence of

the electric field[49], as has been studied in detail[17]. The electron photocurrents are more dispersive than the hole photocurrents, because electron transport might be more sensitive to an ambient environment (such as oxygen and moisture) than hole transport, resulting in more electron trapping sites inside the device, and causing the ToF photocurrent to become more dispersive.

The calculated mobility is shown as a Poole-Frenkel plot in figure 5.1.2, showing virtually no electric field dependence at room temperature, which is comparable to that reported in the literature[51] for TPD. We note that, although our sample is a hole transport material, the electron mobilities ($7x10^{-4}cm^2/Vs$) in the TPD sample are of the same magnitude as the hole mobilities ($1x10^{-3}cm^2/Vs$). This strongly suggests that a TPD device can transport both holes and electrons with a very similar velocity.

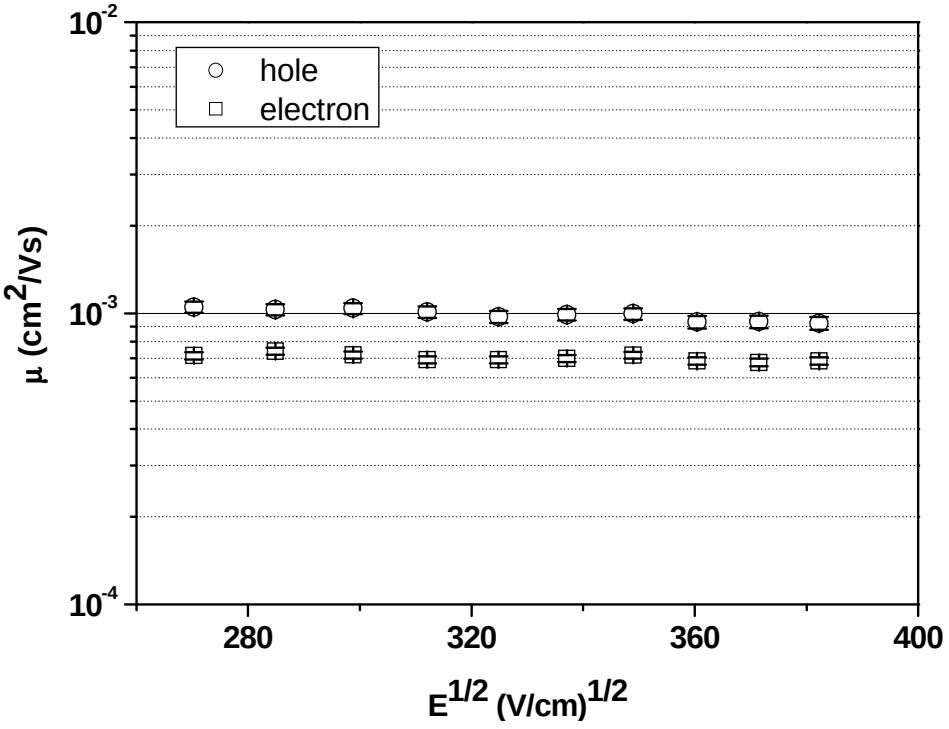

Figure 5.1.2 Poole-Frenkel plot of the hole and electron mobility

Figure 5.1.3 shows the hole and electron drift velocities as a function of the applied field, the slope of linear fit gives a mobility value of $(9.72\pm0.45)\times10^{-4}$ cm^2/Vs for hole transport and $(6.97\pm0.19)\times10^{-4}$ cm^2/Vs for electron transport. Both linear fits pass through the origin, which means that both electron and hole mobility is electric field independent, and this agrees with figure 5.1.2. Both hole and electron mobility was measured once again, and presented in figure 5.1.4

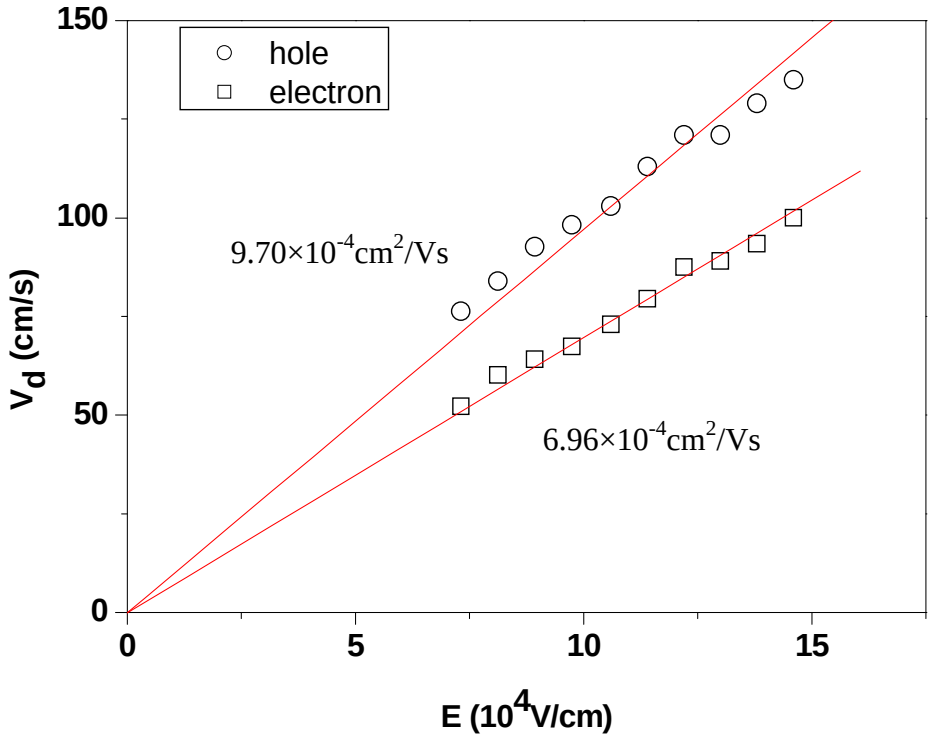

Figure 5.1.3 Velocities of both hole and electron as a function of electric field, at room temperature

The fittings are forced to go through the original coordinate, with R at more than 0.99.

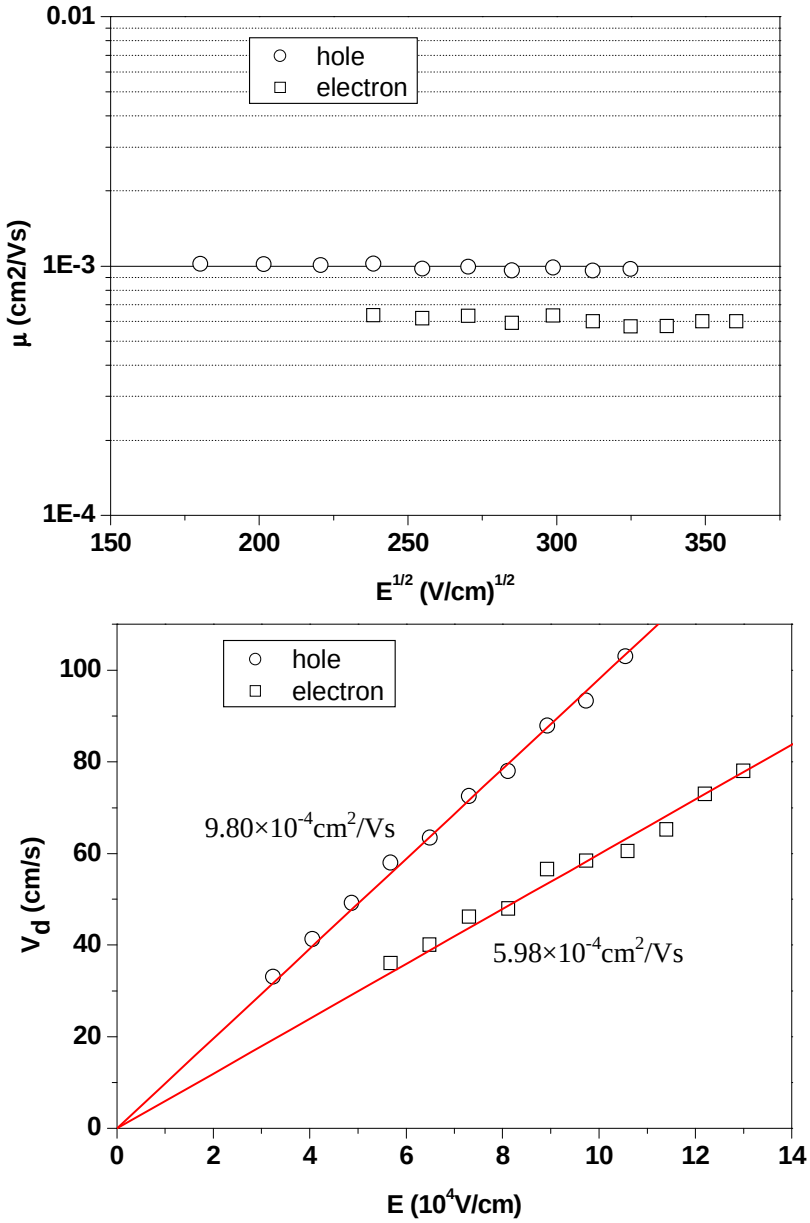

Figure 5.1.4 Repeats of the hole and electron mobility, Poole-Frankel plot (top) and v_d versus electric field (bottom).

5.1.2. Discussion

(TPD) is a well known hole transporter[52-54] and is widely used as a hole transport layer in organic light-emitting diodes (OLED)[55]. For a very long time it has only

been considered as a hole transport material, and hole mobility has been widely reported ranging from pure TPD samples to doped mixtures at various temperature ranges [56-58]. Electron mobilities have not been generally considered, until now there has been only few reported papers on the electron mobility in TPD[59], their results are much lower than what we have observed. But they did not present the measuring technique and method, and the way to retrieve their data is unknown. Since the light emission is found in TPD-only devices [30, 48], this is a firm evidence that TPD contains excited states during operation, implying that both holes and electrons must be injected into the device, and transported by the organic to meet and form excitons. This could mean that hole transport organics can also transport electrons. Indeed, the hole and electron mobilities for vapour-deposited TPD films are measured by the time-of-flight (ToF) method. The hole mobility for the TPD device at room temperature is around $1x10^{-3}$ cm^2/Vs, which is comparable with the literature[60], and the electron mobility for the same device under the exactly same condition is around $7x10^{-4}$ cm^2/Vs

In conclusion, we have measured a reproducible mobility for both holes and electrons travelling in TPD (figure 5.1.4). We suggest that the reason it has been defined as a hole transporting material is not because of its hole-only transporting characteristics, as the mobility of both hole and electron carriers are quite similar. Thus, the reasonable explanation could depend on contact resistances (the energy barrier between the electrodes and the organics). The energy difference between the work function of ITO (4.9eV) and HOMO level of TPD (5.5eV) is smaller than that between the work function of aluminum (4.3eV) and LUMO level of TPD (2.55eV), as a result the hole extraction is much more efficient than the electrons.

5.2. DI for thin TPD device

After succeeding with the organic polymer P3HT, we tried another small molecular organic called N,N'-diphenyl-N,N'-bis(3-methylphenyl)-4,4'-diamimobiphenyl (TPD) to test the general validity of our theory among organic semi conductive materials, and also to complete our theory. There is, nevertheless, still one flaw with the P3HT experiment, exciton formation inside the device could lead to a light output of the diode, although no luminescence has been detected from P3HT, this could be caused by the relatively longer electroluminescence wave length (660 nm), which is far from the sensitive region (~520 nm) of our photo-detector. Luckily the electroluminescence of TPD is around 520 nm and light output can be detected.

Compared to P3HT, TPD is relatively more stable in atmosphere and less dispersive. So, the time-of-flight method is also considered to reinforce our theory in another aspect. So considering the experimental consistency and the familiar techniques which have already been successful with P3HT, dark injection measurement has still been chosen to confirm our theory at this stage, while time-of-flight technique will be discussed in the following chapter.

5.2.1. Results

Although the sample is an ambipolar device, hole DI transients show a clear space-charge cusp, as presented in figure 5.2.1 (a). This suggests that the electron injection within these TPD devices is not balanced to that of the holes.

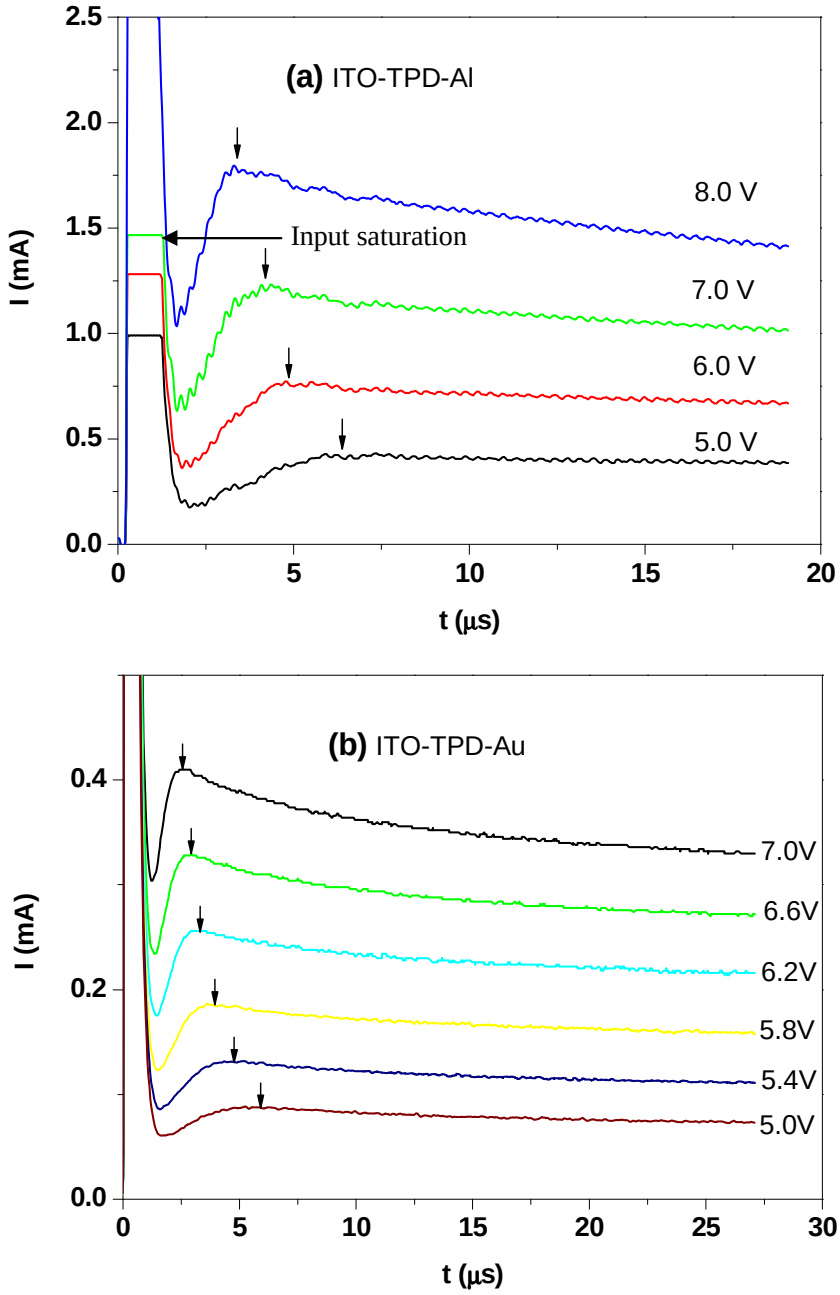

Figure 5.2.1 Original dark injection data recorded from the oscilloscope

Figure 5.2.1 (a) shows the DI transients obtained under different bias without offset in an ambipolar (ITO-TPD–Al) sample. Figure 5.2.1 (b) shows the DI transients obtained under different bias without offset in a unipolar (ITO–TPD-Au) sample. In both graphs the peak time t_{DI} scales correctly with applied bias and is clearly detectable.

The resulting calculated mobility and drift velocity at different fields are shown in figure 5.2.2 and 5.2.3, for the ambipolar and unipolar sample respectively. Both of them show slight field dependence. More importantly, both of them are comparable to those reported in the literature[60], thus confirming our experimental techniques.

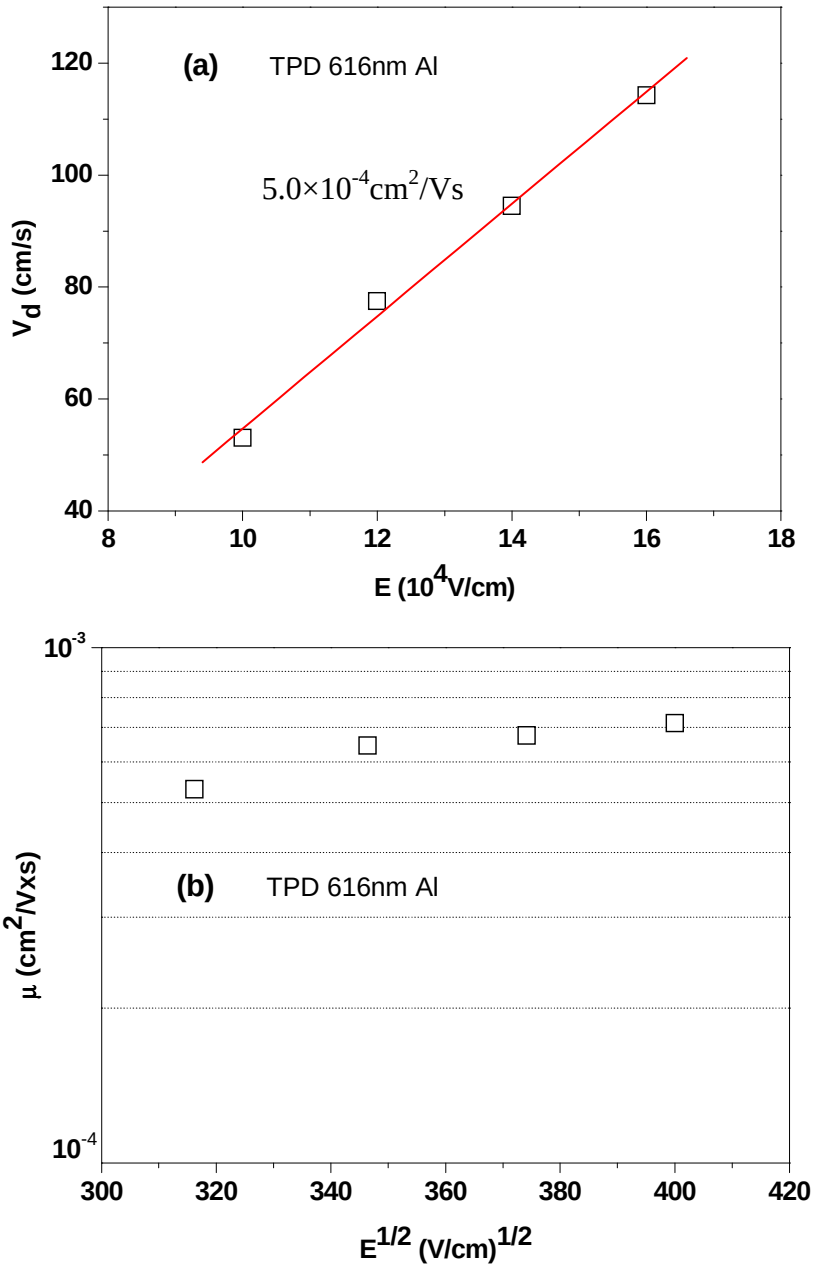

Figure 5.2.2 Mobility of ambipolar device (ITO-TPD-Al)

Figure 5.2.2(a) represents the hole drift velocity versus electric field, and figure 5.2.2(b) is the Poole–Frenkel plot of hole mobility

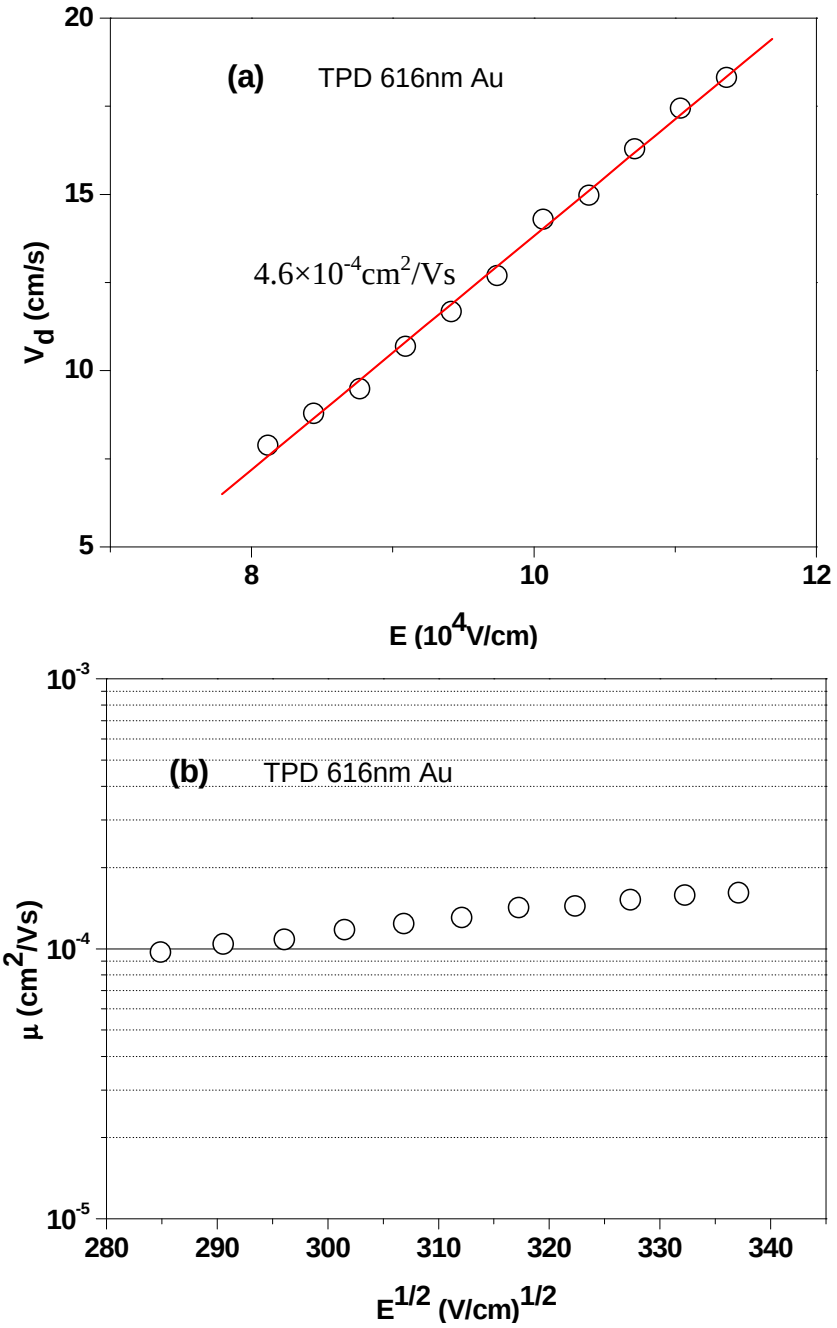

Figure 5.2.3 Mobility of the unipolar device (ITO-TPD-Au)

Figure 5.2.3 (a) shows the drift velocity of holes versus electric field, and figure 5.2.3(b) is the Poole–Frenkel plot of hole mobility in the unipolar TPD device.

We note that the average zero offset TPD hole mobilities for the two types of sample (unipolar and ambipolar) are slightly different but still the same order of magnitude.

Given sample to sample variation, the mobility of the ambipolar and unipolar devices are μ_{ITO-Al}^{hole} = (5.0±0.7) ×10^{-4} cm^2/Vs and μ_{ITO-Au}^{hole} = (1.6±1.2) ×10^{-4} cm^2/Vs. This difference in the samples may be due to the use of gold or aluminum as the top contact, such as metal diffusion into the device or different contact resistance.

The DI experiments carried out with zero offset on the ambipolar sample of figure 5.2.1 (a), and the DI transit at different voltage steps with 4V offset on the same sample, are shown in figure 5.2.4. The DI is detectable and the cusp peak clearly scales with the electric field.

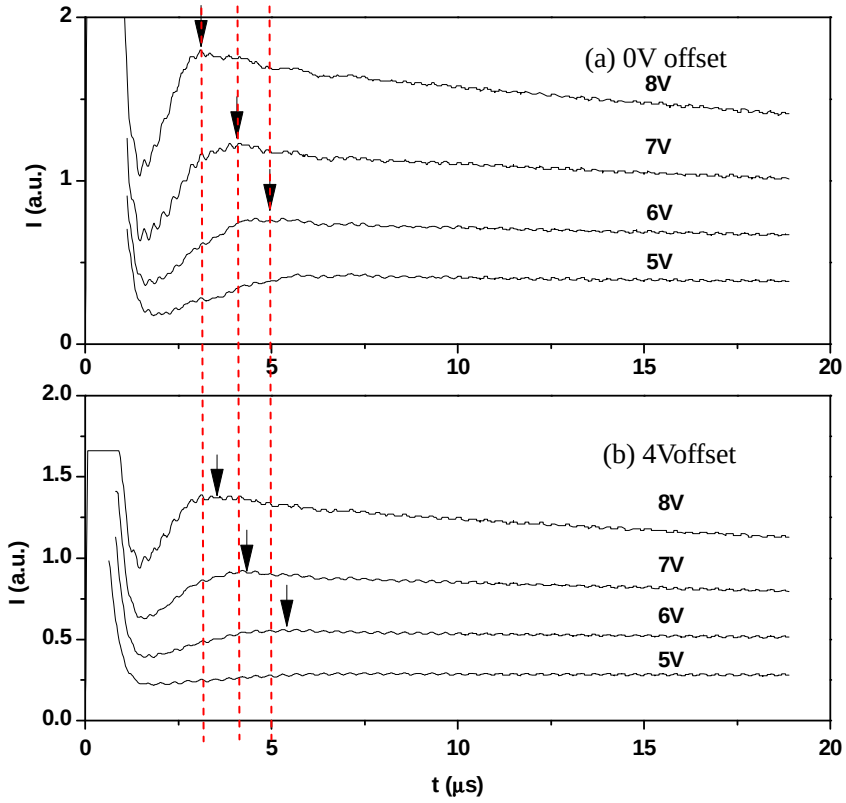

Figure 5.2.4 (a) The current trace of the ambipolar TPD device without offset, (b) the current trace of the same device with 4V offset at different fields.

The calculated hole mobilites with and without offset are illustrated in figure 5.2.5. They show a slight electric field dependence, both with and without offset, in this specific case the offset voltage is 4V, where, both lines of best fit do not pass through

the origin. In these graphs it clearly shows that under the same electric field, the mobility of the ambipolar device with 4V offset voltage (1.87×10^{-4}cm^2/Vs) is obviously less than that with zero offset voltage (2.30×10^{-4}cm^2/Vs).

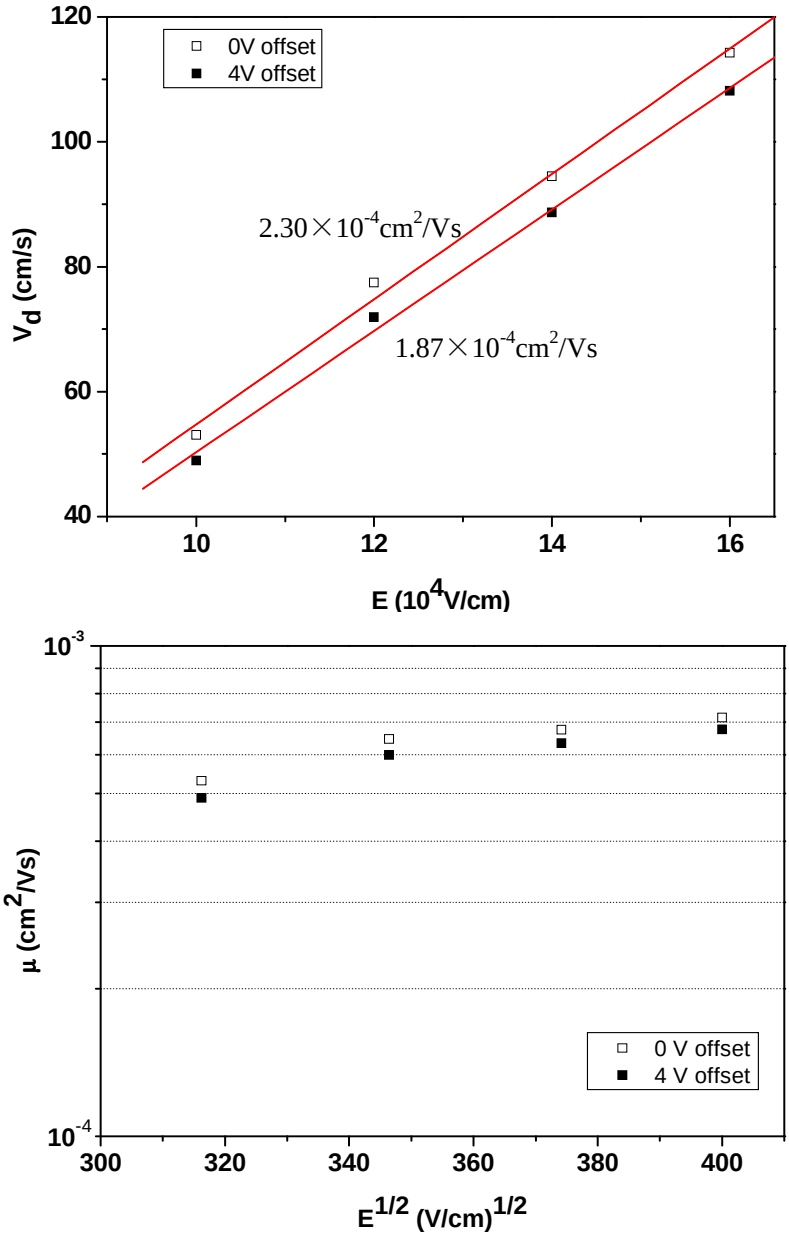

Figure 5.2.5 Poole–Frenkel plot of hole mobility (a) and drift velocity versus the electric field (b) in the ambipolar device both with and without offset voltage. The hollow squares represent the mobility of the device with zero offset voltage, and the filled squares represent the mobility with 4 V offset.

Another way of studying the effect of an offset is to keep the same electric field and vary the offset bias. Figure 5.2.6 presents the raw dark injection curves for the ambipolar device, with all the measurements taken under 7V voltage step. As the offset voltage increases, the DI transit peak shifts to longer times, which indicates that an increase in offset voltage can lead to a mobility decrease in the ambipolar TPD device.

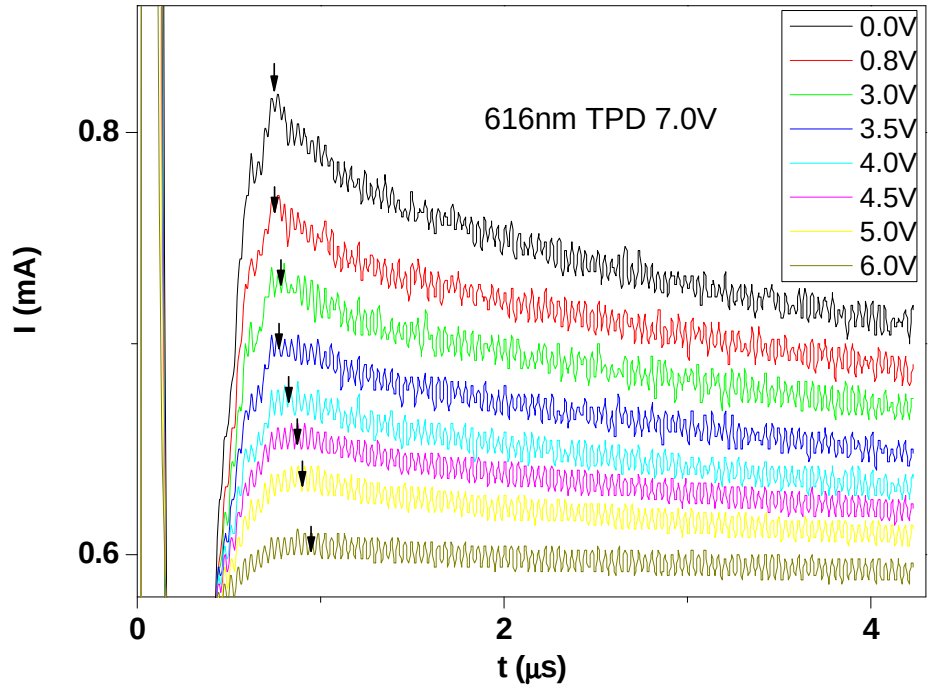

Figure 5.2.6 Current versus time for the ambipolar device under different offset voltage. The measurement pulse is 7 V.

The thickness of this ambipolar device is 610 nm. The offset voltage varies from 0.0 volts to 6.0 V, the absolute voltage applied to the device was kept at 7.0 V through the whole experiment, ensuring that all the data is collected under the same condition.

In contrast to figure 5.2.6, figure 5.2.7 shows the current versus time for the unipolar device (data collected under a 7V voltage step). In figure 5.2.7 the DI transit time does not vary with offset voltage, which indicates that the mobility is not related to

the offset voltage in the unipolar device.

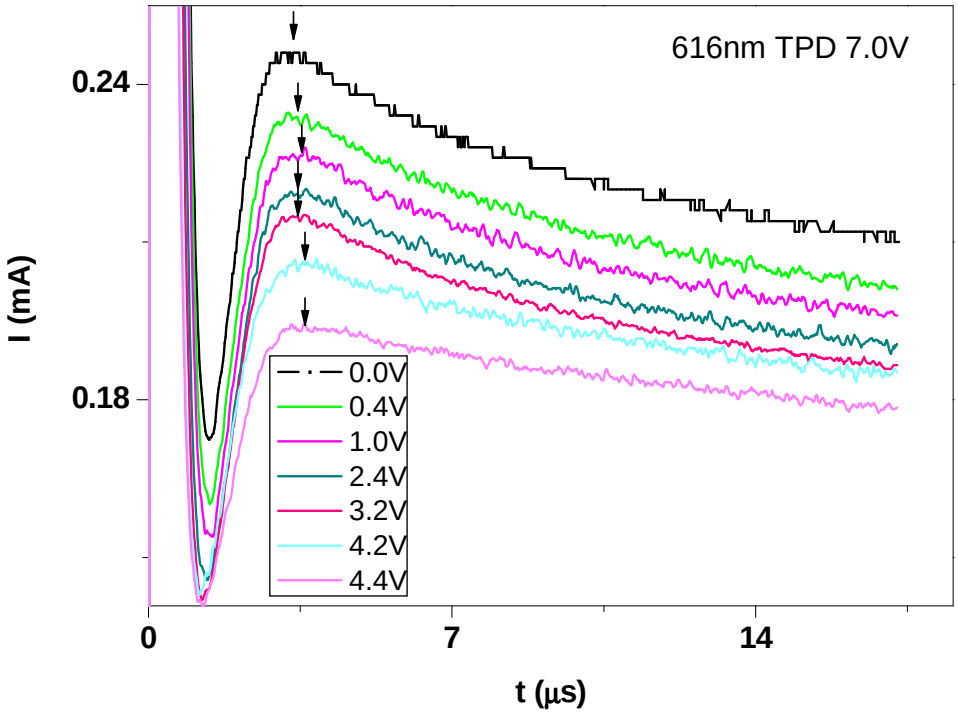

Figure 5.2.7 Current versus time for the unipolar device under different offset voltage. The measurement pulse is 7V.

5.2.2. Discussion

Figure 5.2.8 shows the mobility ratio (as defined in section 3.3 as μ(offset≠0)/μ(offset=0)) versus the offset for two hole-only (Au–TPD-Au) and two ambipolar (Au–TPD-Al) devices. All the DI meaurements are taken under 7 V voltage pulse. The hole-only devices do not show significant change in hole mobility, up to 5 V, strongly suggesting that, at the experimental carrier concentrations, all hole traps are filled (if there were unfilled hole traps, then an increase in measured mobility would result from the increased offset). For offset voltages below ~1.6 V, the data obtained for ambipolar devices shows a slight increase with offset bias, suggesting that the experimental carrier concentrations could be too low to fill up all hole traps. Enhancing the offset voltage could cause more and more traps to be filled,

hence the mobility of the device is slightly increased. When the offset voltage >~1.6 V, however, we observe a marked decrease in mobility with increasing offset in the case of ambipolar devices only.

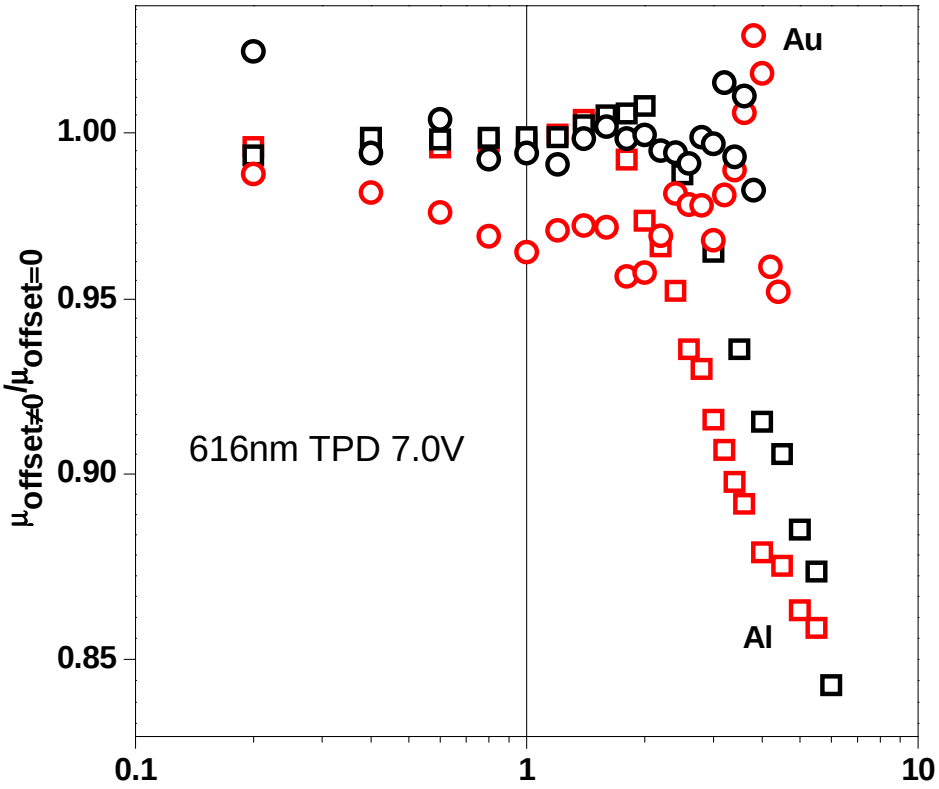

Figure 5.2.8 Mobility ratio versus offset voltage in TPD devices

Two unipolar (ITO-TPD-Au) devices (circular dots) and two ambipolar (ITO-TPD-Al) devices (square dots) are used to check the reproducibility of this experiment.

Figure 5.2.10 (a) shows the current-voltage characteristics of the two types of device investigated by DI. The ambipolar structures show typical diode device behavior consisting of a hole-only current at low voltages, a sharp increase in current at ~1.2 V (the turn on, associated with the onset of electron injection), and a space-charge limited ($I \propto V^2$) regime developing at high voltages. We note that the onset of electron injection in figure 5.2.10 (a) (~1.2 V) corresponds to the onset of mobility

reduction (~1.4 to 1.6 V) seen in figure 5.2.8. It also shows much higher current densities at lower voltage for the unipolar device compared to the ambipolar structure. This can be due to a combination of factors such as interpenetration of the evaporated gold within the organic layer (effectively reducing the device thickness) and efficient hole injection and extraction by gold or the contact resistance of electrodes. Before turn on, the current of the ambipolar device (ITO-TPD-Al) is extremely low (around 10^{-11} A) in figure 5.2.10, under this current density not many carriers have been injected into the device, therefore hole traps are not filled by the carriers. Increasing the voltage results in more and more carriers being injected into the system, these carriers will gradually fill up the hole traps and cause the measured mobility to increase until the dc offset voltage reaches the turn on voltage (~1.2 V in figure 5.2.10), and this is consistent with figure 5.2.8, where there is a slight increase of the mobility as the offset voltage is below ~1.4-1.6V. However, according to figure 5.2.10 the current of the unipolar device (ITO-TPD-Au) is roughly 10^{-9} A if the voltage is below 1.2V, with this much current flowing through the sample, the charge concentration is sufficient to fill all hole traps inside the device.

The different current before turn on voltage is quite likely due to the different leakage currents. Since the current is extremely low (around nA and pA), the absolute difference of these currents is not significant. Due to sample to sample variation the leakage current may slightly different as well, this is quite common in semiconducting devices. There is also a turn on behaviour in the ITO-TPD-AU device, this may be caused by the mismatch of electrodes.

From studies done on wide varieties of organic materials with different metal interfaces, it is concluded that there is a relation between the dipole formation, work function for the organic material and the work function of the metal used [61, 62]. A main trend observed is that there is always a negative vacuum level shift, which causes a lowering of the vacuum level. Based upon this trend, the origin of the dipole

at the interface and the cause of the vacuum level shift were explained by Ishii *et al*. and the mechanism was illustrated in Figure 5.2.9 (adapted from Ref. [61]). The main cause of the dipole can be electron transfer between the metal and the organic, as shown in Figure 5.2.9, causing the positive and negative charges to separate across the interface. The origin of the charge separation at the interface (and resulting electric field) is similar to conventional band bending, which also results from the charge transfer across an interface. In the case of the interfacial dipole, however, the electric field is confined to a very narrow region, not more than 1-2 nm[63]. This kind of electron transfer occurs for combinations of a strong donor organic-high work function metal as shown in Figure 5.2.9 (a), or a strong acceptor organic-low work function metal as shown in Figure 5.2.9 (b)[37].

(a) (b)

Figure 5.2.9 the interface dipolar at the metal organic interface

It is well recognized that oxidative treatments such as oxygen plasma or UV ozone could dramatically enhance hole injection. Oxidative treatments incorporate more oxygen onto the surface, and this could cause a surface rich in negatively charged oxygen resulting in a dipole layer formation near the surface region of ITO, hence increasing the work function of the ITO anode.

Therefore the dipolar structure at the ITO-TPD interface could be different from that at the TPD-AU interface, and this dipolar structure could change the work function of the electrodes, and resulting in two mismatched electrodes.

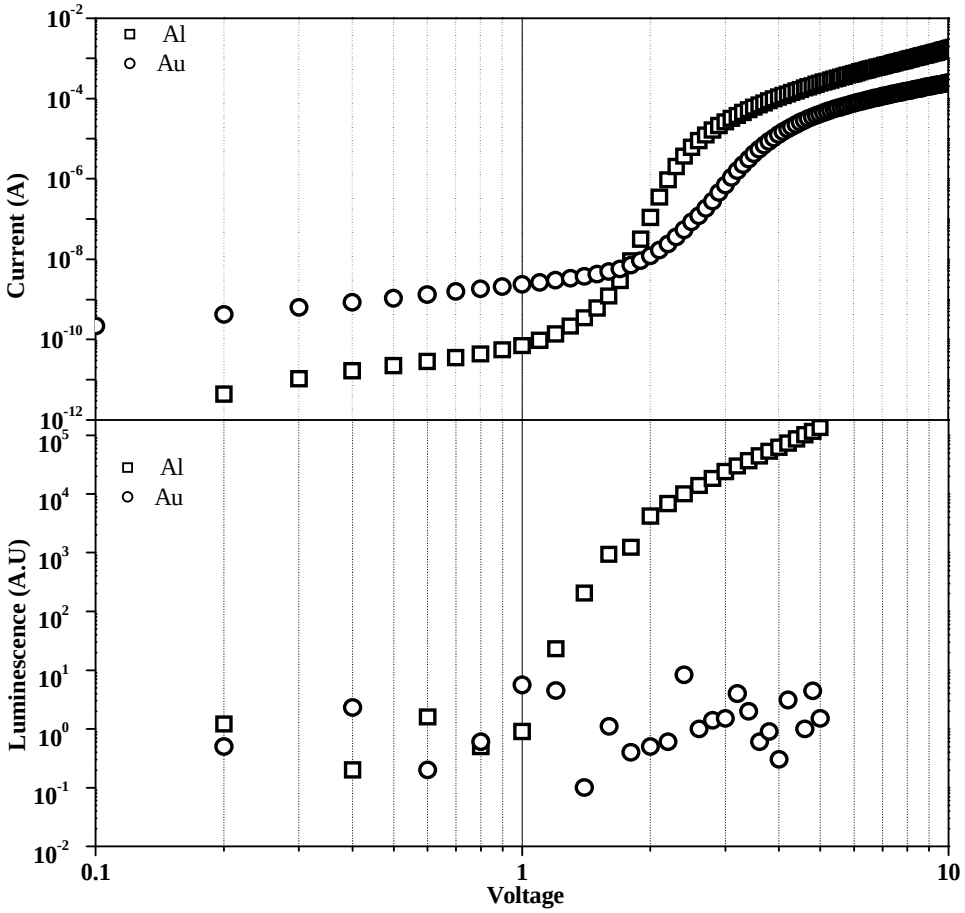

Figure 5.2.10 IV characteristics and luminescence plot of TPD devices

On top are the IV characteristics of both the unipolar and ambipolar devices. Before turn on point (~1.2V), the current of the ambipolar (ITO-TPD-Al) device is almost two orders of magnitude lower than the unipolar device (ITO-TPD-Au). The bottom graph presents the luminescence characteristics of TPD devices. In both graphs, circles represent the unipolar device, and squares indicate the ambipolar device.

It should also be noted that light output can be observed from the ambipolar (ITO-TPD-Al) device but not from the unipolar (ITO-TPD-AU) device. This was measured using a square wave from a pulse generator and detected using a Thorn EMI 9202V S-20 Photomultiplier and SignalRecovery 7265 lock-in amplifier. All

sample measurements (I-V-L and DI) were carried out in a vacuum (~7×10^{-5} mbar) to reduce device degradation.

We are able to unequivocally link the reduction in hole mobility (above ~1.6V in figure 5.2.7) to the presence of excited states, as it is not only consistent with the inflection point in the IV curve of an Al cathode sample occurring at ~1.4V (see figure 5.2.10), but also with significant light output from such a device occurring above ~2 V (see figure 5.2.10). This is further confirmed by the Au sample results, where there is no significant change in hole mobility up to offset voltages of 4.5V (figure 5.2.8), consistent with the lack of luminescence shown in figure 5.2.10.

We attribute the reduction in hole mobility (Fig. 5.2.8) to interactions of the holes with excited states present in the TPD materials, and the mechanisms are exactly the same as we discussed in chapter 2.3 for P3HT materials. First, if the transiting hole has the same spin state as the hole on the triplet, then the exciton acts as a blocked site for the transiting hole and will reduce the mobility. Secondly, if the transiting hole has a different spin state to that on the exciton, then there are two possibilities. The triplet can be quenched by the free carrier or can interact with it, leaving a hole and triplet, resulting in an effective scattering interaction. Both of these processes will slow down the charge carriers and reduce the hole mobility.

Until now, the hole mobility in both poly-(3-hexylthiophene) and TPD samples are measured by the dark injection transient technique in both hole-only and ambipolar devices. By applying a small offset bias prior to the voltage step, electronic excited states are generated in the ambipolar but not in the hole-only devices. The presence of excited states reduces the room temperature hole mobility by as much as 15% compared to that measured without offset, in contrast to the hole-only devices where no significant mobility reduction is seen at the same, or indeed higher, current densities. We attribute the lower mobility to interactions between the charge carriers and the long-lived triplet states and to an effective reduction in the number of

transport sites available.

5.3. ToF with forward bias

5.3.1. Results

A voltage pulse is triggered 700ns before the laser pulse to pre-generate excitons inside the ambipolar device, and the voltage step lasts approximately 30ms which is long enough to provide the electric bias for the whole ToF measurement. Figure 5.3.1 presents the ToF curve on the oscilloscope. The voltage step started at -7×10^{-4} s (given the first RC discharge peak), which means it started 700ns before the laser pulse is triggered (given the second RC discharge peak, and this is counted as the starting time of the measurement, defined as zero), and this period is certainly long enough for triplet formation. During laser pulse incidence a thin layer of free carriers can be generated into the system, and as a result the current density is enhanced after the laser is triggered. By analysis the carrier transit time t_{trans} and the hole mobility of the sample device can be obtained. Typical current-time traces are shown in figure 5.3.1 for varying bias 3 Vto 10 V.

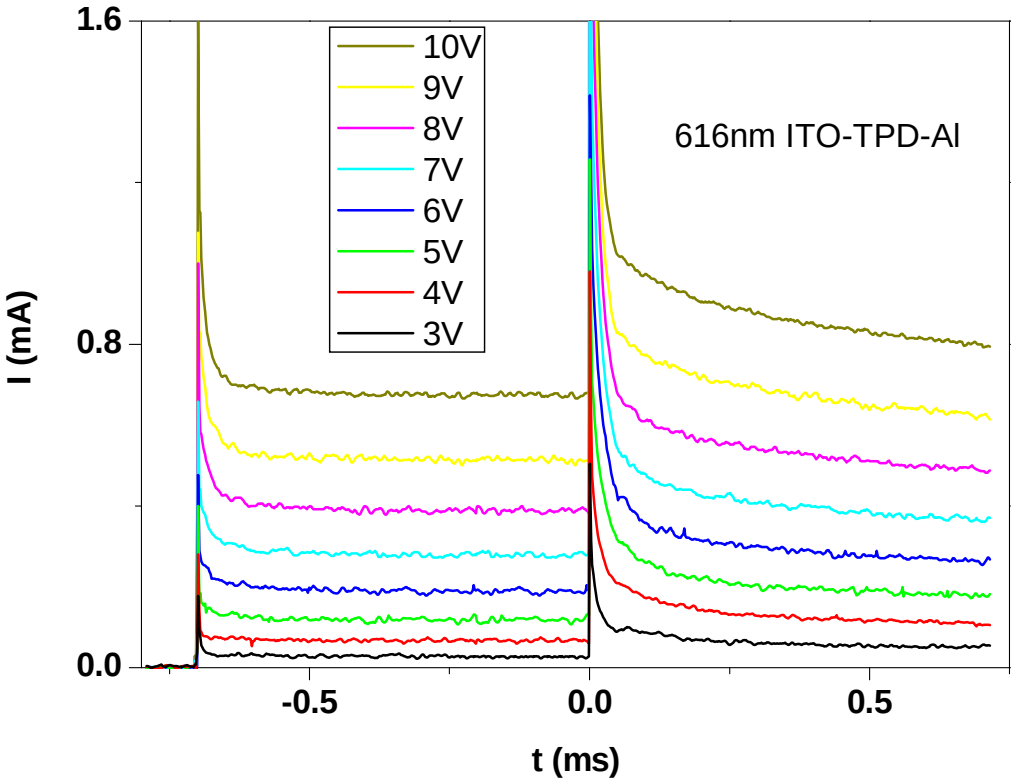

Figure 5.3.1 Raw ToF data from oscilloscope

The first peak around -7×10^{-4} s is the RC displacement current caused by the voltage step, and is followed by a constant dark current. The second peak around 0s is the photocurrent caused by the laser pulse. For times $t>0$ the resulting current is simply the sum of the dark current and photocurrent.

In order to analyse the ToF photocurrent the pre-laser dark current is subtracted and the resulting photocurrent plotted in figure 5.3.2. Both graphs show a clear transit "knee" on the *I-t* curves which indicates this material is not too dispersive.

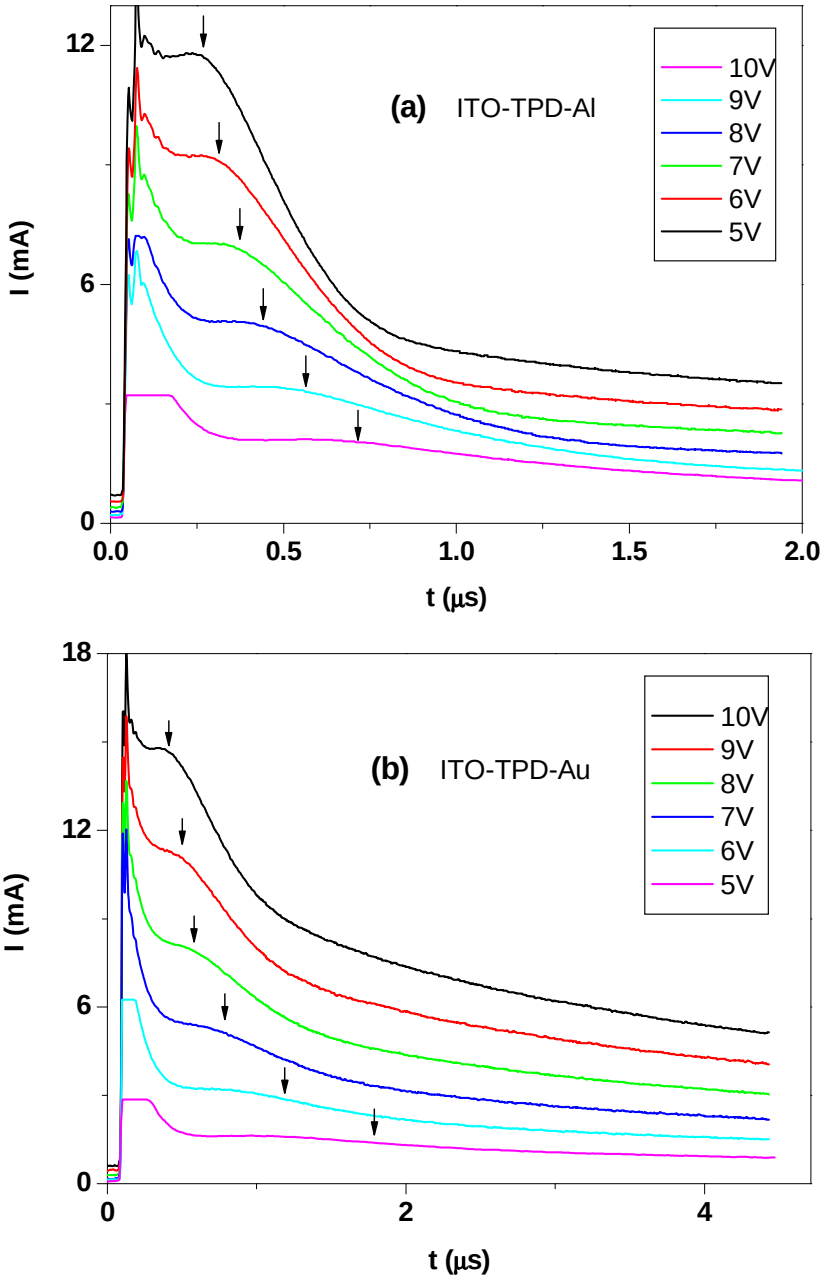

Figure 5.3.2 *I-t* curves of both unipolar and ambiploar devices.

Figure 5.3.2 (a) indicates the ambipolar device, and figure 5.3.2 (b) shows the current trace of the unipolar device, all devices are measured in a voltage range between 5 V to 10 V.

5.3.2. Discussion

Using the arrival times from figure 5.3.2, a Poole–Frenkel plot of hole mobility from both unipolar and ambipolar devices is displayed in figure 5.3.3. Two ITO-TPD-Au devices and two ITO-TPD-Al samples were measured to check the reproducibility. In the Poole-Frenkel plot, the unipolar device shows an increase of hole mobility with the square root of electric field typical of organics, however, the ambipolar device shows no such increase.

For the unipolar device there is an absence of pre-generated excitons, therefore in the Poole–Frenkel plot the mobility is slowly increasing with the electric field just like other disordered semi conducting materials that are electric field dependent. The reason for this increase has already been discussed in chapter 1.2. using equation 1.2.2. However, inside the ambipolar device, the triplet states are pre-generated, therefore free charge carriers could be scattered by the excited sites with a relatively longer lifetime, this affects the mobility in the Poole–Frenkel plot. Unlike the mobility behaviours inside the unipolar device, instead of going up, the hole mobility of the ambipolar device almost remains the same with the increase of electric field. The current before laser pulse in the ambipolar device is higher, if there is any trap filling, the mobility of the ambipolar sample should increase, but in contrast there is no such increase, implying that the mobility of the field independent behaviour in the ambipolar device is due to the triplets blocking and scattering. However there is another possibility that the traps have already been filled by the excess injected charges due to the higher current density.

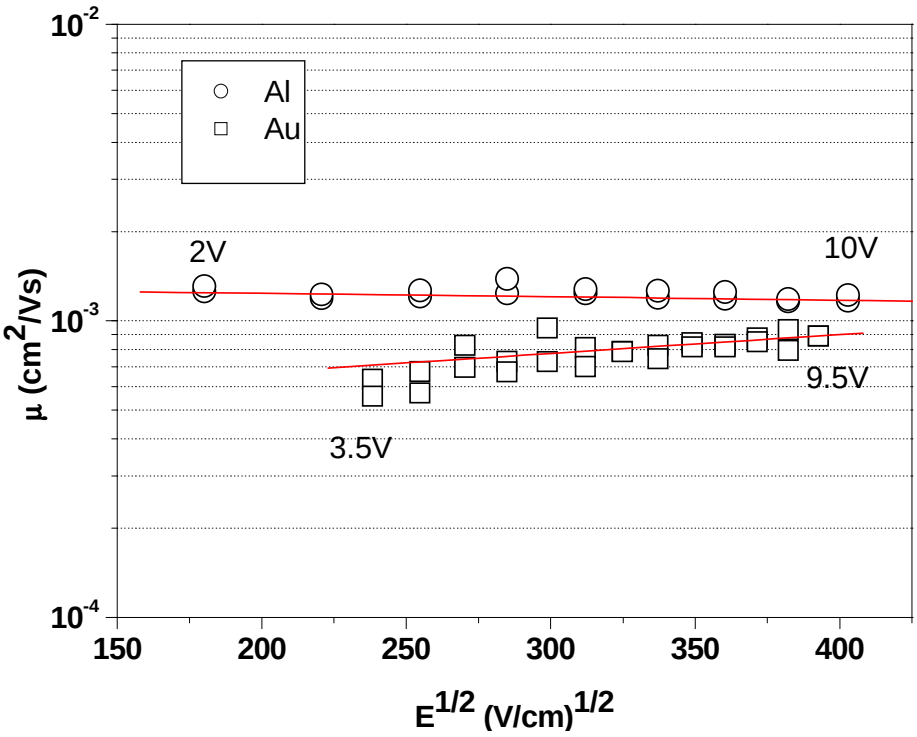

Figure 5.3.3 Poole–Frenkel plot of hole mobility in TPD device

Two unipolar devices and two ambipolar devices are tested to check the reproducibility of this experiment. Clearly in this electric field range, the mobility of unipolar devices increases, but the mobility of ambipolar devices remains almost the same, or even decreases a little bit.

The hole mobility in TPD samples are measured by time of flight technique in both hole-only and ambipolar devices. By applying a step voltage pulse prior to the laser pulse, electric-excited states are generated inside the ambipolar but not in the hole-only devices. The presence of excited states affects the room temperature hole mobility quite obviously compared to that measured without in the hole-only devices. We attribute the effect of mobility to interactions between the charge carriers and relatively long lived triplet states, and to an effective reduction in the number of transport sites available. Therefore, both dark injection and time of flight experiments are in agreement with our assumption, which has confirmed our theory.

5.4. Magnetoresistance (MR) measured by DI

5.4.1. Results

Figure 4.7.1 presents dark injection transit curves for the ambipolar device (ITO-TPD-Al) both with (figure 5.4.1 (b)) and without (figure 5.4.1 (a)) an applied magnetic field under 0.6 volts offset voltage (voltage step V_0=5 V). The DI transit peak in figure 5.4.1 (a) is marked by the red line and extended to figure 5.4.1 (b), and there is no significant difference of t_{DI} between two graphs. The small offset voltage could result in this small mobility change, as the offset bias is less than the turn on voltage (see figure 5.2.10 (a)), only holes can be injected into the sample, since there are no excited states, so t_{DI} should not be affected by the magnetic field.

Figure 5.4.2 presents dark injection transit curves for the ambipolar device (ITO-TPD-Al) both with (figure 5.4.2 (b)) and without (figure 5.4.2 (a)) an applied magnetic field under 3.5 volts offset voltage (V_0=5 V). The DI transit peak in figure 5.4.2 (a) is marked by the red line and also extended to figure 5.4.2 (b), and there is an obvious decrease in t_{DI} under the influence of the magnetic field (figure 5.4.2 (b)). The higher offset voltage results in an obvious mobility improvement, with the offset bias above the turn-on voltage (see figure 5.2.10 (a)), triplet states can be generated in the bulk of the TPD device, and applying a magnetic field could lead to a reduction of triplet states due to intersystem crossing, hence improving the sample mobility.

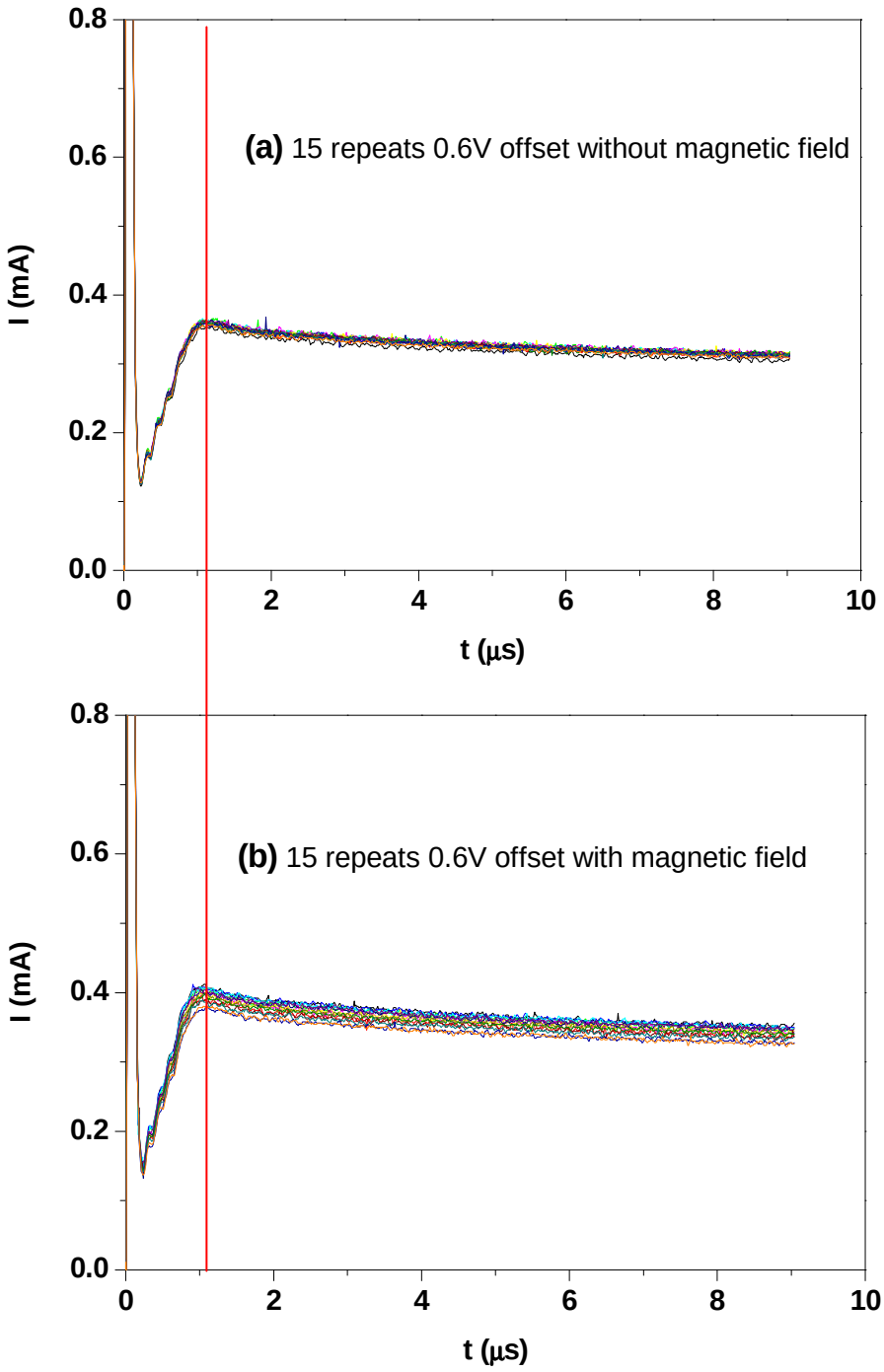

Figure 5.4.1 DI transit curves of the ambipolar device under 0.6 V offset voltage

Figure 5.4.1 (a) is the sample absence of magnetic field and figure 5.4.1 (b) presents the sample under 0.5 T magnetic field, and there is not much difference of t_{DI} between the two figures.

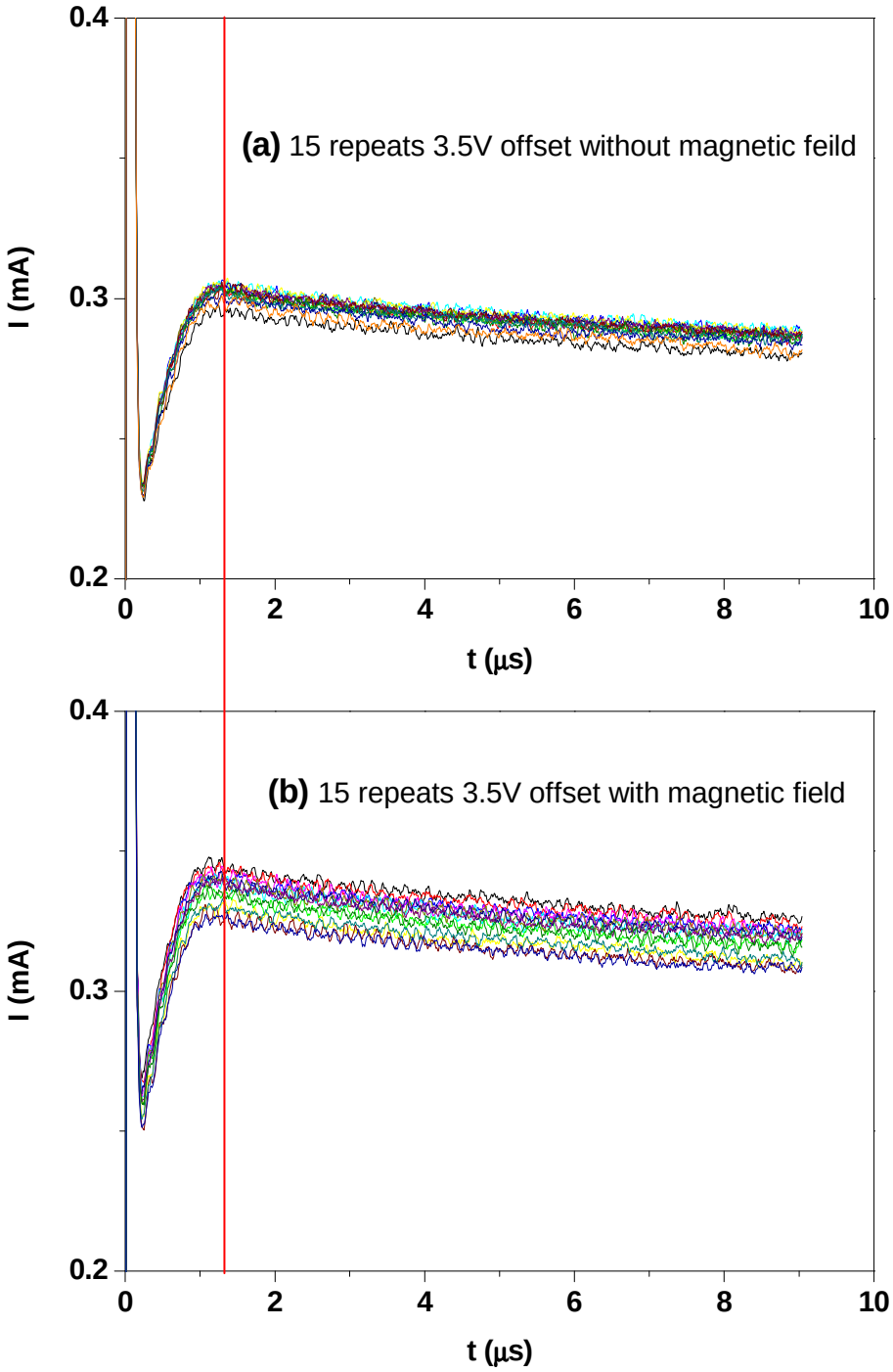

Figure 5.4.2 DI transit curves of the ambipolar device under 3.5 V offset voltage

Figure 5.4.2 (a) is the sample absence of magnetic field and figure 5.4.2 (b) presents the sample under 0.5 T magnetic field, and there is an obvious decrease of t_{DI} when magnetic field is applied, indicating the mobility increases under the magnetic field.

Figure 5.4.3 shows the DI transit curve of the unipolar device (ITO-TPD-Au) with and without a magnetic field. All these measurements are under zero offset bias. The DI transit peak in figure 5.4.3 (a) is also marked by a red line, and extended to figure 5.4.3 (b). It is clear that under zero offset voltage there is no significant difference in t_{DI} between these two graphs. This indicates that the magnetic field does not have any effect on charge transport in the unipolar device.

Figure 5.4.4 presents the DI transit curve of the unipolar device (ITO-TPD-Au) with and without applying magnetic field, using a 3.5 V offset. The DI transit peak in figure 5.4.4 (a) is marked by a red line, and extended to figure 5.4.4 (b). Again, it is clear that even with 3.5 V offset there is still no significant difference in t_{DI} between the two graphs.

It is safe to conclude that the magnetic field does not affect the charge transport in the unipolar device, irrespective of the applied offset bias. The reason for this is that only holes can be injected and transported inside a unipolar device, therefore it is very difficult to generate excited states inside unipolar architecture. Due to the absence of triplet states scattering/blocking the free charge carriers, theoretically, the magnetic field should not change the dark injection transit time t_{DI} in a unipolar device.

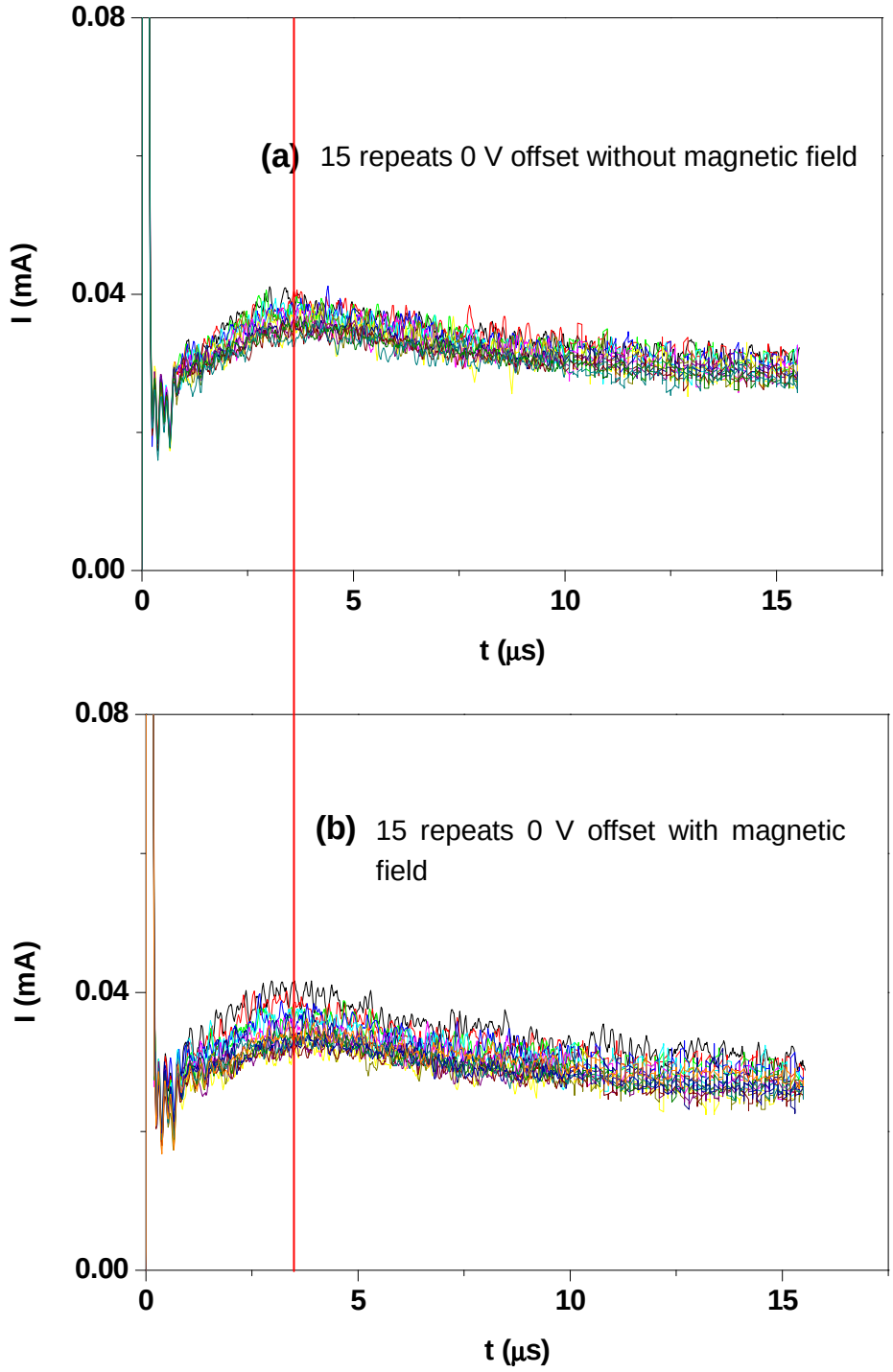

Figure 5.4.3 DI transit curve of unipolar device at 0.6 V offset voltage

Figure 5.4.3 (a) is the I-t curve for device without a magnetic field and figure 5.4.3 (b) represents the I-t curve for device under 0.5 T magnetic fields.

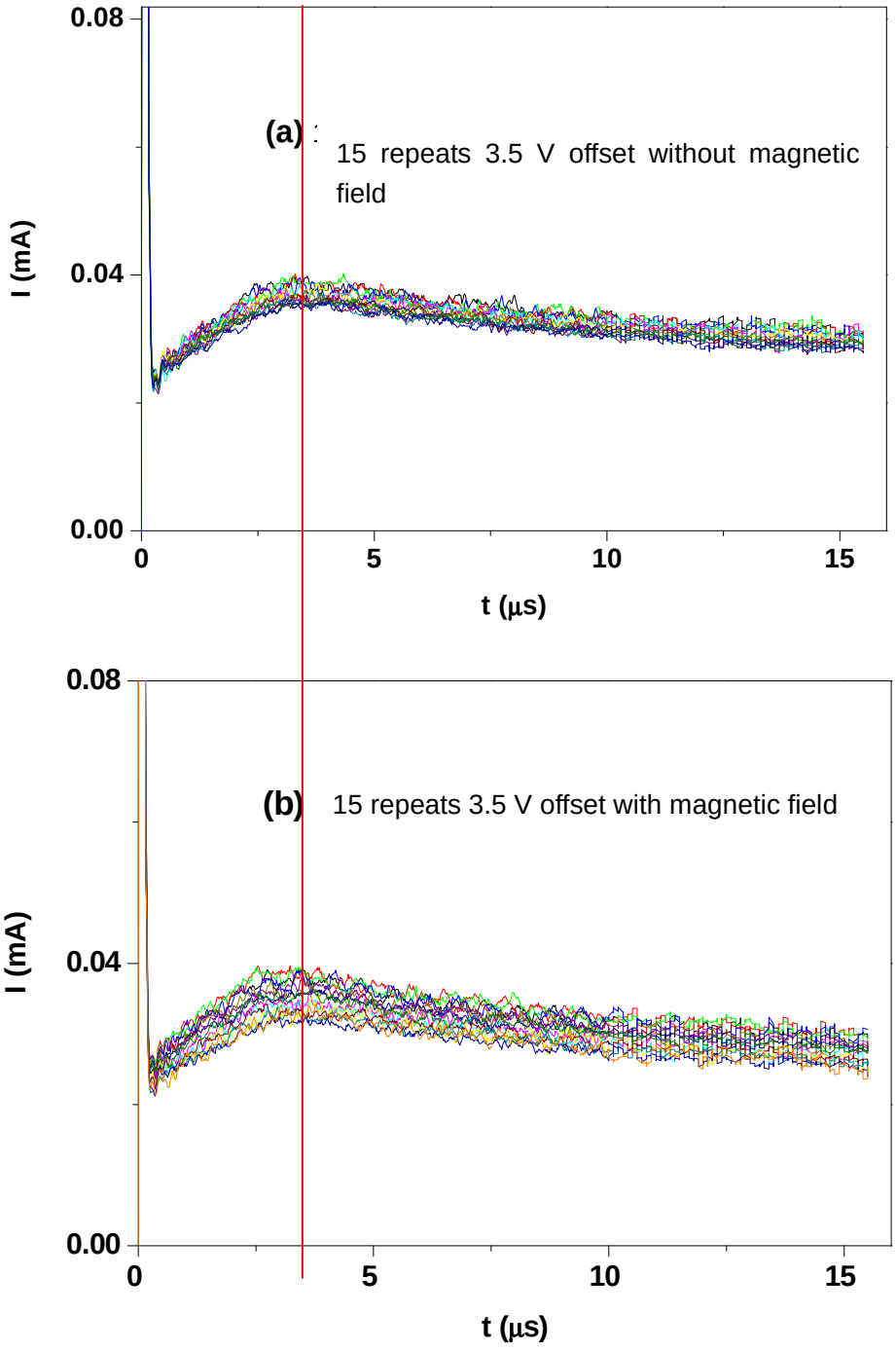

Figure 5.4.4 DI transit curve of the unipolar device under 3.5 V offset voltage

Figure 5.4.4 (a) is the device without a magnetic field and figure 5.4.4 (b) represents the device under 0.5 T magnetic fields.

Because the working current density in a semi-conducting device is highly related to the sample mobility, the device steady state current must behave similarly to the carrier mobility under the influence of a magnetic field. As the magnetic field is able to enhance hole mobility as a function of offset voltage in an ambipolar device, then the improvement of steady state dark current (space charge limited current I_{SCL}) ($\Delta I_{SCL} = I_{SCL/magnet\neq 0} - I_{SCL/magnet=0}$) should also follow the same pattern as the mobility improvement. On the other hand, in a unipolar device, the improvement in hole mobility is not affected by the offset voltage, hence any improvement in steady state dark current ($\Delta I_{SCL} = I_{SCL/magnet\neq 0} - I_{SCL/magnet=0}$) should also remain the same under different offset bias.

Figure 5.4.5 presents the steady state dark current $I_{SCL,}$ both with (figure 5.4.5(b)) and without (figure 5.4.5(a)) a magnetic field for the ambipolar device at 0 V offset. In this figure the average steady state dark current I_{SCL} increased by less than 0.005 mA (the increase is about 4.5%) due to the effect of magnetic field. More importantly a statistical analysis will be presented in the discussion to establish whether the change is significant or not.

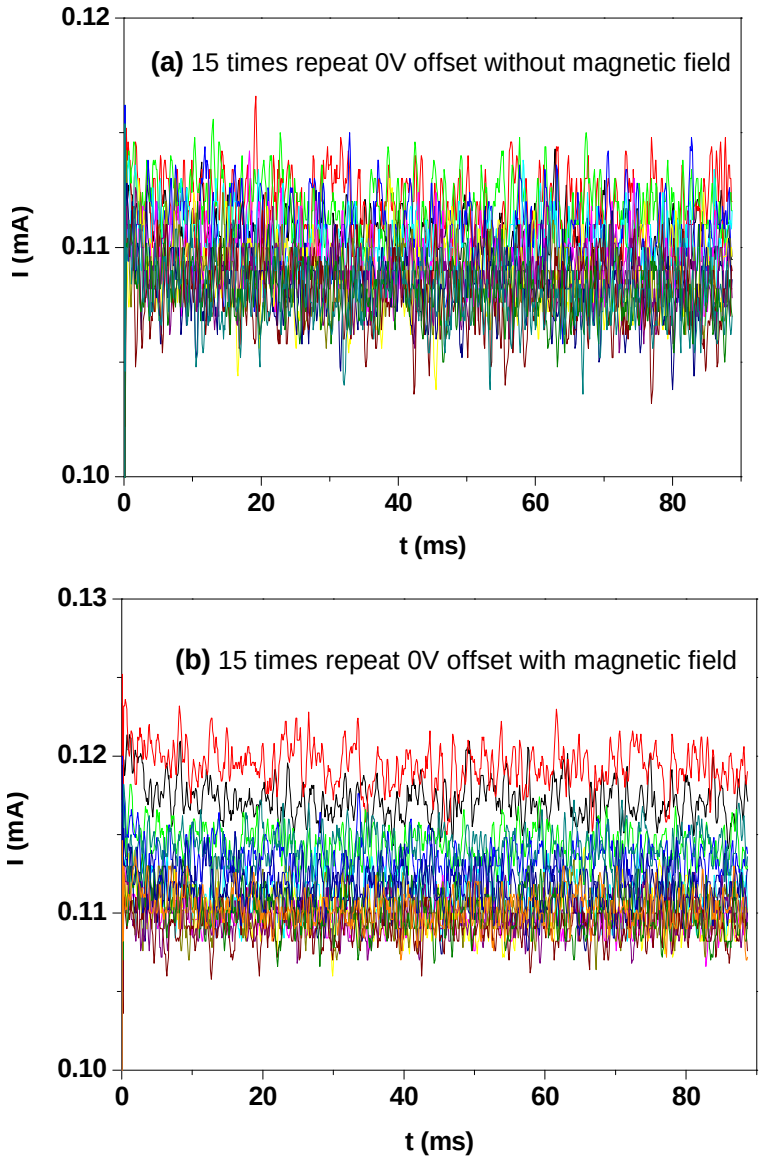

Figure 5.4.5 DI steady state current I_{SCL} plot of the ambipolar device under 0V offset voltage

Figure 5.4.5 (a) is I_{SCL} versus time under no magnetic field and figure 5.4.5 (b) represents it under 0.5 T magnetic fields.

If a 3.5 V offset voltage is applied to the ambipolar device, a remarkable increase of steady state dark current ΔI_{SCL} (approaching 0.01mA, this may looks not significant enough. However, if judged by the percentage, the improvement almost reached 10%, the small absolute improvement is just due to the small current flow in the sample) is

observed in figure 5.4.6, resulting from the presence of magnetic field. This increase (~ 10%) of I_{SCL} in figure 5.4.6 is much more significant, if compared to that in figure 5.4.5. (~ 4.5%)

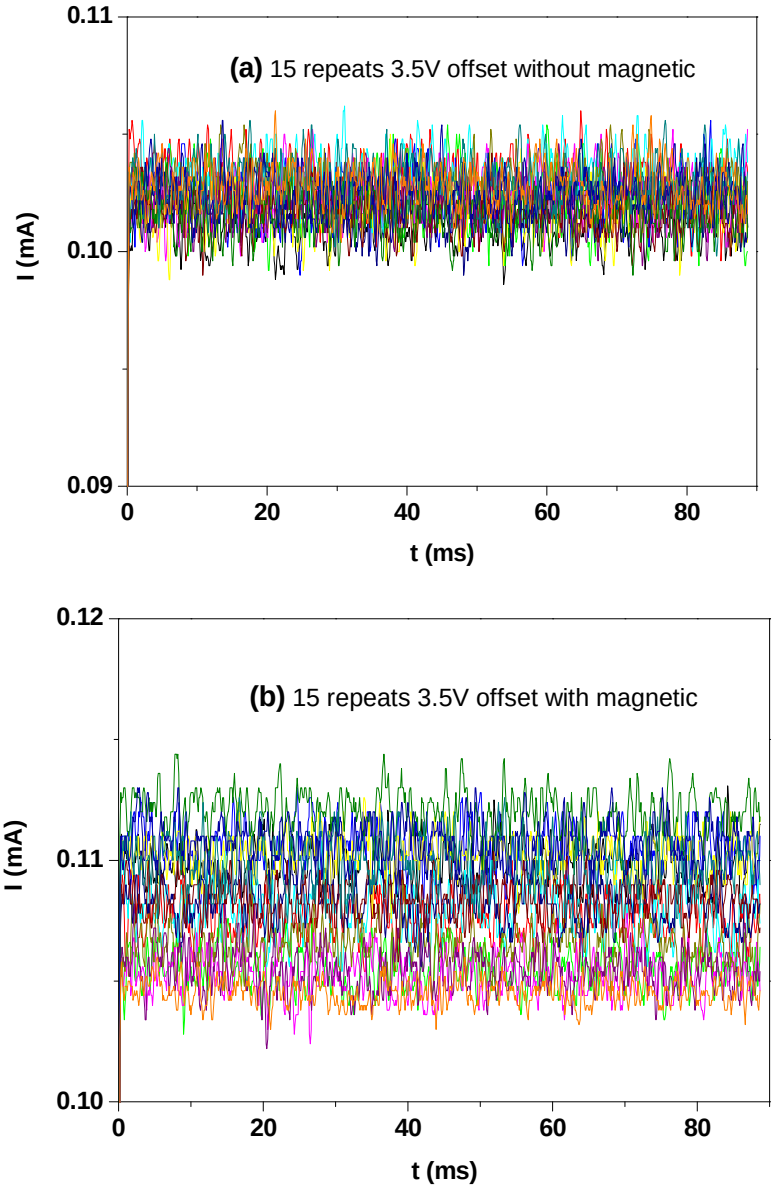

Figure 5.4.6 DI steady state current I_{SCL} plot of the ambipolar device under 3.5 V offset voltage. Figure 5.4.6 (a) is I_{SCL} versus time without magnetic field and figure 5.4.6 (b) represents it under 0.5 T magnetic fields.

In order to make a comparison, DI steady state currents I_{SCL} are also measured in the

unipolar device. In figure 5.4.7, I_{SCL} is measured at 0 volts offset bias both with (figure 5.4.7 (b)) and without (figure 5.4.7(a)) the magnetic field. The steady state current change (J(t) | t≥ 40 ms used) is too small to be observed (if take the average value both with and without B field, and the difference is only about 1 μA).

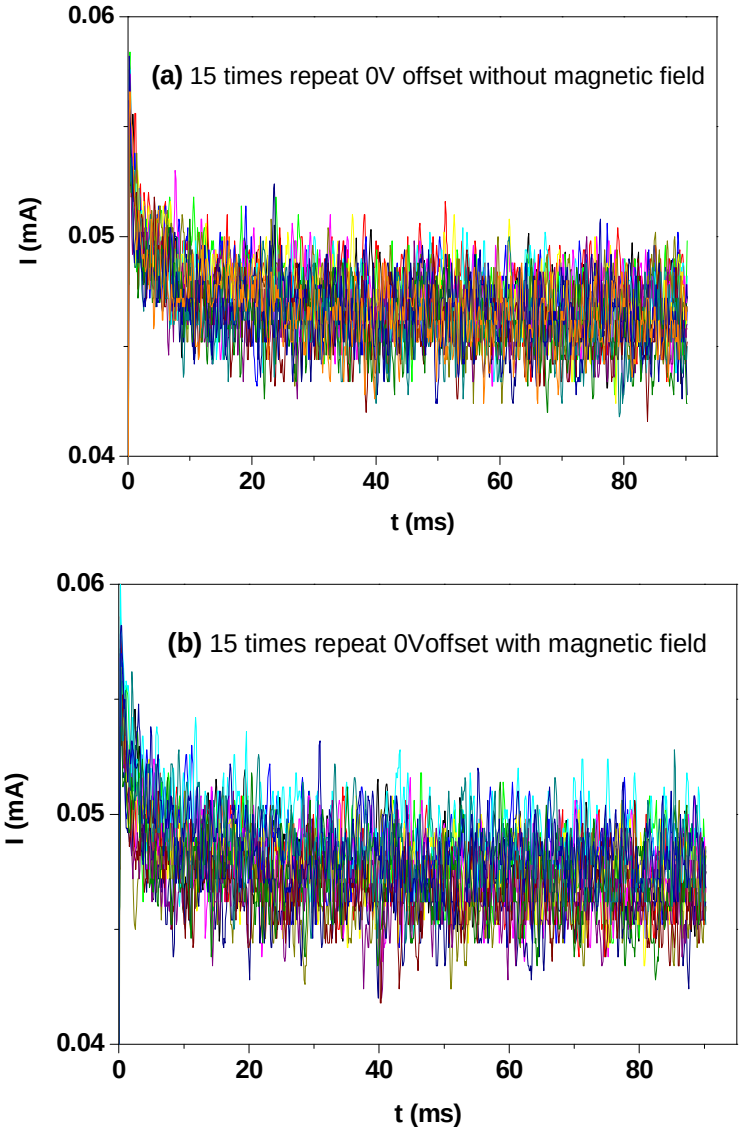

Figure 5.4.7 DI steady state current I_{SCL} plot of the unipolar device under 0V offset voltage. Figure 5.4.7 (a) is I_{SCL} versus time without magnetic field and figure 5.4.7 (b) represents it with 0.5 T magnetic field, there is little difference between these two graphs, and it is too small to be detected.

Even if the unipolar device is at 3.5 volts offset bias (figure 5.4.8), the steady state current change $\Delta I_{SCL,}$ due to the magnetic field is extremely small and difficult to distinguish (the difference of the average value is about 0.1μA).

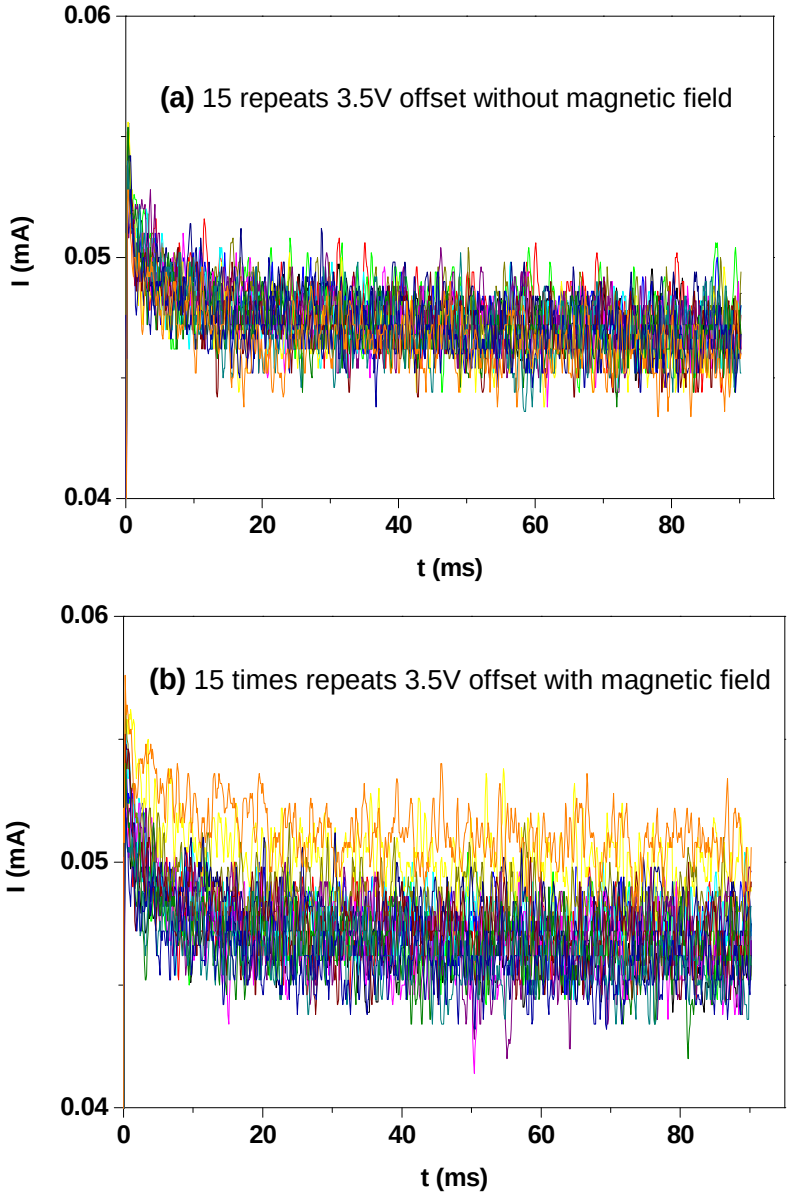

Figure 5.4.8 DI steady state current I_{SCL} plot of the unipolar device under 3.5 V offset voltage. Figure 5.4.8 (a) is I_{SCL} versus time without magnetic field and figure 5.4.8 (b) represents it with 0.5 T magnetic field, there is almost no difference between these two graphs.

5.4.2. Discussion

By fitting the data near DI peak, as described in section 4.2, the hole mobility is calculated for each experimental result from figure 5.4.1 to figure 5.4.4. Figure 5.4.9 shows the calculated hole mobility in an ambipolar device (ITO-TPD-Al) and a unipolar device (ITO-TPD-Au) under different DC offset voltage (0.6 volts and 3.5 volts) both with and without a magnetic field. In order to reduce the noise, each experiment was repeated 15 times. With a small offset voltage (0.6V in the ambipolar device), the average mobility in the ambipolar sample increased very little ～2% as a result of the magnetic field. However if the DC offset voltage is increased to 3.5 volts, by applying a magnetic field the average mobility in the ambipolar device increased by ～7%. This phenomenon is consistent with the conclusion reached in chapter 5.2 (see figure 5.2.8). Since almost no triplet states exist at a low offset voltage (below the turn-on voltage of the ambipolar device), as confirmed by IV characteristics and lack of luminescence in figure 5.2.10, there are no mobility changes in figure 5.2.8 and very little mobility improvement due to magnetic field in figure 5.4.9. With a 3.5V offset, the mobility in the ambipolar TPD device decreased by more than 10% in both figure 5.2.8 and figure 5.4.9. Since light output has been detected in figure 5.2.10(a), this implies that triplets have been generated inside the ambipolar sample at 3.5 volts offset. As the magnetic field can convert these triplets to singlets, this leads to a 7% increase in hole mobility, much higher than the 2% at 0.6 volts offset.

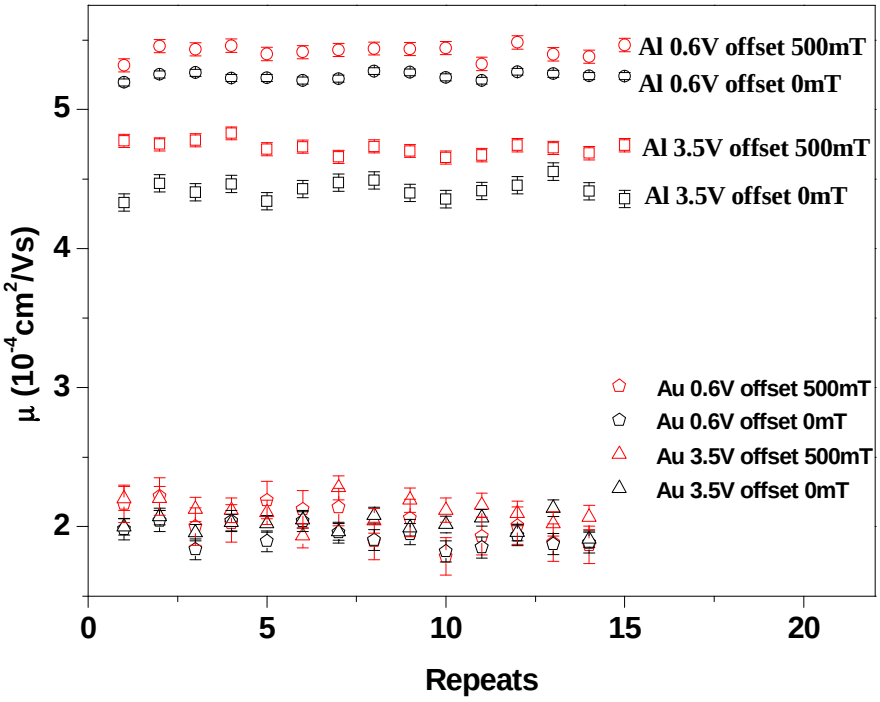

Figure 5.4.9 Mobility in TPD devices with and without magnetic field at two different offset voltages

Theoretically, there are no excited states inside the unipolar device, as only holes can be injected into the system, but in practice a small amount of electrons could be injected into the unipolar system, as a result of the large voltage step supplied by the pulse generator for the DI measurement. After applying a magnetic field to the unipolar device, the mobility shows a small increase (see figure 5.4.10), but this was not influenced by the offset voltage and remained roughly constant under different offset (see figure 5.4.10). This phenomenon confirms our suggestion that the electron injection is caused by the pulse voltage from the generator, which remains constant throughout all experiments, meaning that any resulting exciton concentration is constant in measurements. Thus any mobility improvement would also remain the same, irrespective of the offset voltage (see figure 5.4.10).

When the offset voltage is higher than the turn-on voltage of the ambipolar TPD devices (≥1.2 V), the mobility improvement $\Delta\mu$ ($\mu_{magnet\neq0}-\mu_{magnet=0}$) in the unipolar

system is much less than that in the ambipolar device. We believe that there is a higher triplet concentration in the ambipolar device than exists in the unipolar system under these conditions. This is because the excited states inside the unipolar device are only generated by the voltage pulse from the power source, but for the ambipolar device they are primarily generated by the offset bias, applying a magnetic field can convert more triplets to singlets in the ambipolar device, causing the mobility improvement $\Delta\mu$ in the ambipolar device to be greater than the unipolar system (at 3.5 V offset).

This is consistent with the ambipolar structures showing a drop in the zero magnetic field mobility of ~15% between the 0.6 V and 3.5 V offset (figure 5.2.8), whereas for the unipolar sample there is no effect due to the offset voltage.

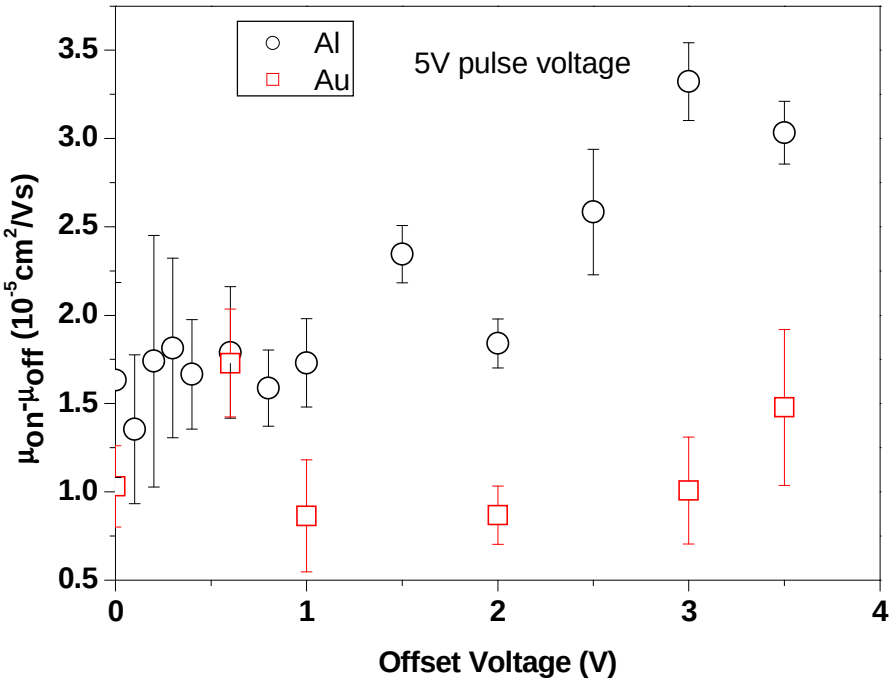

Figure 5.4.10 The plot of mobility increase in a magnetic field, under different offset voltages. Each data point is the average value after 15 repetitions to reduce the white noise, and the circles represent the mobility improvement of the ambipolar device, while the squares indicate the mobility improvement of the unipolar device.

The hole mobility improvement ($\Delta\mu = \mu_{magnet\neq 0} - \mu_{magnet=0}$) caused by the presence of the magnetic field versus offset voltage is shown in figure 5.4.10. Each data point is averaged over all 15 measurements to minimise noise. We note that the mobility improvement in the unipolar device remains roughly constant ($\Delta\mu \approx 1.1\times10^{-5}$ $cm^2V^{-1}s^{-1}$) irrespective of offset voltage (from 0V to 3.5 V). This is in contrast to the mobility improvement in the ambipolar device which changes from 1.7×10^{-5} $cm^2V^{-1}s^{-1}$ at 0V offset voltage to 3.0×10^{-5} $cm^2V^{-1}s^{-1}$ at 3.5 V offset. The increase in mobility improvement is due to a magnetic field in the presence of a large number of excited states and provides the most striking confirmation of the role of excited states in organic magnetoresistance (OMR) The differences between the absolute values of hole mobility measured in the Al and Au electrode samples can be accounted for by sample to sample variation or different contact resistance, and in any case do not affect any of the arguments presented so far, as the relative changes in measured mobility *in a given sample*, due to either excited states or a magnetic field are discussed. The offset independent magnetic field mobility enhancement displayed by the Au electrode sample may be due to the small number of excited states generated by the DI measurement pulse itself, although we note that it is not inconsistent with OMR theories which do not require ambipolar injection[35]. The same mechanisms can explain the relatively small magnetic field mobility enhancement seen in the Al electrode sample below turn-on. Thus, the most conservative interpretation of the results is that the microscopic magneto-resistance mechanism, which requires excited states, is at least equal in magnitude to one which does not, simply by looking at the (roughly doubling of the) magnetic field mobility increase as the Al sample is measured below and above turn-on.

In order to link the mobility improvement (due to the MR effect) to the steady state current improvement (also due to the MR effect), ΔI_{SCL} is also fully investigated, by averaging each noisy DI steady state current I_{SCL} from figure 5.4.5 to figure 5.4.8 in

section 5.4.1, and plotted in figure 5.4.11. Also, in order to reduce the errors, each measurement is repeated 15 times. In this graph it is obvious that the steady state current I_{SCL} increased significantly (ΔI_{SCL}=6.0 μA) in the ambioplar device under 3.5 V offset, compared to that under 0 V offset (ΔI_{SCL}=3.0 μA). This enhancement in I_{SCL} is attributed to the higher triplet concentration inside the ambipolar device at a higher offset voltage (3.5 V). In the presence of a magnetic field, more triplet states could transfer to singlet states via inter-system crossing, hence more charge blocking sites (triplets) would disappear, leading to a large I_{SCL} improvement.

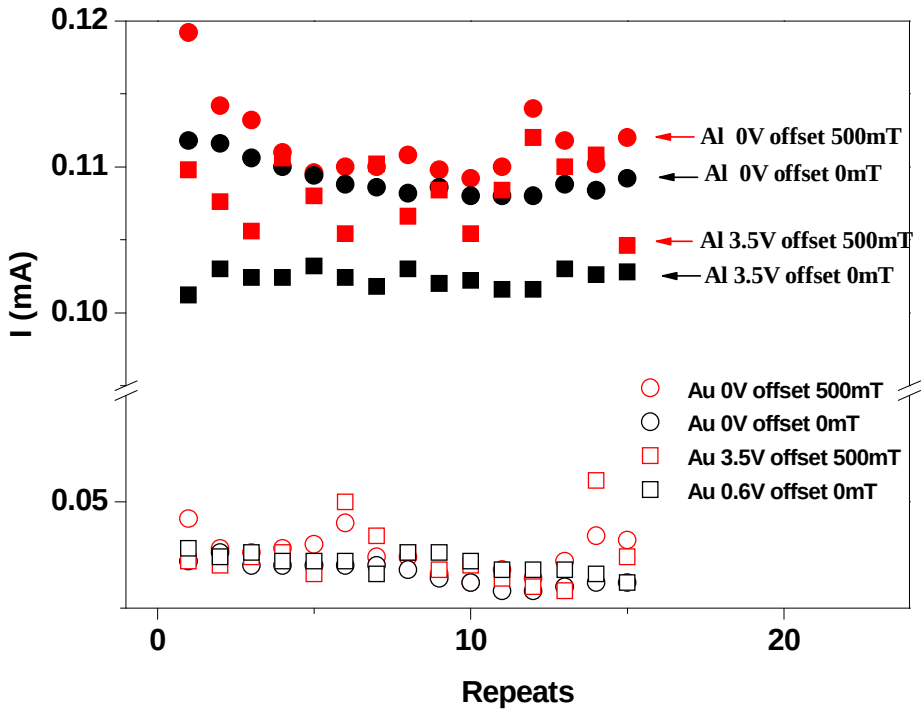

Figure 5.4.11 DI steady state current (I_{SCL}) plot both with and without presence of magnetic field at two different offset voltages. Repeat measurements of I_{SCL}, using unipolar (Au cathode) and ambipolar (Al cathode) samples, in the presence (red dots) and absence (black dots) of a magnetic field. The two offset values, 0 V (top) and 3.5 V (bottom), have been chosen to correspond to regions below and above device turn-on respectively in the ambipolar sample. The two offset voltages for the unipolar sample, 0 V and 3 V, are virtually indistinguishable.

In contrast to this, in the unipolar device, no significant improvement of I_{SCL} is observed even at higher (3.5 V) offset. This can be explained, since as a result of the electrodes used, there are few excited states inside a unipolar device even under a large offset bias. Any excitons are solely generated by the step voltage from the power source, which remains constant during all measurements. So, in the unipolar system the magnetic field should not significantly affect the working current, as there are only a few blocking sites.

Before future discussion, there is a very important phenomenon which must be pointed out. Since the space charge limited (SCL) current (see figure 5.4.5 and figure5.4.6) is very noisy under the magnetic field, it is hard to judge whether the SLC current increase is due to the big noise or the influence of magnetic field. Clearly in figure 5.4.11, the SCL current is increased every single time when a magnetic field is applied, the only difference is the amount of improvement. Therefore, the noise in figure 5.4.5 is literally caused by these various improvements. If take these SLC current values and present it separately (see figure 5.4.11), it is quite obviously that the SCL current consistently increased under the influence of magnetic field, just the absolute improvement value is varying during each measurements. So there is no doubt, that the SCL current is truly increased after applying a magnetic field and this is definitely not a disguise of those noise.

The behaviour of the steady state current improvement in figure 5.4.11 agrees with the mobility improvement in figure 5.4.9. This confirmed our MR measurements with the magnetically mediated steady state current (as measured in “traditional” OMR experiments).

To investigate the relationship between offset voltage and steady state dark current improvement ΔI_{SCL}, figure 5.4.12 shows the measured ΔI_{SCL} under different offset. It is clear that the steady state dark current improvement ΔI_{SCL} increases as a function of applied offset bias in the ambipolar device. This kind of behaviour is expected, as

increasing the offset voltage means more triplets are generated inside the device, with the applied magnetic field reducing the number of blocking sites and leading to a larger increase of I_{SCL}.

In a unipolar device, however, only few excited states are generated by the pulse voltage for the DI measurement, hence only a few blocking sites can be converted, irrespective of the offset voltage. Therefore the steady state dark current improvement ΔI_{SCL} should not vary with offset bias, and remains almost constant.

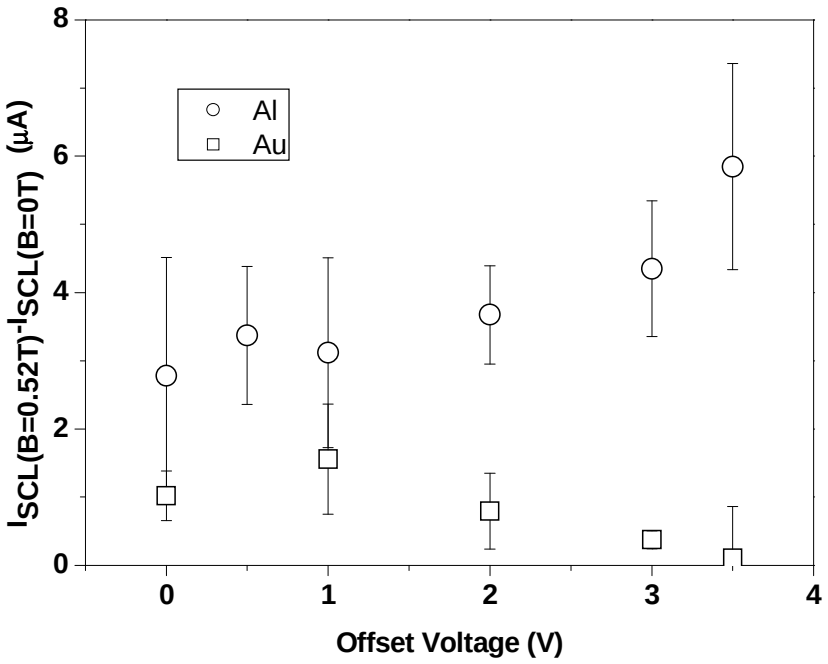

Figure 5.4.12 DI steady state current improvement versus offset voltage

Each point here is averaged over 15 times to reduce the experimental errors. The circles represent the ambipolar device (ITO-TPD-Al), and the squares indicate the current change of the unipolar device (ITO-TPD-Au).

With the large error bars in figure 5.4.12, it is hardly to argue that there is a real mobility increase in the ambipolar system. In order to confirm whether the mobility increase trend in the ambipolar device is significant or not, a statistical trend analysis is plotted in figure 5.4.13 (a), also another statistical trend analysis for the unipolar device is presented in figure 5.4.13 (b), for comparison purpose.

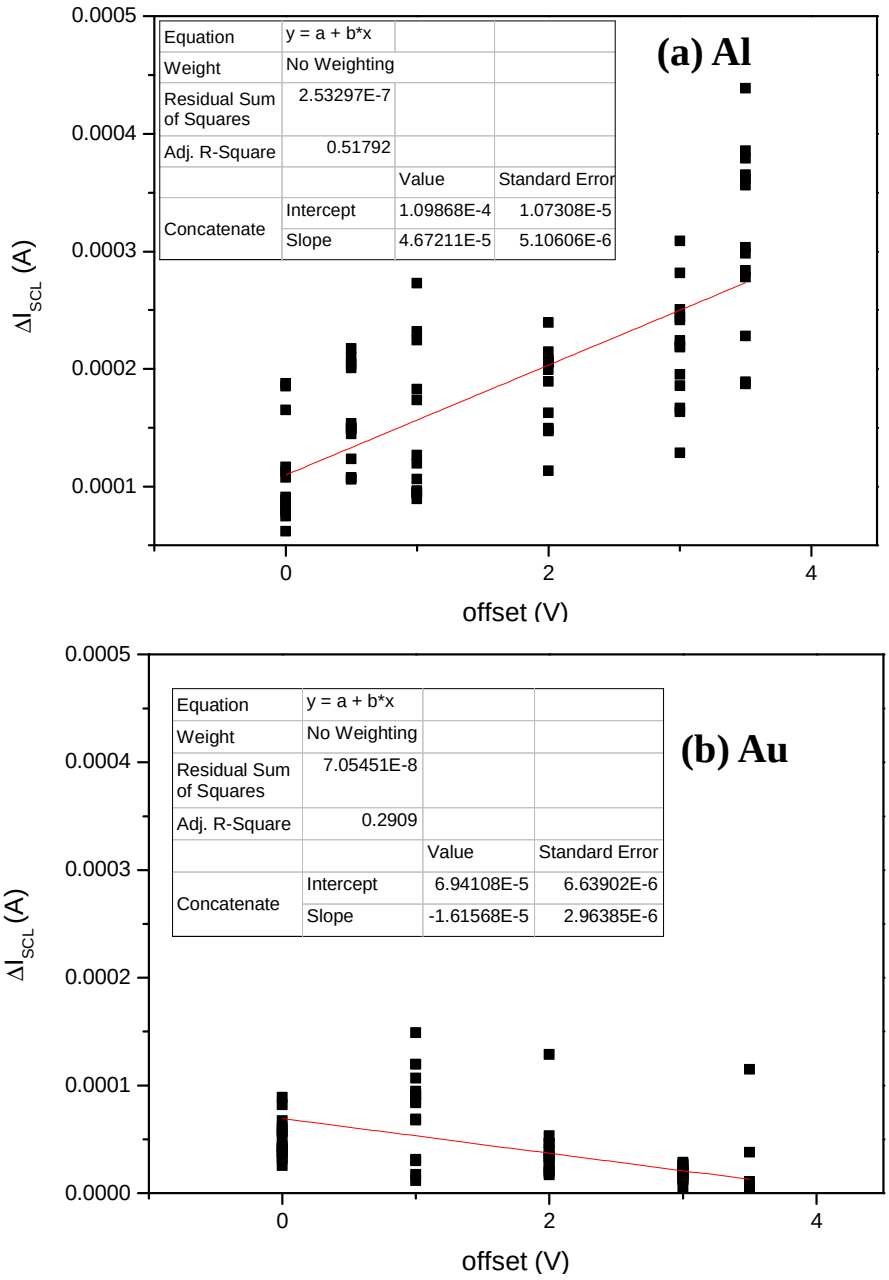

Figure 5.4.13 statistical trend analysis for both ambipolar device (ITO-TPD-Al), see figure 5.4.13 (a), and unipolar device (ITO-TPD-Au), see figure 5.4.13 (b).

The changes in hole mobility with magnetic field measured in TPD (see figure 5.4.10) can be compared with the change in the steady state current after the DI pulse (see figure 5.4.12). In the steady state for the unipolar sample the triplet concentration will be independent of the offset voltage as it is determined by the magnitude of the

DI pulse. This is indeed the case, and for the samples with the gold cathode the OMR was 7.5±4.7%, whereas for the aluminum cathode the OMR 8.7±3.0%. These values are the same as the mobility changes measured, within experimental error, and support the view that the change in current can be attributed to the change in mobility. Moreover, if the applied voltage and device structure are fixed, then the current density in a working device should be proportional to the sample mobility. Hence, we plot the mobility improvement ($\Delta\mu$) due to magnetic field, versus steady state dark current improvement (ΔI_{SCL}) also due to magnetic field in figure 5.4.14. It shows a clearly linear relationship between the two in the ambipolar device. The fitted red line is forced though zero coordinates with the slope around 2 (1.96), and this perfectly matched with the relationship between current and mobility, which further confirmed our assumption.

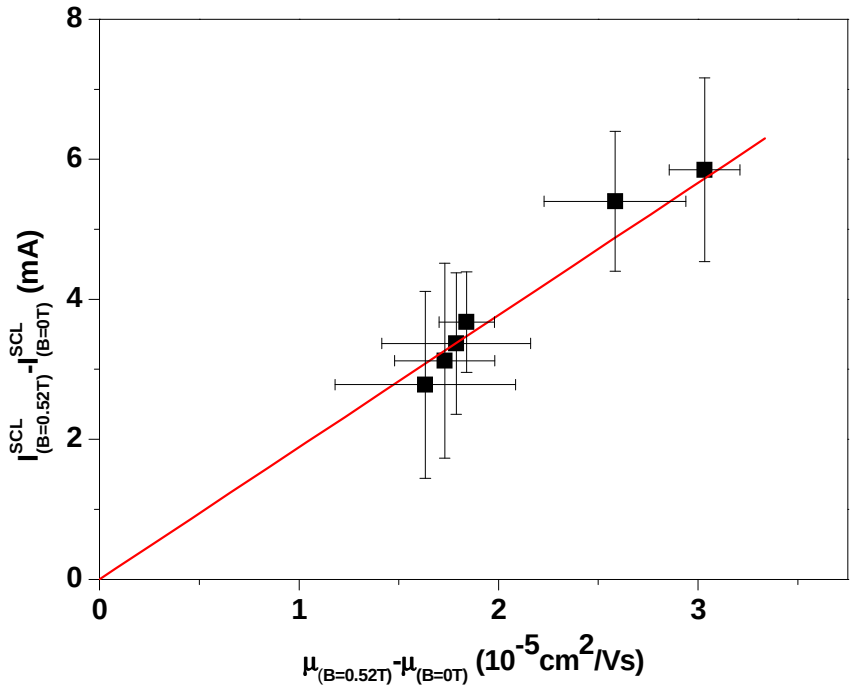

Figure 5.4.14 ΔI_{SCL} versus $\Delta\mu$ plot in ambipolar device

The linear fitting (with the slope around 1) matches the relationship between current and mobility, which relates the magneto-resistance to the mobility change.

The magneto-resistance of organic semiconductors can be explained as follows. The microscopic mechanism for OMR, proposed by our group, states that the primary action of a magnetic field on an OLED is to increase the singlet concentration within the organic layer[31], resulting in improved efficiency, at the same time it also reduces the triplet concentration. By reducing the triplet concentration, their effect on the mobility is also reduced. We have proposed that there are three primary mechanisms through which triplets can affect mobility [30, 31, 35, 64-67] depending on the relative spin states of the polaron and triplet. If a polaron encounters an exciton in the triplet state, and its spin state is the same as the corresponding electron or hole of the triplet, then the site is blocked (see figure 2.1.1) and the mobility is decreased, as the polaron has to find an alternative route. However, if the polaron has the opposite spin state, then it can interact with the triplet molecule, and here there are a number of possible outcomes, again depending on the spin conditions (see figure 2.1.1). The polaron can depart the molecule leaving a triplet behind, although both polaron and triplet may exchange their spin to result in different spin states, or the polaron can quench the triplet leaving just the polaron [31]. Both of these processes will change the mobility of the polaron and, in addition, they would likely have some magnetic field dependence, which would be convolved with the magnetic field dependence of the triplet population (caused by the change in the intersystem crossing mentioned earlier). This probably accounts for the observed difference between the magnetic field dependence of the device efficiency and current seen in OMR experiments [30, 31, 64, 68].

In this chapter, hole mobility in thin films of *N*,*N*'-diphenyl-*N*,*N*'-bis(3-methylphenyl)-(1,1'-biphenyl)-4,4'-diamine (TPD) has been measured by the method of dark injection transients (DI). These measurements were performed in the presence of a small variable offset bias in unipolar and ambipolar samples, with and without an applied magnetic field. The application of a magnetic field (~500 mT) has

the effect of increasing the measured mobility by a few percent. The magnetic field mobility increase is enhanced by the presence of excited states in ambipolar samples (from ~1.7×10^{-5} $cm^2V^{-1}s^{-1}$ below turn-on to ~3.3×10^{-5} $cm^2V^{-1}s^{-1}$above), as opposed to the unipolar samples, where it remains constant (~1.1×10^{-5} $cm^2V^{-1}s^{-1}$). This enhancement is interpreted as resulting from a magnetically mediated increase in the intersystem crossing rate between the majority, site blocking, triplet states and the short lived singlet states (the short lifetime means that they are more likely to decay before they have led much site blocking effect) and provides direct measurement of a microscopic mechanism accounting for the phenomena of organic magneto-resistance.

5.5. MR measured by ToF

The time of flight technique was also used to test our hypothesis. In order to ensure these experiments are valid, both hole and electron mobility were measured and compared to the literature. The raw ToF data is shown in figure 5.5.1 where the ToF transit time scales correctly with electric field both in hole and electron measurement, and the measured mobilities are presented in figure 5.5.2, with the hole mobility around 1×10^{-3} $cm^2V^{-1}s^{-1}$, which is absolutely comparable with the literature[51], the electron mobility is around $6.5\times10^{-4}cm^2V^{-1}s^{-1}$, which also agrees with that measured in chapter four ($7.0\times10^{-4}cm^2V^{-1}s^{-1}$), given the sample to sample variation.

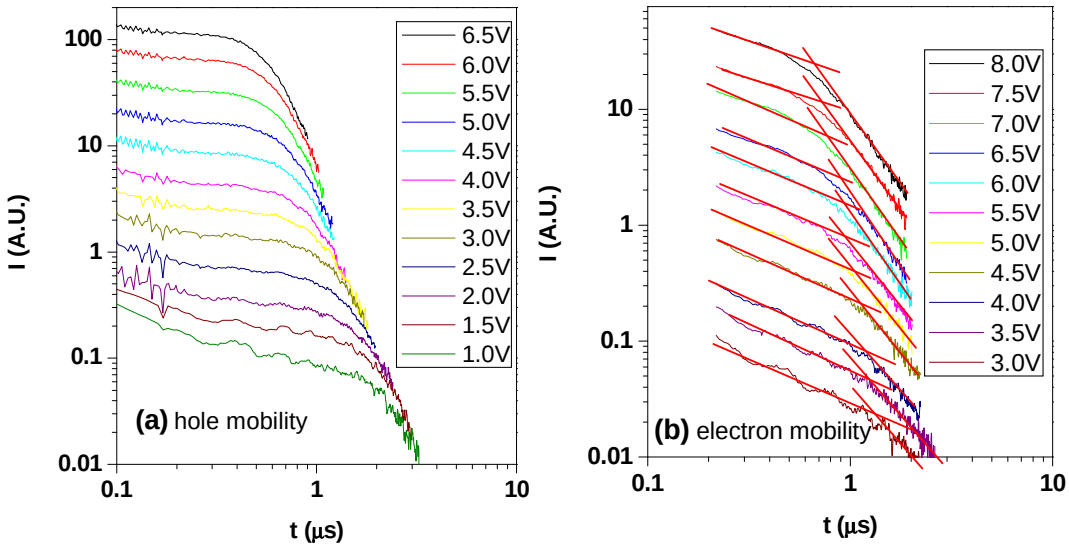

Figure 5.5.1 Time of flight transit curve of TPD device

Figure 5.5.1 (a) hole transit curve under varied electric field, (b) electron transit curve under different electric field, both measured under reverse bias.

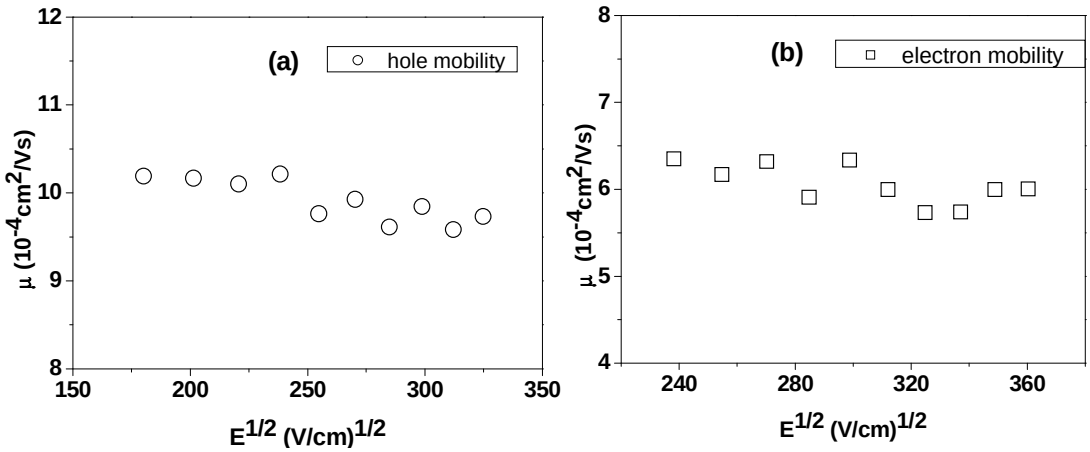

Figure 5.5.2 Time of flight mobility of TPD

Figure 5.5.2 (a) presents the hole mobility obtained by ToF, and figure (b) shows the electron mobility of TPD, both of which are electric field independent.

In order to reduce noise, both hole and electron mobility was measured by repeatedly (15 times) placing and removing a small U shape neodymium magnet, and the calculated mobility is presented in figure 5.5.3. As expected, the hole and electron mobilities remain unaffected by the magnetic field, under reverse bias, subject to random variation. This is quite understandable: during time of flight measurement, electric-excitation is prohibited due to the blocking contacts, so all excited states inside the sample are solely caused by photo-excitation and are mainly singlet states with extremely short lifetimes. They do not cause any significant site blocking effect, so applying magnetic field can not affect the ToF mobility due to absence of triplet excitons, if these short lifetime singlets could convert to triplets, these could cause the mobility decrease. The average electron mobility under magnetic field is 8.70×10^{-4} cm^2/Vs, and it is 8.86×10^{-4} cm^2/Vs with zero magnetic field, the average hole mobility is identical around 1.02×10^{-3} cm^2/Vs.

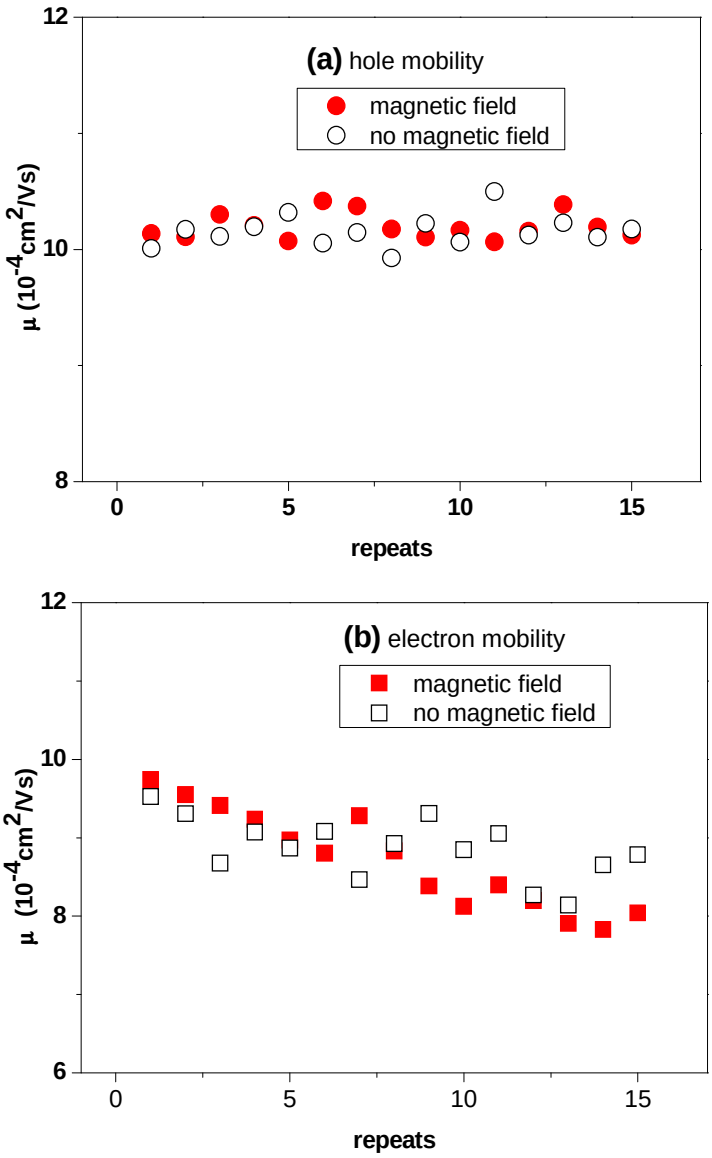

Figure 5.5.3 ToF mobility both with and with out magnetic field

Figure 5.5.3 (a) presents the hole mobility carried out by repeatedly placing and removing magnetic field, and figure (b) shows the electron mobility carried out in the same conditions, both have not shown any magnetic field dependence.

In conclusion, charge mobility is measured by dark injection and time of flight, both with and without magnetic field, and the only difference between DI and ToF is the existence of excited triplet states, therefore, this comparison is a double confirmation that the magneto-resistance inside organic diodes is truly due to the inter-system

crossing between triplets and singlet states, as the triplets can block and interact with free charge carriers.

5.6. TPD with ferromagnetic electrodes

As discussed before, magnetic field can change the balance between singlet and triplet states, and some other mechanisms can also affect this equilibrium, such as doping and spin state controlling. It is not surprising, therefore, that the use of ferromagnetic electrodes can also influence the excited states conformation due to the spin state control of injected charge carriers, which eventually leads to a balance shifting between singlets and triplets

Thus nickel-iron anode has been used for hole injection, as its work function is quite close to the HOMO level of TPD. During the sample preparation, the evenly mixed nickel-iron powder (with 21% of nickel and 79% of iron) is compressed into a nickel-iron tablet using a hydraulic press. This is then placed on a tungsten boat in the evaporator, evaporated and deposited on an etched ITO substrate as an anode electrode. The sample structure is exactly like the one made for DI in chapter three: the semi-conducting layer is still TPD, and the cathode electrode is still aluminium, except that the anode contact is changed from gold to nickel iron mixture.

The sample is immediately transferred to the sample holder after fabrication and evacuated though the vacuum port using a pumping station giving pressures of ~10^{-5}mbar. It is then measured by standard dark injection technique to check the efficiency of hole injection, and hole transport mobility.

Figure 7.1.1 shows the original *I-t* curve of DI measurement, which had very good charge injection, and the transit peak scales correctly with the applied electric field, which indicates that this ferromagnetic device can be used to accomplish further experiments.

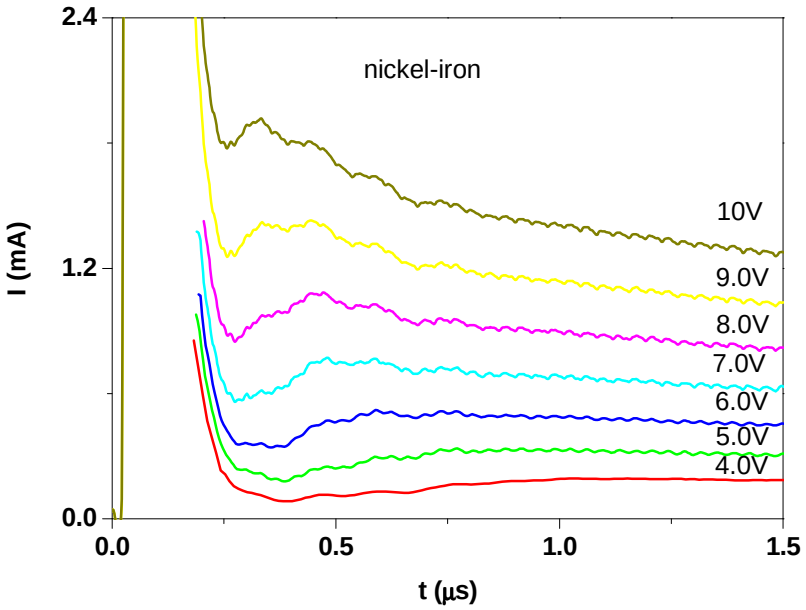

Figure 7.1.1 Original *I-t* curve of DI measurement

Dark injection transit curve for nickel-iron/TPD/Al device, the transit time tDI scales perfectly with pulse voltage.

Figure 7.1.2 presents the drift velocity versus electric field: the slope of this fitted line is the mobility of this device, as it does not go though the origin, which means the sample mobility is slightly field dependent, this is shown in the Poole-Frenkel plot of figure 7.1.3. The mobility of this device shows a slight increase with electric field. The calculated average hole mobility of this ferromagnetic device is around $4 \times 10^{-4} cm^2 V^{-1} s^{-1}$, which agrees with that measured from the ITO anode in chapter five ($6 \times 10^{-4} cm^2 V^{-1} s^{-1}$) given sample to sample variations.

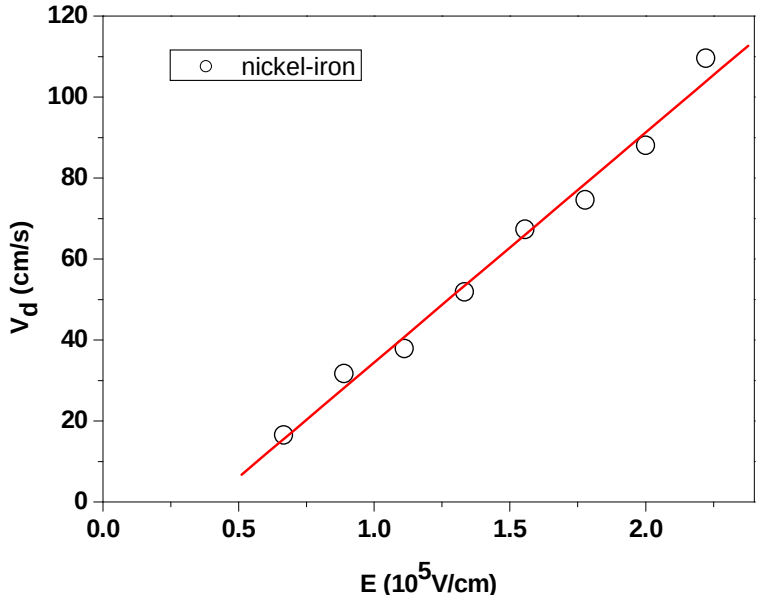

Figure 7.1.2 drifting velocity versus electric field in nickel iron device

The scattering drifting velocity data is fitted with linear function and represented by the red line

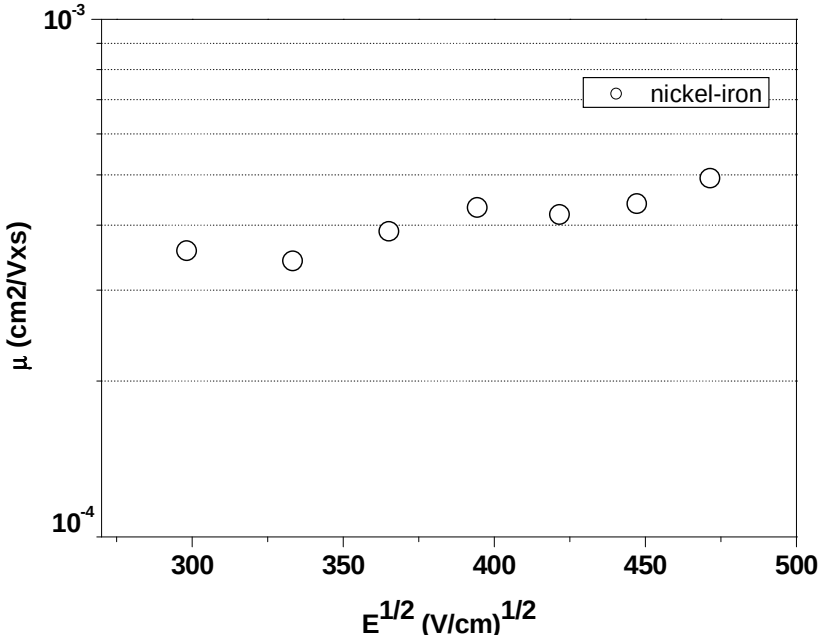

Figure 7.1.3 Poole-Frenkel plot of nickel iron device

The hole mobility shows just a slight increase with electric field.

Chapter six: Discussion

6. Discussion

In this thesis, we have measured the hole mobility in both P3HT and TPD in section (4.3.2) and section (5.2.2), in both cases obtaining results in good match with literature. Our work shows that for a unipolar P3HT device we see no change in mobility with DC bias, whereas for the ambipolar device we obtain a reduction in mobility（～15%) that can be perfectly correlated with the turn on voltage in I-V characterisation. This behaviour is not only observed in P3HT devices but also demonstrated in TPD devices, and the reduction in mobility is still around 15%, irrespective of the material. In TPD the mobility reduction perfectly correlates with both the turn-on voltage in IV characterisation and light emission, strongly suggesting that excitons play a critical role in reducing the mobility in organic semiconductors. These two experiments confirmed the generality of the site blocking mechanism, which solely depends on the spin states of injected charges and on the formation of excited states (primarily triplet). The actual semi-conducting organic material is not important in the theory and we measured essentially identical behaviour in two very different materials, note for example the similarities between figure 6.1.1 and figure 6.2.2.

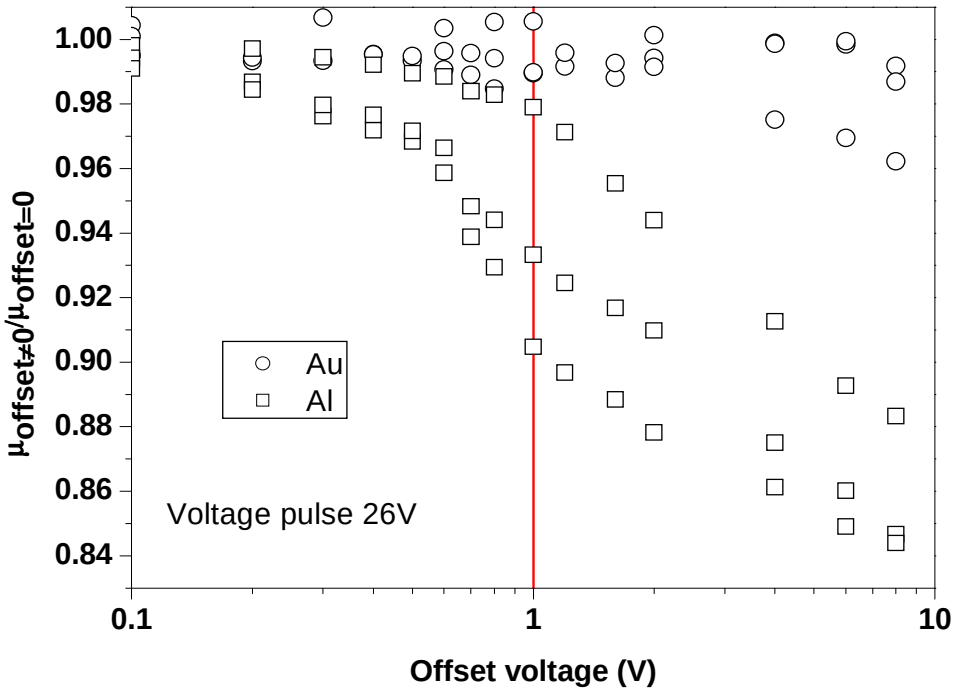

Figure 6.1.1 Mobility ratio versus the offset voltage in P3HT devices

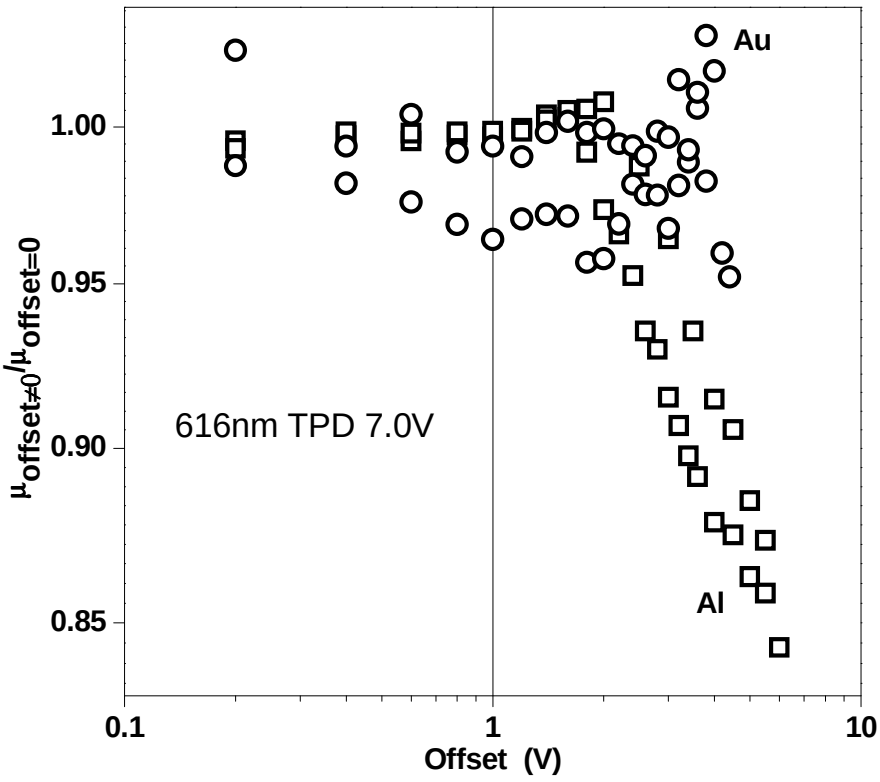

Figure 6.1.2 Mobility ratio versus offset voltage in TPD devices

The site blocking theory is also supported by the ToF results with forward bias in section (5.3.1). In the unipolar device the mobility increases with the applied electric field (this may be due to a number of causes, as commonly observed in organic semiconductors), however, in the ambipolar device the mobility remains constant with electric field, and this is consistent with the excited state blocking/interacting effect, suppressing any mobility increase. However due to higher dark current density in ambipolar device, this phenomenon could be caused by trap filling as well. The DI and ToF are consistent and support the role of excited states in charge transport. From these experiments, we can safely conclude that the mobility reduction in the ambipolar devices is due to the presence of excited states (triplets) and that these excited states are blocking/interacting with the carriers. There are several ways to confirm our hypothesis. First, even though the architecture of both unipolar and ambipolar samples is identical and the current density in both devices is quite similar (even higher in the unipolar device), the mobility reduction can only be observed in a given ambipolar device, but not in a unipolar sample. This indicates that the mobility reduction in the ambipolar device is due to the exciton generation, which can not occur in the unipolar device. Also, the mobility reduction can not be caused by the increased current density, since the dark current in the unipolar device is higher than the ambipolar sample. Second, the mobility reduction starts after the turn on of the ambipolar sample, see figure 6.1.1 and figure 6.1.2, which is also correlated to the light emission. Before this critical value, no excitons are generated, so mobility is roughly the same (or even slightly increased in the TPD device). After turn on, since electrons and holes are injected into the device and can form excitons, light emission is observed in ambipolar TPD samples. This can easily confirm the existence of excited states. Therefore the mobility reduction after this threshold value (turn on voltage) is direct evidence of excited states blocking/interacting with carriers. In ambipolar samples (eg: Au-P3HT-Al) in our experiments, the hole DI transients

show a clear space-charge cusp and the transit time scales correctly with the applied voltage pulse. This suggests that the electron injection and transport within these devices is not balanced with that of the holes. We also note that the average P3HT hole mobilities for the two types of sample (unipolar and ambipolar) are in agreement, given sample to sample variation, being $\mu_{Au-Au}=(5.1\pm0.9)\times10^{-5}$ cm^2/Vs and $\mu_{Au-Al}=(4.8\pm1.8)\times10^{-5}$ cm^2/Vs. This shows that we perform valid measurement of hole mobility in the organic irrespective of cathode material, as a matter of fact only the anode is crucial for the DI measurement, which needs to by Ohmic contact for good charge injection.

The excited states (triplets) blocking/interacting mechanism is strongly supported when measuring the effect of a magnetic field on the mobility of holes in TPD under different bias conditions. The magnetic field results in a significant increase in mobility for the ambipolar sample but not in the unipolar sample, and this can be explained by the intersystem crossing between long-lived triplets and short lifetime singlet states. With an applied magnetic field, triplets generated inside the ambipolar device can inter-convert to singlet states, and lead to a reduction of blocking sites, hence increasing the mobility and steady state current. No such mechanism is possible in unipolar samples. In figure 6.1.3, the ambipolar sample displays a clear increase in mobility and steady state current density with magnetic field in contrast to unipolar results. So, the increase of dark current is not due to exciton dissociation, but simply caused by the increase of mobility

Since a magnetically mediated mobility improvement is measured in the samples at the same time, as a magnetically mediated increase in steady state current (as measured in “traditional” OMR experiments), we can directly compare the two. In figure 6.1.4, we show a direct correlation between improved mobility and current density, which only occurs in ambipolar samples.

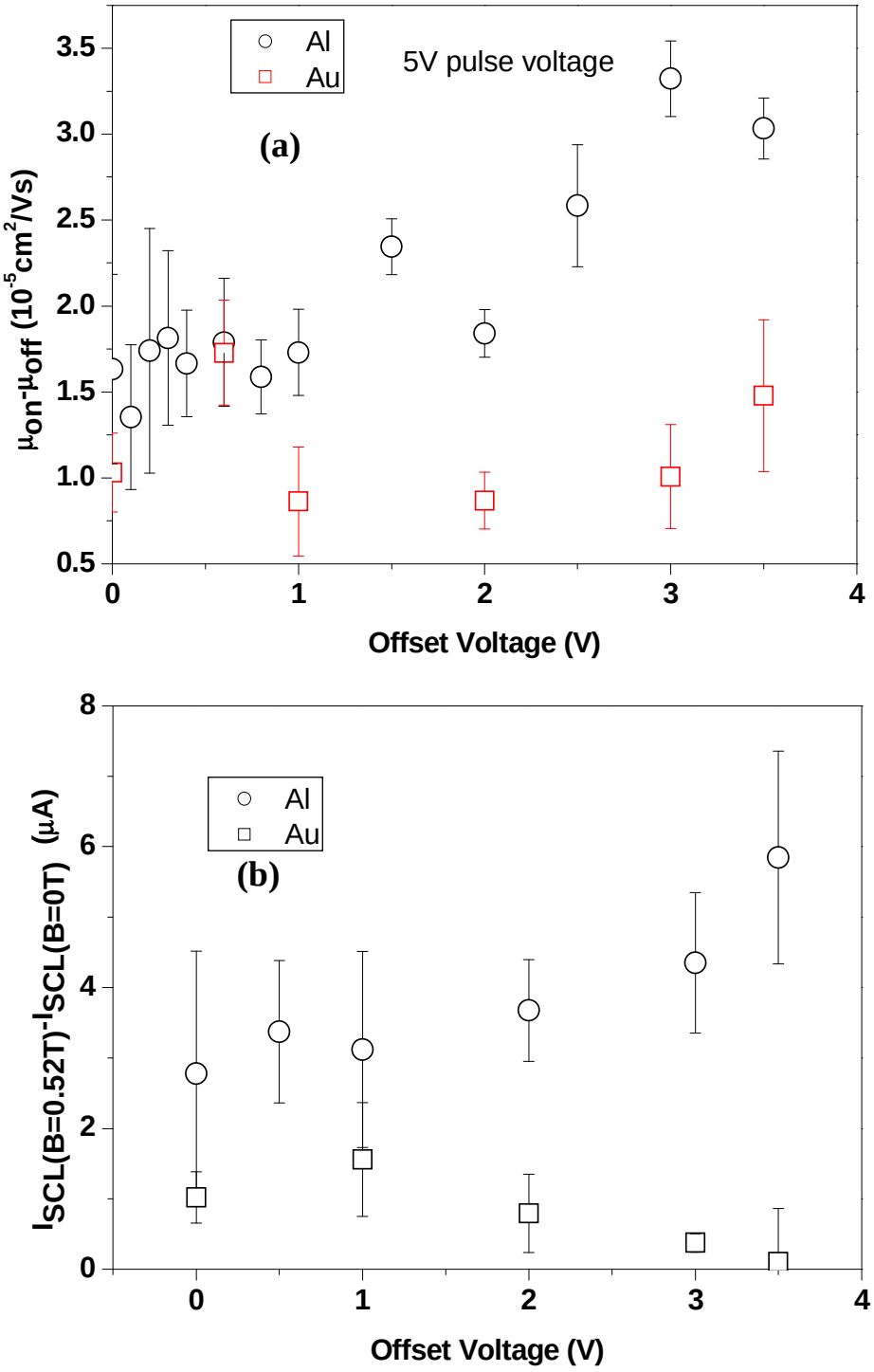

Figure 6.1.3 (a) the plot of mobility increase in a magnetic field, under different offset voltages, figure (b) DI steady state current improvement versus offset voltage

These results conflict with the bipolaron theory, where the mobility and current density change is solely caused by bipolaron formation and this should not be affected by the electrode choice. That is, according to this theory, the magnetically mediated increase in mobility and current density should be observed in both unipolar and ambipolar devices. We see a much greater effect (more than two times) in the ambipolar case. As the current flows through the device, the injected charges can either hop to an empty site, forming a polaron, or hop onto an occupied site, forming a bipolaron. So, bipolaron formation can occur before the turn on voltage, even though only one type of charge is injected. This indicates a magnetically mediated increase in current should be observed when there is any current flow in the sample. We observed significantly higher magnetically mediated current in ambipolar case above turn on, and this points directly to the formation of excitons, which can only be generated above the turn on voltage. According to bipolaron theory, OMR should behave similarly in both unipolar and ambipolar devices. However in our experiments both the magnetically mediated mobility and the magnetically mediated current are very different between the unipolar and ambipolar samples. See figure 6.1.3 (a) and (b), there is a significant increase in mobility and current density for the ambipolar sample but not in the unipolar sample, this is directly linked to the formation of excitons, which can only occur in the ambipolar sample but not in the unipolar device. However, in both figures there is a small magnetically mediated mobility and current density in unipolar device, which could be due to the measurement voltage pulse, or the bipolaron mechanism, or both of these effects.

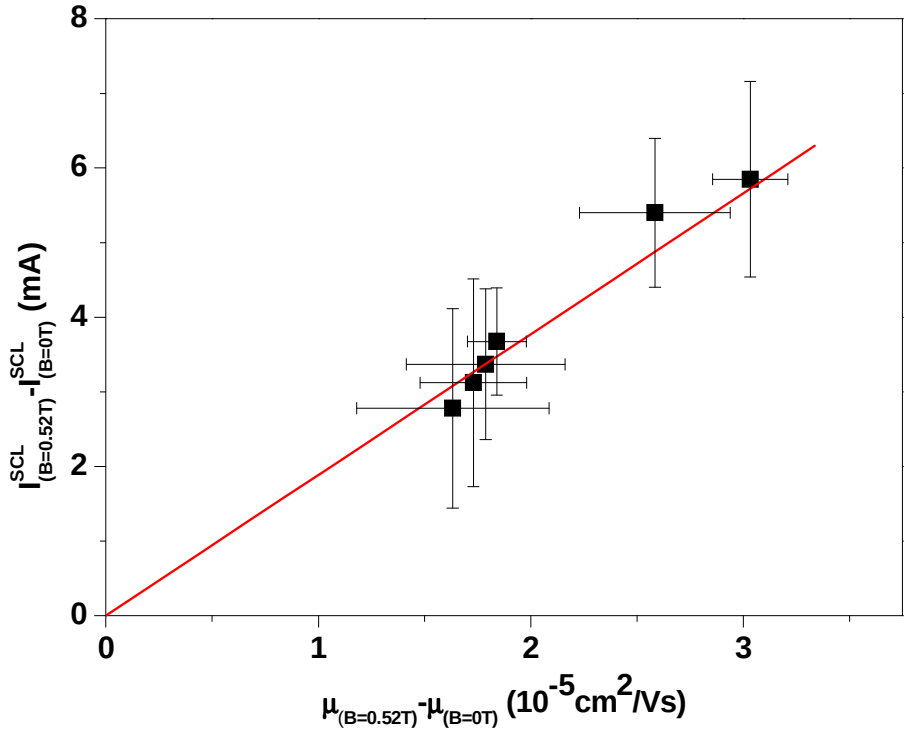

Figure 6.1.4 ΔI_{SCL} versus $\Delta\mu$ plot in ambipolar device

We can also rule out a columbic trapping mechanism as an explanation for mobility reduction in ambipolar devices. According to this theory, the hole mobility should not be affected by the external magnetic field, as the population of electron trapping centers is not influenced by the external magnetic field. This suggestion is in direct conflict with our observation and offers no mechanism for explaining our results.

TPD is a sufficiently different molecular system to the previously reported P3HT to confirm the site-blocking mechanism as a general feature of long lived excited states in organic semiconductors. These results therefore strengthen the view that excitons have a significant effect on carrier mobility, thus providing support for the TPI model of organic magneto-resistance. Furthermore, our results may have more far-reaching implications, for instance in device modeling, where the role of excitons on current transport in OLEDs has been overlooked until now. Indeed, if even the very low exciton concentrations present in our structures (due to the considerably smaller

electron injection compared to holes) can reduce mobilities by 15%, then the level of excitons present in functional OLEDs should cause significant changes in mobility. This may be, at least in part, the origin of the commonly observed turnover in current voltage characteristics observed for OLEDs with increasing drive voltage.

Chapter seven: Conclusions

7. Conclusions

In final summary, since both DI and ToF techniques have been used to complete our experiments, as well as two organic materials (P3HT and TPD) have been involved to check the generality of our theory. It is safe to suggest that the excited states (specifically long lived triplet states) play a critical role in reducing the mobility in organic semiconductors. The hole mobility decrease, which was observed in an ambipolar system, can be attributed to the triplets site blocking and interaction with charge carriers, hence affecting the charge transport in organic semiconducting system. Due to the intersystem crossing mechanism, the long lived triplets can be inter-converted to singlets (much shorter lifetime) by the presence of a magnetic field. So the reduced mobility due to excited states (primarily triplets) can be recovered in the presence of a magnetic field, hence providing a direct microscopic mechanism for OMR. The understanding of these basic principles behind the organic semiconductors may lead to the possibility of improving the performance of organic devices, e.g. the efficiency of OLED and OPV.

References

1. Tang, C.W., *Two-layer organic photovoltaic cell.* Applied Physics Letters, 1985. **48**: p. 2.
2. Tang, C.W.V., S. A., *Organic electroluminescent diodes.* Applied Physics Letters, 1987. **11**: p. 2.
3. Burroughes, J.H., et al., *Light-Emitting-Diodes Based on Conjugated Polymers.* Nature, 1990. **347**(6293): p. 539-541.
4. Burroughes, J.H., Bradley, D. D. C., Brown, A. R., Marks, R. N., Mackay, K., Friend, R. H., Burns, P. L., and Holmes, A. B., *Electroluminescence in conjugated polymers.* Nature, 1999. **397**(6715): p. 121-128.
5. Lilienfeld, J.E., US Patent 1 745 175, 1930.
6. Tsumura, A. and H. Koezuka, *Macromolecular Electronic Device: Field-Effect Transistor with a Polythiophene Thin Film.* Applied Physics Letters, 1986. **49**: p. 2.
7. Mcculloch, I., Heeney, M., Bailey, C., Genevicius, K., Macdonald, I., Shkunov, M., Sparrowe, D., Tierney, S., Wagner, R., Zhang, W. M., Chabinyc, M. L., Kline, R. J., Mcgehee, M. D., and Toney, M. F., *Liquid-crystalline semiconducting polymers with high charge-carrier mobility.* Nature Materials, 2006. **5**(4): p. 328-333.
8. Peumans, P., V. Bulovic, and S.R. Forrest, *Efficient, high-bandwidth organic multilayer photodetectors.* Applied Physics Letters, 2000. **76**(26): p. 3855-3857.
9. Tang, C.W., S.A. Vanslyke, and C.H. Chen, *Electroluminescence of Doped Organic Thin-Films.* Journal of Applied Physics, 1989. **65**(9): p. 3610-3616.
10. Garnier, F., Hajlaoui, R., Yassar, A., and Srivastava, P., *All-Polymer Field-Effect Transistor Realized by Printing Techniques.* Science, 1994. **265**(5179): p. 1684-1686.
11. Tang, C.W., *2-Layer Organic Photovoltaic Cell.* Applied Physics Letters, 1986. **48**(2): p. 183-185.
12. Sirringhaus, H., Brown, P. J., Friend, R. H., Nielsen, M. M., Bechgaard, K., Langeveld-Voss, B. M. W., Spiering, A. J. H., Janssen, R. A. J., Meijer, E. W., Herwig, P., and de Leeuw, D. M., *Two-dimensional charge transport in self-organized, high-mobility conjugated polymers.* Nature, 1999. **401**(6754):

p. 685-688.
13. Helfrish, W. and W.G. Schneider, *Recombination radiation in anthracene crystals.* Phys. Rev. Lett., 1965. **14**: p. 2.
14. Desai, P., *Organic-Magnetoresistance in Aluminium tris(8-hydroxyquinolinate) Light Emitting Diodes.* PhD thesis, 2008.
15. Poplavskyy, D., *Hole injection and transport in organic semiconductors.* PhD thesis, 2003.
16. Hill, I.G., Kahn, A., Soos, Z. G., and Pascal, R. A., *Charge-separation energy in films of pi-conjugated organic molecules.* Chemical Physics Letters, 2000. **327**(3-4): p. 181-188.
17. Bassler, H., *Charge Transport in Disordered Organic Photoconductors - a Monte-Carlo Simulation Study.* Physica Status Solidi B-Basic Research, 1993. **175**(1): p. 15-56.
18. Hill, R.M., *Poole-Frenkel Conduction in Amorphous Solids.* Philosophical Magazine, 1971. **23**(181): p. 59-&.
19. Dunlap, D.H., P.E. Parris, and V.M. Kenkre, *Charge-dipole model for the universal field dependence of mobilities in molecularly doped polymers.* Physical Review Letters, 1996. **77**(3): p. 542-545.
20. Novikov, S.V., Dunlap, D. H., Kenkre, V. M., Parris, P. E., *Essential role of correlations in governing charge transport in disordered organic materials.* Physical Review Letters, 1998. **81**(20): p. 4472-4475.
21. Parris, P.E., D.H. Dunlap, and V.M. Kenkre, *Energetic disorder, spatial correlations, and the high-field mobility of injected charge carriers in organic solids.* Physica Status Solidi B-Basic Research, 2000. **218**(1): p. 47-53.
22. Mott, N.F. and R.W. Gurney, *Electronic Processes in Ionic Crystals* Oxford University Press, New York, 1940.
23. Greenham., N.C. and R. Friend, *Semiconductor Device Physics of Conjugated Polymers.* Solid State Physics, 1995. **49**.
24. Griffiths, D.J., *Introduction to quantum mechanics.* 1995.
25. Walser, A.D., R. Priestley, and R. Dorsinville, *Temperature dependence of the singlet excited state lifetime in Alq(3).* Synthetic Metals, 1999. **102**(1-3): p. 1552-1553.
26. R.E.Merrifield, *Diffusion and mutual annihilation of triplet Excitons in organic crystal.* Accounts of chemical research, 1968. **1**.
27. Kalinowski, J., Cocchi, M., Virgili, D., Di Marco, P., and Fattori, V., *Magnetic field effects on emission and current in Alq(3)-based electroluminescent diodes.* Chemical Physics Letters, 2003. **380**(5-6): p. 710-715.
28. Groff, R.P., Avakian, P., Suna, A., and Merrifie.Re., *Magnetic Hyperfine Modulation of Dye-Sensitized Delayed Fluorescence in an Organic Crystal.* Physical Review Letters, 1972. **29**(7): p. 429.

29. Groff, R.P., Avakian, P., Suna, A., and Merrifie.Re., *Magnetic Hyperfine Modulation of Dye-Sensitized Delayed Fluorescence in Organic Crystals.* Physical Review B, 1974. **9**(6): p. 2655-2660.
30. Shakya, P., Desai, P., Kreouzis, T., and Gillin, W. P., *Magnetoresistance in triphenyl-diamine derivative blue organic light emitting devices.* Journal of Applied Physics, 2008. **103**(4): p. -.
31. Desai, P., Shakya, P., Kreouzis, T., Gillin, W. P., Morley, N. A., and Gibbs, *Magnetoresistance and efficiency measurements of Alq(3)-based OLEDs.* Physical Review B, 2007. **75**(9): p. -.
32. Ern, V. and R.E. Merrifield, *Magnetic Field Effect on Triplet Exciton Quenching in Organic Crystals.* Physical Review Letters, 1968. **21**: p. 2.
33. Frankevich, E.L., Lymarev, A. A., Sokolik, I., Karasz, F. E., Blumstengel, S., Baughman, R. H., and Horhold, H. H., *Polaron-Pair Generation in Poly(Phenylene Vinylenes).* Physical Review B, 1992. **46**(15): p. 9320-9324.
34. Kalinowski, J., J.D. Szmytkowski, and W. Stampor, *Magnetic hyperfine modulation of charge photogeneration in solid films of Alq(3).* Chemical Physics Letters, 2003. **378**(3-4): p. 380-387.
35. Bobbert, P.A., Nguyen, T. D., Van Oost, F. W. A., Koopmans, B., and Wohlgenannt, *Bipolaron mechanism for organic magnetoresistance.* Physical Review Letters, 2007. **99**(21).
36. Wagemans, W., Bloom, F. L., Bobbert, P. A., Wohlgenannt, M., and Koopmans, B.,Wagemans, W., *A two-site bipolaron model for organic magnetoresistance.* Journal of Applied Physics, 2008. **103**(7): p. -.
37. Tuladhar, P.S., *Charge Injection and Magneto-transport Studies in Small Molecule Organic Light Emitting Diodes.* PhD thesis, 2008.
38. Lampert, M.A. and P. Mark, *Current injection in solids.* Academic Press, New York, 1970.
39. Many, A. and G. Rakavy, *Theory of Transient Space-Charge-Limited Currents in Solids in the Presence of Trapping.* phys. Rev. Lett., 1962. **126**(6): p. 8.
40. Rossiter, E., P. Mark, and M.A. Lampert, *Unusual Field Phenomena Associated with Majority-Carrier Injection from a Point Contact.* Solid-State Electronics, 1970. **13**(4): p. 491-&.
41. Tse, S.C., S.W. Tsang, and S.K. So, *Polymeric conducting anode for small organic transporting molecules in dark injection experiments.* Journal of Applied Physics, 2006. **100**(6): p. -.
42. Poplavskyy, D., Kreouzis, T., Campbell, A., Nelson, J., and Bradley, D., *Injection and charge transport in polyfluorene polymers.* Organic and Polymeric Materials and Devices-Optical, Electrical and Optoelectronic Properties, 2002. **725**: p. 67-77
43. Kepler, R.G., *Charge Carrier Production and Mobility in Anthracene Crystals.* Physical Review Letters, 1960. **119**(4): p. 3.

44. LeBlanc, O.H., *Electron Drift Mobility in Liquid n□Hexane.* Journal of Chemical Physics, 1959. **30**(6): p. 4.
45. Mozer, A.J., Sariciftci, N. S., Pivrikas, A., Osterbacka, R., Juska, G., Brassat, L., and Bassler, H., *Charge carrier mobility in regioregular poly(3-hexylthiophene) probed by transient conductivity techniques: A comparative study.* Physical Review B, 2005. **71**(3): p. -.
46. Choulis, S.A., Kim, Y., Nelson, J., Kim, Y., Poplavskyy, D., Kreouzis, T., Durrant, J. R., and Bradley, D. D. C., *High ambipolar and balanced carrier mobility in regioregular poly(3-hexylthiophene).* Applied Physics Letters, 2004. **85**(17): p. 3890-3892.
47. Rackovsky, S. and H. Scher, *On the drift mobility of a molecular polaron in the presence of Coulomb traps.* Journal of Chemical Physics, 1999. **111**(8): p. 7.
48. Baldo, M.A. and S.R. Forrest, *Transient analysis of organic electrophosphorescence: I. Transient analysis of triplet energy transfer.* Physical Review B, 2000. **62**(16): p. 10958-10966.
49. Choulis, S.A., Kim, Y., Nelson, J., Kim, Y., Poplavskyy, D., Kreouzis, T., Durrant, J. R., and Bradley, D. D. C., *Investigation of transport properties in polymer/fullerene blends using time-of-flight photocurrent measurements.* Applied Physics Letters, 2003. **83**(18): p. 3812-3814.
50. Barard, S., *Separate charge transport pathways determined by the time of flight method in bimodal polytriarylamine.* Journal of Applied Physics, 2009. **105**(1): p. -.
51. Mori, T., E. Sugimura, and T. Mizutani, *Estimate of hole mobilities of some 1 organic photoconducting materials 1 ,using the time-of-flight method.* JOURNAL OF PHYSICS D-APPLIED PHYSICS, 1993. **26**(3): p. 3.
52. Naka, S., Okada, H., Onnagawa, H., Yamaguchi, Y., and Tsutsui, T., *Carrier transport properties of organic materials for EL device operation.* Synthetic Metals, 2000. **111**: p. 331-333.
53. Mattoussi, H., Murata, H., Merritt, C. D., Iizumi, Y., Kido, J., and Kafafi, Z. H., *Photoluminescence quantum yield of pure and molecularly doped organic solid films.* Journal of Applied Physics, 1999. **86**(5): p. 2642-2650.
54. Malagoli, M. and J.L. Bredas, *Density functional theory study of the geometric structure and energetics of triphenylamine-based hole-transporting molecules.* Chemical Physics Letters, 2000. **327**(1-2): p. 13-17.
55. Tang, C.W. and S.A. Vanslyke, *Organic Electroluminescent Diodes.* Applied Physics Letters, 1987. **51**(12): p. 913-915.
56. Shen, Y.L., Klein, M. W., Jacobs, D. B., Scott, J. C., and Malliaras, G. G., *Mobility-dependent charge injection into an organic semiconductor.* Physical Review Letters, 2001. **86**(17): p. 3867-3870.
57. Hartenstein, B., Bassler, H., Heun, S., Borsenberger, P., Vanderauweraer, M.,

and Deschryver, F. C., *Charge-Transport in Molecularly Doped Polymers at Low Dopant Concentrations - Simulation and Experiment.* Chemical Physics, 1995. **191**(1-3): p. 321-332.

58. Campbell, A.J., Bradley, D. D. C., Laubender, J., and Sokolowski, M., *Thermally activated injection limited conduction in single layer N,N '-diphenyl-N,N '-bis(3-methylphenyl)1-1 '-biphenyl-4,4 '-diamine light emitting diodes.* Journal of Applied Physics, 1999. **86**(9): p. 5004-5011.
59. Yamada, T., Sato, T., Tanaka, K. and Kaji, H., *Percolation paths for charge transports in N,N '-diphenyl-N,N '-di(m-tolyl)benzidine (TPD).* Organic Electronics, 2010. **11**(2): p. 255-265.
60. Mori, T., Sugimura, E., and Mizutani, T., *Estimate of Hole Mobilities of Some Organic Photoconducting Materials Using the Time-of-Flight Method.* Journal of Physics D-Applied Physics, 1993. **26**(3): p. 452-455.
61. Ishii, H., Sugiyama, K., Ito., Seki, K., et al., *Energy Level Alignment and Interfacial Electronic Structures at Organic/Metal and Organic/Organic Interfaces.* Advanced Materials, 1999. **11**.
62. Hill, I.G., A. Rajagopal, and A. Khan, *Molecular level alignment at organic semiconductor-metal interfaces.* 1998. **73**.
63. Paasch, G., Peisert, H., Knupfer, M., Fink, **J** and Scheinert, S., *Electronic properties of interfaces between different sexithiophenes and gold.* Journal of Applied Physics 2003. **63**.
64. Desai, P., Shakya, P., Kreouzis, T., and Gillin, W. P., *The role of magnetic fields on the transport and efficiency of aluminum tris(8-hydroxyquinoline) based organic light emitting diodes.* Journal of Applied Physics, 2007. **102**(7).
65. Shakya, P., Desai, P., Somerton, M., Gannaway, G., Kreouzis, T., and Gillin, W. P., *The magnetic field effect on the transport and efficiency of group III tris(8-hydroxyquinoline) organic light emitting diodes.* Journal of Applied Physics, 2008. **103**(10).
66. Rolfe, N., Desai, P., Shakya, P., Kreouzis, T., and Gillin, W. P., *Separating the roles of electrons and holes in the organic magnetoresistance of aluminum tris(8-hydroxyquinoline) organic light emitting diodes.* Journal of Applied Physics, 2008. **104**(8).
67. Song, J.Y., Stingelin, N., Kreouzis, T., and Gillin, W. P., *Reduced hole mobility due to the presence of excited states in poly-(3-hexylthiophene).* Applied Physics Letters, 2008. **93**(23): p. -.
68. Desai, P., Shakya, P., Kreouzis, T., and Gillin, W. P., *Magnetoresistance in organic light-emitting diode structures under illumination.* Physical Review B, 2007. **76**(23).